2009

Classification of Urban features using Airborne Hyperspectral Data

Bharath Ganesh Babu
Indiana State University

CURRICULUM VITAE

EDUCATION

Ph.D., Indiana State University, 2009.
Major: Physical Geography
Dissertation Title: Classification of Urban Features using Airborne Hyperspectral Data
M.Sc., University of Madras, 1997.
Major: Applied Geography
Study Focus: Satellite image interpretation and digital mapping techniques.
B.Sc., Madras Presidency College, 1995.
Major: Geography

TEACHING EXPERIENCE

Instructor, Valparaiso University, 2006 - 2009.
Introduction to GIS, Advanced GIS, Remote Sensing, Advanced Remote Sensing, Environmental Conservation, Biogeography, Globalization and Development, Introduction to Meteorology Lab
Teaching Assistant/Instructor, Indiana State University, 2004 - 2006.
World Regional Geography, Global Geography
Guest Lecturer, Madras University, 1998.
Cartography, Regional Geography of India, GIS Techniques Lab

PROFESSIONAL EXPERIENCE

Interactive and Multimedia Designer, 2005 - 2006
Interactive and Multimedia Design Services, CIRT, Indiana State University
Graphic/Web Designer, 2005 - 2006
Spectral Interactions with Earth Features, An educational module part of a five year NASA REASoN grant supporting the project *Measuring Vegetation Health*, Geo-Education Center, Indiana State University
Project Collaborator, 2005
Darwin's Fox Research and Conservation Project in Chiloé Island, Chile, funded by Darwin's Initiative, and Department of Environment, Food and Rural Affairs, UK

PROFESSIONAL MEMBERSHIPS

Member, Association of American Geographers, 2000 - Present.
Senior Director, Geography and Environmental Studies, Indiana Academy of Social Sciences, August 2009 - August 2010.
Director, Geography and Environmental Studies, Indiana Academy of Social Sciences, August 2008 - August 2009.
Junior Director, Geography and Environmental Studies, Indiana Academy of Social Sciences, August 2007 - August 2008.

CLASSIFICATION OF URBAN FEATURES USING AIRBORNE HYPERSPECTRAL DATA

A Dissertation

Presented to

The School of Graduate and Professional Studies

Department of Geography, Geology, and Anthropology

Indiana State University

Terre Haute, Indiana

In Partial Fulfillment

of the Requirements for the Degree

Doctor of Philosophy

---

by

Bharath Ganesh Babu

December 2009

Keywords: Hyperspectral, Remote Sensing, Classification, Urban, Land Use Land Cover

COMMITTEE MEMBERS

Committee Chair: Paul Mausel, Ph. D.

Professor Emeritus of Geography

Indiana State University

Committee Co-Chair: Susan Berta, Ph. D.

Associate Professor of Geography

Indiana State University

Committee Member: Jay Gatrell, Ph. D.

Associate Professor of Geography

Indiana State University

Committee Member: Rusty Gonser, Ph. D.

Assistant Professor of Biology

Indiana State University

Committee Member: James Speer, Ph. D.

Associate Professor of Geography and Geology

Indiana State University

ABSTRACT

Accurate mapping and modeling of urban environments are critical for their efficient and successful management. Superior understanding of complex urban environments is made possible by using modern geospatial technologies. This research focuses on thematic classification of urban land use and land cover (LULC) using 248 bands of 2.0 meter resolution hyperspectral data acquired from an airborne imaging spectrometer (AISA+) on 24th July 2006 in and near Terre Haute, Indiana. Three distinct study areas including two commercial classes, two residential classes, and two urban parks/recreational classes were selected for classification and analysis. Four commonly used classification methods – maximum likelihood (ML), extraction and classification of homogeneous objects (ECHO), spectral angle mapper (SAM), and iterative self organizing data analysis (ISODATA) - were applied to each data set. Accuracy assessment was conducted and overall accuracies were compared between the twenty four resulting thematic maps. With the exception of SAM and ISODATA in a complex commercial area, all methods employed classified the designated urban features with more than 80% accuracy. The thematic classification from ECHO showed the best agreement with ground reference samples. The residential area with relatively homogeneous composition was classified consistently with highest accuracy by all four of the classification methods used. The average accuracy amongst the classifiers was 93.60% for this area. When individually observed, the complex recreational area (Deming Park) was classified with the highest accuracy by ECHO, with an accuracy of 96.80% and 96.10% Kappa. The average accuracy amongst all the classifiers was 92.07%. The commercial area with relatively high

complexity was classified with the least accuracy by all classifiers. The lowest accuracy was achieved by SAM at 63.90% with 59.20% Kappa. This was also the lowest accuracy in the entire analysis. This study demonstrates the potential for using the visible and near infrared (VNIR) bands from AISA+ hyperspectral data in urban LULC classification. Based on their performance, the need for further research using ECHO and SAM is underscored. The importance incorporating imaging spectrometer data in high resolution urban feature mapping is emphasized.

ACKNOWLEDGEMENTS

My grandfather had a favorite Tamil saying that roughly translates as, "If you prop me up and tie my loincloth for me, I too will stand like a lion!" A multitude of people have propped me up and led me by hand to this humbling moment of success.

My parents patiently sat with me while I reluctantly did my homework in primary school. My brother Sundar kept me interested in the splendor of science, history, and literature merely through engaging conversations - a feat that no classroom could accomplish. Mrs. Joseph, my tenth grade math teacher cared enough and enabled me to take another step forward. In high school it was Ms. Padmavati who showed me that I was good in geography. I remember the day my aunts stood in queue with me late in the night to get me enrolled in college. Later, during my Master's Dr. Sivagnanam took me under his wing and helped me find direction. My cousin Kannan virtually wrote my application letters and gave me confidence to pursue higher education in the United States. Dr. Venugopal introduced me to Dr. Paul Mausel.

I could not have arrived at this moment without Dr. Mausel's patient and insightful guidance. I do not have enough words to thank him for meticulously editing my drafts often in brutally short time. Most of all, I thank him for not giving up on me. I constantly strive to imitate his equanimity, objectivity, and clarity of thought while interacting with my own peers and students. I am fortunate to have had the opportunity to learn from him. I still use notes from his classes. I also remind myself to be unconditionally kind to others, for my life is fruitful because of

the kindness shown to me by Dr. William Dando and Mrs. Caroline Dando. I thank them for their warm embrace and support.

My life experience is enriched by the memorable times I had with friends in Indiana. I have learnt in many ways from my friends and colleagues Vijay Lulla, Ajay Singh, Nelson Dias, Idrissa Tiemogo, Cameron Craig, Adil Wadia, Ishwari Sivagnanam, Nicole Wright, Amy Deane, Ravi Visvanadha, Srinivas Pandeshwar, and Sara Brown. My heartfelt gratitude extends to Jaishankar Raman and Jayashree Raman at Valparaiso, for their friendship and the many meals they share with me. I am also lucky to know my wonderful friends Teresa Bals-Elsholz and Kurt Elsholz, who cheered me on during difficult days.

I am grateful to my committee members Dr. Rusty Gonser, Dr. Susan Berta, and Dr. James Speer, whose valuable suggestions have helped me shape this research. I specifically thank Dr. Jay Gatrell whose encouraging words helped me complete this work. I also offer my sincere appreciation to administrative assistants in all the departments who might have forwarded numerous forms and papers on my behalf. Particularly, Suzanne Walters in the Geography department has helped me navigate the administrative Everglades for many years.

TABLE OF CONTENTS

COMMITTEE MEMBERS ii

ABSTRACT iii

ACKNOWLEDGEMENTS v

TABLE OF CONTENTS vii

LIST OF TABLES x

LIST OF FIGURES xii

INTRODUCTION 1

1.1 Research Objectives 3

1.2 Hypotheses 4

BACKGROUND AND CONTEXT 5

2.1 Introduction 5

Value of Remote Sensing in Urban Research 6

Significance of Data Resolution in Remote Sensing 7

2.2 Hyperspectral Remote Sensing 10

AISA+ Hyperspectral Sensor 12

2.3 Land Use and Land Cover Classification 15

2.4 Band Reduction and Digital Image Classification 20

Data Dimensionality 20

Principal Components Analysis (PCA) 21

Minimum Noise Fraction (MNF) 24

Thematic Classification of Remote Sensor Data 24
Maximum Likelihood Classification (MLC) 25
Extraction and Classification of Homogeneous Objects (ECHO) 26
Spectral Angle Mapper (SAM) 29
Iterative Self Organizing Data Analysis Technique (ISODATA) 29
2.5 Accuracy Assessment 30
STUDY AREA AND DATA CHARACTERISTICS 32
3.1 Study Area 32
3.2 Data Characteristics 34
In Situ and Ancillary Data 34
AISA+ Hyperspectral Data 34
METHODOLOGY 44
4.1 Field Sampling and Ancillary Information 44
4.2 Land Use and Land Cover Classification Scheme 46
Built up Class 46
Vegetation Class 47
Non-Urban or Non-Vegetated Bare Surfaces, and Water Class 48
4.3 Data Processing 48
Spectral Normalization and Data Reduction 48
Sampling 50
4.4 Data Analysis 60
Accuracy Assessment 61
RESULTS AND DISCUSSION 63

5.1 Thematic Classification 63
Commercial Areas 63
Residential Areas 68
Recreational Areas 73
5.2 Classification Accuracies 74
Evaluation of Overall Accuracies and Classification Significance 74
Evaluation of Per Class Accuracies for Commercial Areas 75
Evaluation of Per Class Accuracies for Residential Areas 79
Evaluation of Per Class Accuracies for Recreational Areas 80
CONCLUSIONS 82
6.1 Need for Hyperspectral Remote Sensing 84
6.2 Future Research and Recommendations 86
Classification Scheme 86
Remote Sensing of Urban Features 86
Urban Spectral Libraries 87
Classification Methods 87
REFERENCES 88
APPENDIX A: ERROR MATRICES 98
APPENDIX B: MINIMUM NOISE TRANSFORM COVARIANCE MATRIX 117
APPENDIX C: MINIMUM NOISE TRANSFORM EIGENVALUES 121

LIST OF TABLES

Table 1 Land-Based Classification Standards (LBCS): Criteria relevant to remote sensor data (Jeer 2006). 16

Table 2 Abridged urban classification system based on USGS LULC Classification System (Anderson et al. 1976, Jensen 2007). 17

Table 3 AISA+ Bands and their corresponding wavelengths in the electromagnetic spectrum. 35

Table 4 Modified LULC classification scheme used in the six study areas (Anderson et al. 1976). 47

Table 5 The number of pixels used in training LULC classes across the study subsets is shown. 50

Table 6 Comparison of overall classification accuracies. 74

Table 7 Individual class accuracies (%) for commercial area (1). 78

Table 8 Individual class accuracies (%) for commercial area (2). 78

Table 9 Individual class accuracies (%) for residential area (1). 80

Table 10 Individual class accuracies (%) for residential area (2). 80

Table 11 Individual class accuracies (%) for recreational area (1). 81

Table 12 Individual class accuracies (%) for recreational area (2). 81

Table 13 Percentage difference between classifiers in terms of overall accuracy. 83

Table 14 Commercial (1) error matrix for MLC classification results 99

Table 15 Commercial (1) error matrix for ECHO classification results. 100

Table 16 Commercial (1) error matrix for SAM classification results. 101

Table 17 Commercial (2) error matrix for MLC classification results. 102

Table 18 Commercial (2) error matrix for ECHO classification results. 103

Table 19 Commercial (2) error matrix for SAM classification results. 104

Table 20 Residential (1) error matrix for MLC classification results. 105

Table 21 Residential (1) error matrix for ECHO classification results. 106

Table 22 Residential (1) error matrix for SAM classification results 107

Table 23 Residential (2) error matrix for MLC classification results. 108

Table 24 Residential (2) error matrix for ECHO classification results. 109

Table 25 Residential (2) error matrix for SAM classification results 110

Table 26 Recreational (1) error matrix for MLC classification results. 111

Table 27 Recreational (1) error matrix for ECHO classification results 112

Table 28 Recreational (1) error matrix for SAM classification results. 113

Table 29 Recreational (2) error matrix for MLC classification results. 114

Table 30 Recreational (2) error matrix for ECHO classification results 115

Table 31 Recreational (2) error matrix for SAM classification results. 116

Table 32 A portion of covariance matrix generated from MNF transform of commercial area (1) as an example dataset. 118

Table 33 Eigenvalues for the first 25 bands in each study area. 122

LIST OF FIGURES

Figure 1. Comparison of multispectral and hyperspectral bands using spectral curves of example features. 13

Figure 2. Relationship between USGS LULC classification levels and ground resolution (modified from Jensen 2007)..... 18

Figure 3. Plot of two correlating visible bands (Band A (*axis* x_1) and Band B (*axis* x_2). The principal components transformation generated a new coordinate system (y_1, y_2)..... 22

Figure 4. An example of distribution of pixel values in a two dimensional feature space (developed from AISA+ hyperspectral data)..... 23

Figure 5. Equiprobability contours defined for urban features by maximum likelihood classifier (MLC) in a two band feature space (modified from Lillesand et al. 2008). 27

Figure 6. Two-band representation of classification approach used by SAM. Angle between reference *r* and feature *k* is smaller than feature *t* (modified from Jensen 2005, Shippert 2003). 28

Figure 7. True color digital orthoquad (DOQ) mosaic of Terre Haute, Indiana. 33

Figure 8. An example of validating sample feature from a location using a. Bing Maps™ Bird's Eye; b. Google Maps™ Street View. 36

Figure 9. Study area subsets from AISA+ flight lines, July 2006..... 37

Figure 10. Subset of a commercial area (1) (See 1 in Figure 9): a. AISA+ composite of (RGB 187, 125, 63); b. DOQ; c. High resolution oblique aerial view of a part of subset. 38

Figure 11. Subset of a commercial area (2) (See 2 in Figure 9): a. AISA+ composite of (RGB 187, 125, 63); b. DOQ; c. High resolution oblique aerial view of a part of subset. 39

Figure 12. Subset of a residential area (1) with a spatially dense composition (See 3 in Figure 9): a. AISA+ composite of (RGB 187, 125, 63); b. DOQ; c. High resolution oblique aerial view of a part of subset..... 40

Figure 13. Subset of a residential area (2) with spatially less dense composition (See 4 in Figure 9): a. AISA+ composite of (RGB 187, 125, 63); b. DOQ; c. High resolution oblique aerial view of a part of subset..... 41

Figure 14. Subset of a recreational area (1) (See 5 in Figure 9): a. AISA+ composite of (RGB 187, 125, 63); b. DOQ; c. High resolution oblique aerial view of a part of subset. 42

Figure 15. Subset of a recreational area (2) (See 6 in Figure 9): a. AISA+ composite of (RGB 187, 125, 63); b. DOQ; c. High resolution oblique aerial view of a part of subset. 43

Figure 16. Research methodology..... 45

Figure 17. A comparison between spectral curves developed from a. original data, and b. normalized data. AISA+ false color image is shown in RGB 210, 130, 70 band combination. See Figure 25 for signature legend. 51

Figure 18. ENVI software interface for selecting MNF bands with highest variance. 52

Figure 19. The first 20 principal component images from a Minimum Noise Fraction (MNF) transformation of commercial area (1). 53

Figure 20. The first 20 principal component images from a Minimum Noise Fraction (MNF) transformation of a commercial area (2). 54

Figure 21. The first 20 principal component images from a Minimum Noise Fraction (MNF) transformation of a residential area (1). 55

Figure 22. The first 20 principal component images from a Minimum Noise Fraction (MNF) transformation of a residential area (2). 56

Figure 23. The first 20 principal component images from a Minimum Noise Fraction (MNF) transformation of a recreational area (1). 57

Figure 24. The first 20 principal component images from a Minimum Noise Fraction (MNF) transformation of a recreational area (2). 58

Figure 25. Spectral profiles of select urban features in AISA+ spectral feature space. 59

Figure 26. Classification results of commercial area (1) with a. MLC, b. ECHO, c. SAM, d. ISODATA, and e. Original data are displayed in true color (RGB 135, 75, 25). 65

Figure 27. Classification results of commercial area (2) with a. MLC, b. ECHO, c. SAM, d. ISODATA, and e. Original AISA+ data are displayed in true color (RGB 135, 75, 25). 66

Figure 28. Spectral curves of two different asphalt classes. 67

Figure 29. Classification results of residential area (1) with a. MLC, b. ECHO, c. SAM, d. ISODATA, and e. Original AISA+ data are displayed in true color (RGB 135, 75, 25). 69

Figure 30. Classification results of residential area (2) with a. MLC, b. ECHO, c. SAM, d. ISODATA, and e. Original AISA+ data are displayed in true color (RGB 135, 75, 25). 70

Figure 31. Classification results of recreational area (1) with a. MLC, b. ECHO, c. SAM, d. ISODATA, and e. Original AISA+ data are displayed in true color (RGB 135, 75, 25). 71

Figure 32. Classification results of recreational area (2) with a. MLC, b. ECHO, c. SAM, d. ISODATA, and e. Original AISA+ data are displayed in true color (RGB 135, 75, 25). 72

Figure 33. Comparison of overall accuracies of four classifiers over six urban study areas. 76

Figure 34. Comparison between classification methods when applied to the six study areas. 77

CHAPTER 1

INTRODUCTION

Geographers have a long tradition of urban research. The imminent need for smart and sustainable development of our ever expanding urban areas has only underscored the importance of urban research. Better understanding of urban geography and improved urban modeling are dependent on our knowledge of the causation, impacts, and chronology of urban processes (Herold 2003a, Herold 2003b). Technologies that allow for fast and repeatable monitoring of large areas at a reasonable cost are vital for improved mapping and modeling of urban environments (Roberts et al. 2004). New sources of data and analysis techniques help us better understand the geographical makeup and dynamism of urban areas. Since urban processes have an element of spatial dependence, tools such as remote sensing and Geographic Information Systems (GIS) provide valuable means for modeling spatial data at landscape and cadastral levels (Goodchild 1997).

Detailed and spatially comprehensive urban land use and land cover (LULC) information is required to serve a variety of purposes including residential, industrial, and commercial site selection, population estimates, land and property assessment for taxation, development and implementation of zoning regulations, urban forestry, and public health. Information extracted from remotely sensed data are usually used for further spatial analyses or mapping by various research and administrative entities (Carlson 2003, Cowen et al. 1998, Goodchild 2001). To maintain exchange of spatial information between these entities without ambiguity, spatial scientists follow certain standardized LULC classification schemes.

During the last decade, advances in instrumentation and digital photogrammetry have enabled monitoring of land surface with superior spatial and spectral detail. Airborne imaging spectrometers are increasingly used in a variety of applications (Jensen 2007). However, data obtained by these hyperspectral sensors are often expensive due to flight costs, mission planning and execution, and field sampling. Research and administrative entities that often operate on limited resources are unable to obtain information at a high frequency that is essential for monitoring the frequently changing urban areas. Another challenge with airborne hyperspectral data is that at higher resolutions the tasks of feature identification, data processing, information extraction, and classification of urban objects become arduous and resource hungry (Herold et al. 2003a, Landgrebe 2002). The information derived from airborne hyperspectral sensors make standard LULC classification hard to reconcile. This is only further complicated by the variations in the layout and composition of objects that may often be unique to each urban area.

In recent studies, data from airborne hyperspectral sensors such as AISA+ have been used for identifying surface features that may be often missed by spaceborne multispectral sensors. These studies have mostly limited themselves to specific features or processes. Only a few studies have attempted urban LULC research using hyperspectral data (Herold et al. 2004, Segl et al. 2003, Voss et al. 2008), leaving a need for understanding the usefulness of airborne hyperspectral data in urban LULC classification. The purpose of this study is to quantitatively assess urban LULC classification accuracy by comparing multiple classification methods when applied to select AISA+ hyperspectral data subsets obtained over the city of Terre Haute, Indiana.

1.1 Research Objectives

Accuracy of information extracted from remotely sensed data is dependent on three major factors - nature of the underlying environment, spatial-spectral data characteristics, and classification technique. With these three factors in consideration, the primary objective of this study was to provide quantitative assessment of the suitability of AISA+ hyperspectral data in urban LULC feature classification.

In terms of detecting a larger number of classes with higher accuracy, high dimensional data such as AISA+ can yield more information than multispectral data. However, as dimensionality increases, it is important to address issues such as determining class statistics with precision by intensive sampling, and reducing data dimensionality whereby only the bands with the most spectral variability are used for classification. Treatment of image data by different classification methods also plays an influential role in the thematic outcome. No single method can claim universal superiority. Hence, multiple classification methods need to be applied to the data and the results be compared to field observations to determine their level of accuracy. Given the presence of both homogeneous and heterogeneous spaces in urban environments, it was essential to examine varying scene compositions, such as commercial areas, residential areas, and recreational areas. The specific objectives of this study were as follows:

1. Map urban LULC classes from three representative urban environments - commercial, residential, and recreational using AISA+ hyperspectral data;
2. To achieve the first objective, reduce spectral data dimensionality using the minimum noise fraction (MNF) transformation and select a small subset of MNF bands with the largest spectral variation for classification;

3. Perform unsupervised cluster classification using the iterative self-organizing data analysis (ISODATA) method using the selected MNF band subset;
4. Perform supervised maximum likelihood classification (MLC), extraction and classification of homogeneous objects (ECHO), and spectral angle mapper (SAM) – using the selected MNF band subset;
5. Perform accuracy assessment on maps derived from each classification method implemented on each of the three representative urban environments;
6. Compare results and assess the suitability of AISA+ hyperspectral sensor for urban LULC classification within the context of the specific methods used in this research.

1.2 Hypotheses

The following hypotheses were developed to address LULC classification of AISA+ hyperspectral scenes from Terre Haute, Indiana:

1. Spectral information from AISA+ sensor's VNIR bands can be utilized to classify urban LULC from Level I through Level III, of a modified Anderson's classification, with accuracy of 80% or greater.
2. Iterative self organizing data analysis (ISODATA), extraction and classification of homogeneous objects (ECHO), maximum likelihood classifier (MLC), and spectral angle mapper (SAM) will perform differently when classifying complex urban scenes but will perform in similar manner when classifying homogeneous scenes.

CHAPTER 2

BACKGROUND AND CONTEXT

2.1 Introduction

Remote sensing not only proves useful in repeated earth monitoring at regional and landscape scales, but also plays an important role as a tool for understanding urban structural composition such as surface materials and their arrangement (Herold et al. 2002, Herold et al. 2003a, Priestall et al. 2000), and phenomenal attributes such as land cover change, urban sprawl, climate, and human social interactions (Gatrell et al. 2008, Jensen et al. 1982, Lo et al. 1997, Masser 2000, Voogt et al. 2003). Aerial photography was commonly used by urban researchers for identifying and mapping urban objects that typically have small spatial extents. The recent advancements in high resolution spaceborne remote sensing systems provide a cost effective alternative to aerial photography (Dell'Acqua et al. 2004, Herold et al. 2004, Roberts et al. 2004, Roessner et al. 2001, Segl et al. 2003). Complemented with ground observations and GIS, spaceborne remote sensing is indispensable for global monitoring and spatiotemporal analyses for mapping, modeling features, and forecasting phenomena (Carlson 2003, Gatrell et al. 2008, Kumar, Garg and Khare 2008).

Urban areas are compact in spatial organization and complex in spatial composition and arrangement. They are composed of intimately occurring cultural and natural materials. Spatial and temporal dynamism of these materials further enhances the complexity or urban areas (Cowen et

al. 1998). Given the nature of urban materials, spaceborne multispectral sensors may sometimes lack the ability to differentiate between certain urban features, as their band widths are too broad to sample subtle spectral differences. For this reason, the use of imaging spectrometers is gaining importance and use. Imaging spectrometers can sample a large number of narrow bands of contiguous wavelengths, and facilitate better definition of ground features. Several such instruments exist, and they are increasingly used by researchers for various applications. A need for understanding and processing imaging spectrometer data for accurate thematic classification exists.

Value of Remote Sensing in Urban Research

Research interest in spatial and temporal characteristics of urban areas has been long standing and multifaceted. The need for near real-time information exists in a number of scientific, social, pecuniary, and policy making agencies (Herold 2003). A list of entities that require urban information has been developed by Jensen (2005). He includes councils and legislative bodies, commerce departments, tax assessors, transportation departments, utility companies, public service commissions, parks and recreation departments, emergency and homeland security departments, real estate companies, commercial developers, and scientists. Physical and social scientists play an important role in identifying, extracting, and analyzing diverse urban information that is eventually used by the entities listed earlier. Research such as on urban sprawl (Irwin et al. 2006, Radeloff et al. 2005), urban growth (Fesenmaier et al. 1979), urban forestry (Hardin et al. 2007, Jensen et al. 2009), urban pollution (Bassani et al. 2007, Ben-Dor et al. 2001, Lo et al. 1997), and land cover dynamics (Pozzi et al. 2001) are important to science and society. Being inherently spatial in nature, such research draws heavily from the strengths of geospatial technologies - including GIS (Goodchild 1997, Longley et al. 2005) and remote sensing (Jensen et al. 2005, Jensen et al. 2007, Lillesand et al. 2008, Sabins 1997) - providing valuable support in information gathering, storage, processing,

analysis, and mapping or modeling. Cowen et al. (1998), in their description of urban attributes that are served by remote sensing, include LULC, property infrastructure, transportation network, utility infrastructure, socioeconomic derivatives, energy consumption, meteorology, environmental assessment, disaster management, and urban growth trend forecasting.

Significance of Data Resolution in Remote Sensing

Identification and classification of surface features are the basic goals in most remote sensing applications (Bajcsy et al. 2004). Information acquired through processing of remotely sensed data is often integrated with other spatial and non-spatial attributes to address problems associated with earth environments. Depending on the scale of a study, LULC classification of earth environments can be performed at multiple levels (Anderson et al. 1976). Each level may require optimal amount of spatial clarity that is defined by the *spatial resolution* of data used. For digital sensors, spatial resolution is defined as the ability to distinguish between two closely spaced objects on an image. Spatial resolution is a function of ground area contained within each square pixel (Sabins 1997). It is generally agreed that high resolution data are ideal for effectively identifying features (Jensen 2007). For accurate discrimination between different ground cover, as in agricultural or urban environments, spatial resolution of the order of a few centimeters may be required. However, the amount of synoptic data collected for large areas, even the size of cities, at such a high resolution can be staggering. Therefore, spectral variation, or variation in the reflected or radiated energy from different features, is analyzed by pattern recognition techniques to derive thematic maps of ground cover (Landgrebe 1999). Sensitivity of a detector to the number of wavelengths in the electromagnetic spectrum determines its *spectral resolution* (Jensen 2005, Sabins 1997). Urban remote sensing applications such as in ecology (Hardin et al. 2007), boundary layer climatology (Ben-Dor et al. 2001), energy use (Jensen et al. 2005), pollution (Bassani et al. 2007),

forestry, and distribution and dynamics of social entities (Cowen et al. 1998) have used data with high spectral resolutions in the visible and non visible regions of reflected sunlight. Due to superior spectral sensitivity, hyperspectral remote sensing is proving increasingly useful identifying earth features, especially complex urban areas (Heiden et al. 2007).

Satellite based low spatial resolution data have also been useful in several urban studies. In very early stages, Jensen et al. (1982) conducted change detection of Denver, Colorado using five band low resolution (80 m) multispectral data from Landsat MSS sensor. In their study, residential development in the urban fringe was detected with over 80% accuracy. Jensen et al. (1999) assessed extraction of urban infrastructure and socioeconomic attributes from low resolution satellite data. The complexity of urban environments and the fact that most urban objects were smaller than the smallest pixel resolution in civilian sensors posed challenges for urban research. The pervasive need for improved information extraction and classification accuracies from these datasets led to the development of several application-specific methods. For instance, Gong et al. (1990) presented new methodology using structural information to improve information extraction from SPOT (20 m) data. Other studies have employed various methods including fuzzy statistical technique, neural network classification, continuum based classification, kernel classification, subpixel classification, object oriented classification, and decision tree methods on low resolution image data (Clapham Jr. 2003, Kontoes et al. 2000, Pal et al. 2003, Yang et al. 2003, Zhang et al. 2001). In most studies, aerial photographs were often used as supplements in Level I and Level II classification (Anderson et al. 1976, Cowen et al. 1998, Jensen et al. 1982). They are still used in certain pattern oriented studies as indicated by recent works in urban demographics, climate, vegetation change, urban sprawl, and feature classification that have been conducted with relative success (Li et al. 2005, Lu et al. 2004b, Lu et al. 2005, Lu et al. 2006, Small 2002). Orbital (satellites) remote sensing has also been effective

in urban vegetation and surface temperature studies (Small 2006, Small et al. 1999). Building on previous Landsat TM sensor (30 m) based study (Jensen 2000), Hardin et al. (2007) analyzed the relationship between vegetation leaf area index and urban temperatures using data from ASTER sensor (15 m). ASTER data were used also for explaining relationships between urban forestry and household energy consumption (Jensen et al. 2003b, Jensen et al. 2005). However, in LULC research, it is clear that accurate extraction and classification of urban features is better served by high resolution datasets (Dell'Acqua et al. 2005). As mentioned by Jensen et al. (1982), for good results, sensor spatial resolution should be half the diameter of the smallest object of interest. For instance, a spatial resolution of two and a half meters is required to unambiguously study objects five meters wide. Urban objects often tend to be smaller than approximately ten meters in size, and high resolution data better than five meters is often desirable for detailed urban classification (Jensen 2007, Jensen et al. 1999). Its significance is so vital that in a bid to achieve better ground object separation, many researchers have used data fusion techniques to merge a high resolution panchromatic band or digital orthoquads (DOQ) with low resolution multispectral bands to simulate higher spatial resolution (Shaban et al. 2002, Zhang 1999, Zhang 2001, Zhu et al. 2006).

Availability of high resolution imagery from orbital along track scanning sensors (Lillesand et al. 2008) such as IKONOS (4 m), Orbview (4 m), Quickbird (2.4 m), and GeoEye (1.65 m), often sensitive to visible and near infrared spectral range (VNIR; 400 - 900 nm) contributes immensely towards urban remote sensing, particularly as a cost effective alternative to aerial surveys (Ehlers 2005, Fisher et al. 2001). Even as these datasets help resolve for the high frequency of spatial change in surface features, their broad bandwidths may limit spectral distinction between certain urban materials (Herold et al. 2003a, Roberts et al. 2004). Growing urban settlements pose new challenges in urban mapping for the purpose of target specific studies such as energy conservation analysis

(Medina 2000), LEED certification (Cidell 2009), identification of pollution sources such as asbestos (Bassani et al. 2007), structural vulnerability assessment (Bhaskaran et al. 2004), flood risk assessment based on mapping impervious surfaces (Fisher et al. 2001), water quality (Ridd 1995), and vegetation cover characteristics (Jensen et al. 2009). For such studies, airborne imaging spectrometers that are sensitive to larger and finer spectral ranges, and are able to identify subtle variations in spectral reflectance of features, may provide the necessary data support. This makes them potentially more effective in addressing questions often unexplored by multispectral detectors alone (Roberts et al. 2004)

2.2 Hyperspectral Remote Sensing

Hyperspectral data are distinguished from multispectral data in that the wavelengths of spectral data collected are narrow (less than 10 nm per band) and contiguous. Multispectral data usually contain wide bands with aggregated wavelengths and they are separated by wavelengths that are not sampled (Figure 1). For this reason, hyperspectral remote sensing provides an opportunity for differentiating surface materials using subtle spectral variations in the spectral data (Jensen 2005).

Imaging spectrometers are capable of acquiring several narrow and contiguous spectral bands in the ultraviolet, visible, and infrared spectra (Jensen 2007). They typically collect reflectance information in 60 - 300 narrow and contiguous bands (wavelengths) across major parts of the electromagnetic spectrum. Orbital hyperspectral systems such as the experimental Hyperion and suborbital systems such as the Airborne Visible/Infrared Imaging Spectrometer (AVIRIS), Compact Airborne Spectrographic Imager (CASI), Airborne Imaging Sensor (AIS), HyMap, Digital Airborne Imaging Spectrometer (DAIS), and Airborne Imaging Spectrometer for Applications (AISA) have

been used in several studies with varying degrees of success. While widely used orbital imaging spectrometers such as Moderate Resolution Imaging Spectrometer (MODIS) with 250 m - 1000 m spatial resolution or Hyperion with 30 m resolution, whose availability is very limited, are well suited for small and medium scale studies, their direct relevance is diminished in urban research (Cavalli et al. 2008).

Airborne hyperspectral sensors have shown much promise in several fine scale studies. A few commonly used recurring systems in the literature are NASA's AVIRIS (370 - 2500 nm with 224 bands) (Aardt et al. 2007, Guo et al. 2008), CASI (400 - 1000 nm with 288 bands) (Foody et al. 2004), DAIS (450 - 2450 nm with 72 bands) (Dell'Acqua et al. 2005, Pal et al. 2003), HyMap (450 - 2500 nm with 126 bands) (Bakker et al. 2002), Multispectral Infrared and Visible Imaging Spectrometer (MIVIS; 430 - 830 nm with 20 bands, 1150 - 1550 nm with 8 bands, 1985 - 2479 nm with 64 bands) (Bassani et al. 2007, Cavalli et al. 2008) and AISA+ (400 - 970 nm with 248 bands) (Jensen et al. 2009, Mäkisara et al. 1993, Mausel et al. 2005). The choice of sensor largely depends on the underlying application, spectral sensitivity of sensor, and data availability (Aardt et al. 2007, Buddenbaum et al. 2005, Jensen et al. 2009, Lulla 2009, Pal et al. 2003).

The spectral advantages that help distinguish subtle variations in spectral signatures of underlying features, may also act disadvantageously. Many ground features may not show significant spectral variation in a number of contiguous bands. Such spectral redundancy of bands immediately adjacent to or very near a given hyperspectral band is common. Since feature identification depends on variation in reflectance patterns from one band to another, data with a high inter-band correlation may not provide new information, but only contribute towards noise (Foody et al. 2004). Apart from being problematic for statistical classification algorithms, hyperdimensional datasets also require more computational resources.

Much research has been dedicated to improve information extraction by reducing hyperspectral data dimensionality, using select bands for specific applications, and applying enhanced information extraction and classification techniques (Bajcsy et al. 2004, Dell'Acqua et al. 2006, Segl et al. 2003, Vaiphasa 2006). Methods such as principal components analysis (PCA) (Mausel et al. 1990) and minimum noise fraction (MNF) (Yang et al. 2007a, Yang et al. 2007b) have been used to select bands with the highest spectral variability. Several classification methods have been developed to improve thematic information accuracy from digital imagery (Lu et al. 2007a).

Classification itself is a complex process that depends on factors such as underlying study area characteristics, image data characteristics, ground reference sampling, image processing techniques, and classification algorithms (Tso et al. 2001). Consequently, one method does not fit all remote sensing requirements. It is necessary to identify application, site, and data specific classification techniques that can produce most accurate results.

AISA+ Hyperspectral Sensor

AISA+ is a compact airborne system whose charge-coupled device (CCD) array is sensitive to the VNIR wavelengths of the reflected spectrum. Developed and tested in Finland in 1992 (Braam et al. 1993) as a portable, cost effective, and programmable imaging spectrometer, the AISA+ has a direct sight imaging spectrograph and high performance camera. It has a built-in miniature global positioning system/internal navigation system (GPS/INS) sensor that allows aircraft roll, pitch and yaw information to be encoded for georeferencing (Jensen 2007, Mäkisara et al. 1993). A series of AISA detectors exist in the market today. While AISA+ is a VNIR sensor, AISAHawk is built for shortwave infrared (SWIR) bands, and AISADual is a VNIR/SWIR sensor (SPECIM 2003).

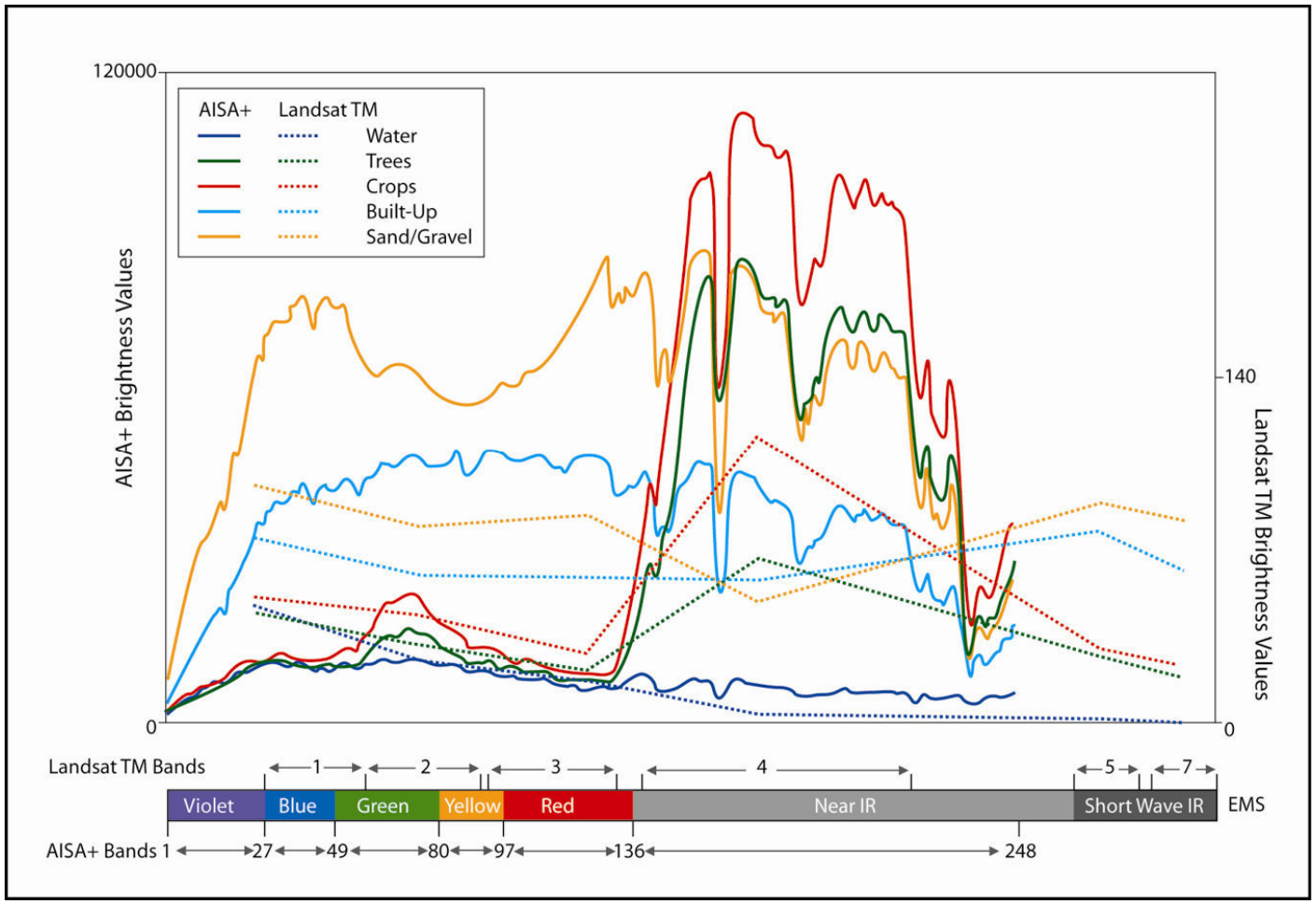

Figure 1. Comparison of multispectral and hyperspectral bands using spectral curves of example features.

Information collected from AISA+ is expected to be useful in understanding terrestrial processes including land use dynamics, urban change, agricultural monitoring, forestry, and transportation. AISA data has been analyzed in many studies involving vegetation related applications. In one of the initial studies using AISA data, a multi-sensor comparative study was conducted for deriving forest inventory. In comparison to other passive systems, estimates resulting from imaging spectrometer data showed very high correlation with field observations (Hyyppä et al. 2000). AISA was exclusively used in a forest inventory study in Finland, where pine and spruce features were extracted using a segmentation approach (Pekkarinen 2002b). In a related study estimating timber volume, image segmentation method was employed to extract information from very high resolution datasets. It was shown that plot level estimates were improved with AISA (Pekkarinen 2002a). In the same year, a Finnish limnology study on water quality using AISA was published, where relatively high information accuracy was achieved on water cloudiness (secchi depth), turbidity, and chlorophyll content (Koponen et al. 2002). Some Israeli research on semi-arid agriculture have also utilized narrow band VNIR capabilities of AISA to assess soil water runoff (Ben-Dor et al. 2004), and effects of using plastics in agriculture on pollution and biodiversity loss (Levin et al. 2007). The sensor was also successfully employed in mapping citrus yields (Ye et al. 2006), and in assessing invasive vegetation (Artigas et al. 2005, Zhou 2007).

In recent studies, AISA+ sensor was flown over the waters of Laguna Madre in south Coastal Texas to conduct preliminary assessment of seagrass distribution and density, and identification of brown tide algal bloom (Mausel et al. 2005). It was also used in mapping coastal mangrove vegetation in an attempt to assess AISA+ data for its capability to distinguish features in coastal environments (Jensen et al. 2007). Jensen et al. (2009) developed urban leaf area index (LAI) models using AISA+ data - a vital indicator of primary productivity - in the city of Terre Haute,

Indiana, and concluded that AISA+ is potentially a good data source for urban LAI measurement. Although AISA+ data are information rich, they pose several challenges in computation and interpretation, for the reasons described previously. Some investigations using AISA+ data have been conducted on impervious surface, soil cover, forests, agricultural areas, aquatic vegetation, and water quality (Artigas et al. 2005, Jensen 2007, Jensen et al. 2009, Koponen et al. 2002, Mausel et al. 2005, Yang et al. 2007a), but very few studies have addressed classification of urban LULC (Fisher et al. 2001, Voss et al. 2008).

2.3 Land Use and Land Cover Classification

There is a need for systematic description of certain observable conditions in the landscape. In this context, *land cover* refers to the physical and biological materials like prairie grass, woody vegetation, lateritic soils and others found on the surface of the land. *Land use* includes the human use of land such as urban commercial areas, roads, and crops. LULC identification, delineation, and classification can be highly subjective. Some agencies have developed specialized exhaustive and hierarchical classification schemes using standardized categories and codes (Wiegand et al. 2002).

Building on an existing land use coding system prescribed in the Standard Land Use Coding Manual (1965), the American Planning Association developed a classification system for urban land use called the Land-Based Classification Standard (LBCS) (Table 1). The LBCS ensures standardized data collection and storage that allows for easy transfer between jurisdictions, agencies, and institutions, especially since most agencies are increasingly relying on GIS data sharing (Jeer 1999).

Table 1

Land-Based Classification Standards (LBCS): Criteria relevant to remote sensor data (Jeer 2006).

Activity: Actual use of land based on its observable characteristics.	Residential Shopping, business, or trade activities Industrial, manufacturing, and waste-related activities Social, institutional, or infrastructure-related activities Travel or movement activities Mass assembly of people Leisure activities Natural resources-related activities No human activity or unclassifiable activity
Function: Economic function or type of enterprise irrespective of type of feature.	Residence or accommodation functions General sales or services Manufacturing and wholesale trade Transportation, communication, information, and utilities Arts, entertainment, and recreation Education, public admin., health care, and other inst. Construction-related businesses Mining and extraction establishments Agriculture, forestry, fishing and hunting
Structural Character: Type of structure or land.	Residential buildings Commercial buildings and other specialized structures Public assembly structures Institutional or community facilities Transportation-related facilities Utility and other non-building structures Specialized military structures Sheds, farm buildings, or agricultural facilities No structure
Site Development Character: Describes "what is on the land" in general physical terms.	Site in natural state Developing site Developed site - crops, grazing, forestry, etc. Developed site - no buildings and no structures Developed site - non-building structures Developed site - with buildings Developed site - with parks Not applicable to this dimension Unclassifiable site development character

Table 2

Abridged urban classification system based on USGS LULC Classification System (Anderson et al. 1976, Jensen 2007).

LEVEL I	LEVEL II	LEVEL III	LEVEL IV
Urban/ Built-up	Residential	Single-family residential	House, house boat, hut, tent Mobile home
		Multiple-family residential	Duplex, Triplex, Apartment complex or condominium, Mobile home (trailer) park
	Commercial and service	Commercial	Automotive, Boat, Department store, Financial and construction, Food and drug, Funeral, Temporary housing, House and garden, Recreation, Utility, Warehousing
		Services	Public buildings and facilities, Medical, Religion
	Transportation, communications, and utilities	Roads and highways	Dirt, Paved, Limited access, Interchange, Parking, Bridge
	Industrial and commercial complexes	Railroad	Track, Marshalling, Terminal, Bridge
		Industrial complex (park) Commercial complex (mall)	
	Mixed urban or built-up		
	Urban or built-up		

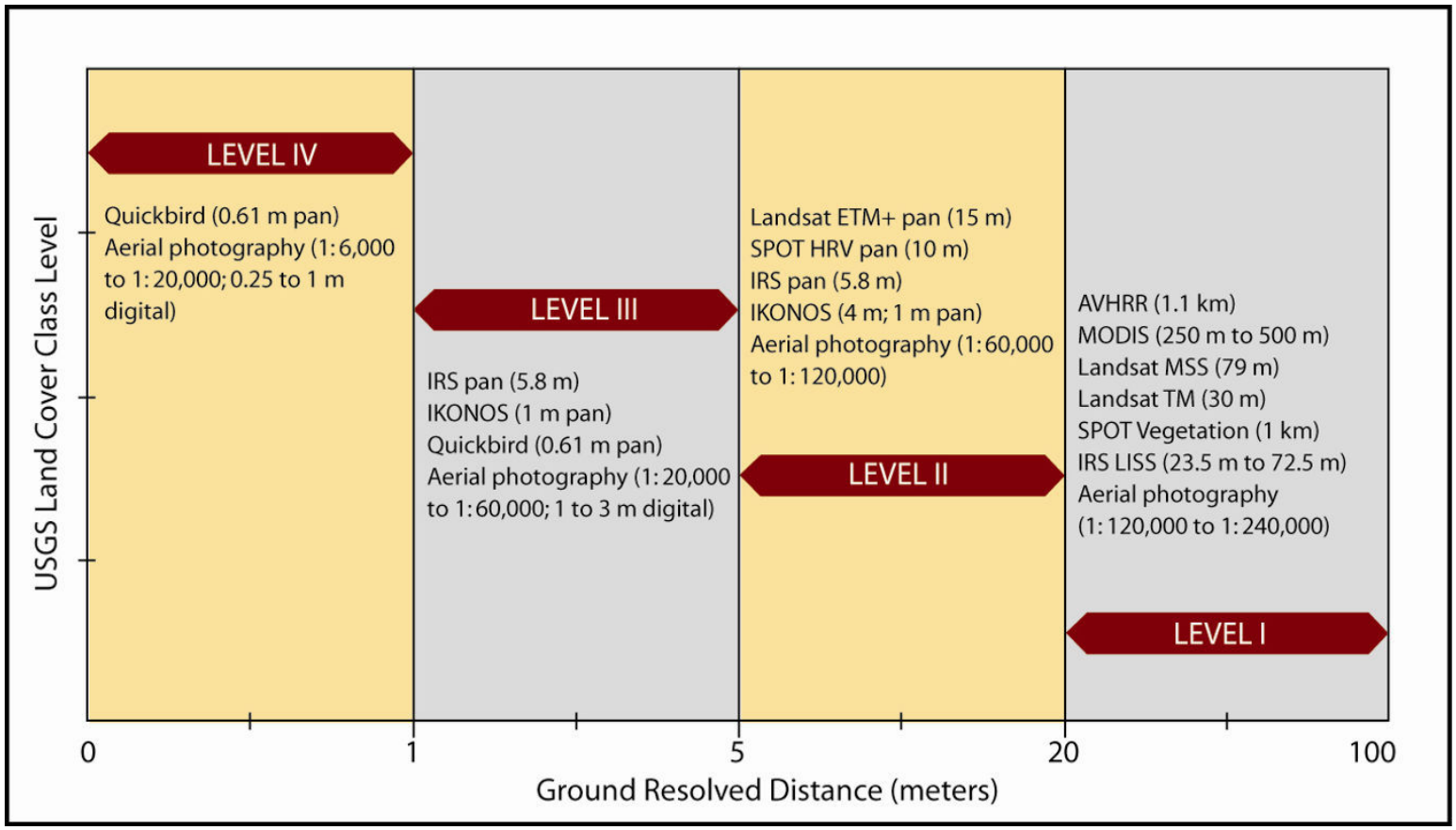

Figure 2. Relationship between USGS LULC classification levels and ground resolution (modified from Jensen 2007).

Anderson et al. (1976), on behalf of the United States Geological Survey (USGS), developed a national LULC classification system for use with remote sensor data. They describe urban or built up land to include residential, commercial and services, industrial, transportation, communications, and utilities, industrial and commercial complexes, mixed urban or built up land, and other urban or built up land. They define ten LULC criteria that must be met for effective orbital or aerial remote sensing: A minimum level of interpretation accuracy of at least 85%, similar accuracy for every class, repeatability of results by different analysts, applicability of classification system over extensive areas, a scheme that permits certain land cover as surrogates for processes, multi-temporal applicability, allowance for effective use of finer scale classes, ability to aggregate classes, ability to compare classes to future land uses, and recognition of multipurpose land uses.

Jensen (2007), has dedicated an entire chapter on remote sensing of urban landscape, where he describes urban classification Levels I - IV. While the original USGS LULC classification was not designed to include detailed urban attributes, several urban studies have used it extensively by fine tuning the classification system with detailed Level III, IV, and V urban classes.

These modified systems are designed to be upwardly compatible with USGS Levels I and II classes. He has consolidated the USGS LULC classification scheme with additional logical extensions. An abridged reproduction of the urban land use classification system can be seen further in this section (Table 2). For urban remote sensing, the general rule is that there needs to be a minimum of four spatial observations (pixels) within an urban object to identify it. At a regional scale, USGS Level I classification is possible with sensors that have more than 100 m spatial resolution. In this case, for example, the difference between built-up land cover and other land covers may be distinguishable. A minimum spatial resolution of 5 - 20 m is required for Level II, and 1 - 5 m is required for detailed Level III, and sub-meter resolution is often best for Level IV

classification (Figure 2). Reference to the standard classification scheme can be found in most remote sensing literature that focus on LULC classification. Discussion on specific urban classification schemes have been addressed by a plethora of remote sensing research (Gatrell et al. 2008, Herold et al. 2002, Herold et al. 2003a, Herold et al. 2004, Irwin et al. 2006, Lo et al. 1990, Lu et al. 2005, Lu et al. 2006, Meinel et al. 1998, Moeller 2005, Zhu et al. 2006).

Geographic information using standardized hard classification schemes often does not precisely represent the ground reality. Thematic information usually transitions from one category to another - such as buffer or transition zone between forest and range land - and therefore needs to be represented using fuzzy definitions. These definitions are typically developed by individual researchers for site-specific studies. Standardized classification is adopted by most researchers because it is based on science and allows for comparison of results from studies conducted by other researchers. However, if needed, individualized fuzzy classification schemes may be developed by modifying existing standardized systems to allow for upward compatibility (Jensen 2005). In high resolution urban remote sensing, the need for such fuzzy definitions is expected to be minor.

2.4 Band Reduction and Digital Image Classification

Data Dimensionality

Hyperspectral data have high dimensionality. In other words, they have numerous spectral bands. With greater dimensionality, image storage and processing systems need to process greater number of pixels that exhaust computing resources (Jensen 2005, Keshava 2001). Hyperspectral data is inherently redundant in spectral information. In other words, if the spectral band width is 2.3 nm, within a given spectral range, earth features may reflect very similarly in several contiguous bands. While the advantage is that subtle variation in radiant flux is recorded in each of these

bands, it is highly likely that the amount of redundant spectral information is significant. Highly correlated bands can be eliminated by statistically deleting unwanted redundant bands or transforming the data to reduce the number of bands without compromising information content. Besides removing noise from the data and improving processing accuracy, band reduction also reduced processing resources and time (Jensen 2005, Landgrebe 2002, Yang et al. 2007a).

Principal Components Analysis (PCA)

PCA has been a frequently used method for band selection in multispectral and hyperspectral remote sensing (Mausel et al. 2005). PCA transforms high dimensional data into equivalent number of dimensions whose first few dimensions contain the most variability (Bajcsy et al. 2004). The workings of PCA can be understood by visualizing a scatterplot of digital numbers (DN) with two spectral bands Band A and Band B represented in the two axes x_1 and x_2 (Figure 3). In this feature space, new axes (y_1 and y_2) are superimposed, with their origin at the mean of the data distribution. Axis y_1 represents the direction of the first principal component, and y_2 represents the direction of second principal component. Simple linear combinations of original data values multiplied by transformation coefficients (eigenvectors) derived from the variance/covariance matrix of the original image data become the principal component image data values. Lillesand et al. (2008) describe the relationship for coordinate system transformation of a data value in the original bands (A and B) to the new axes as $DN_I = a_{11}DN_A + a_{12}DN_B$; $DN_{II} = a_{21}DN_A + a_{22}DN_B$, *where*

DN_I, DN_{II} = digital numbers in new coordinate system

DN_A, DN_B = digital numbers in original coordinate system

a_{11}, a_{12}, a_{21}, a_{22} = coefficients of transformation (eigenvectors derived from variance/covariance matrix for the original image data)

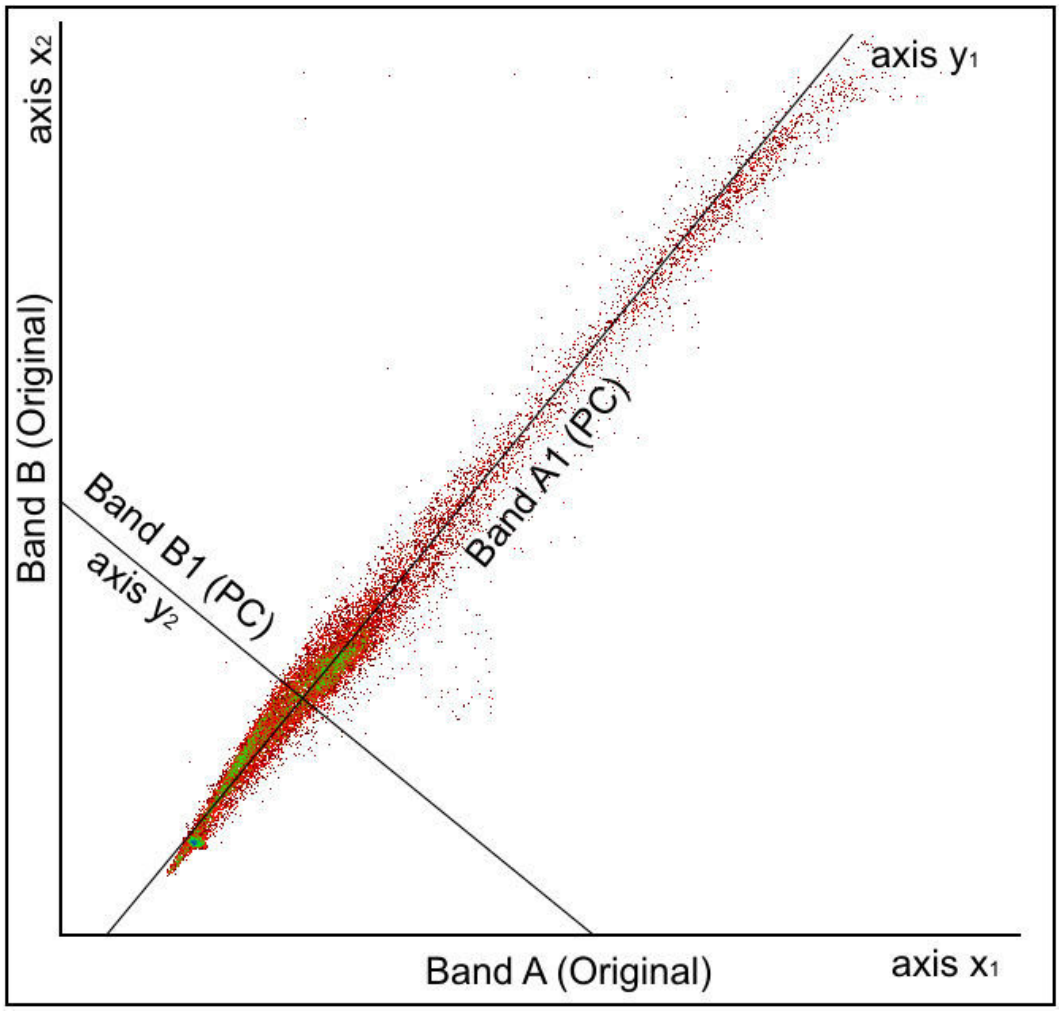

Figure 3. Plot of two correlating visible bands (Band A (*axis* x_1) and Band B (*axis* x_2). The principal components transformation generated a new coordinate system (y_1, y_2).

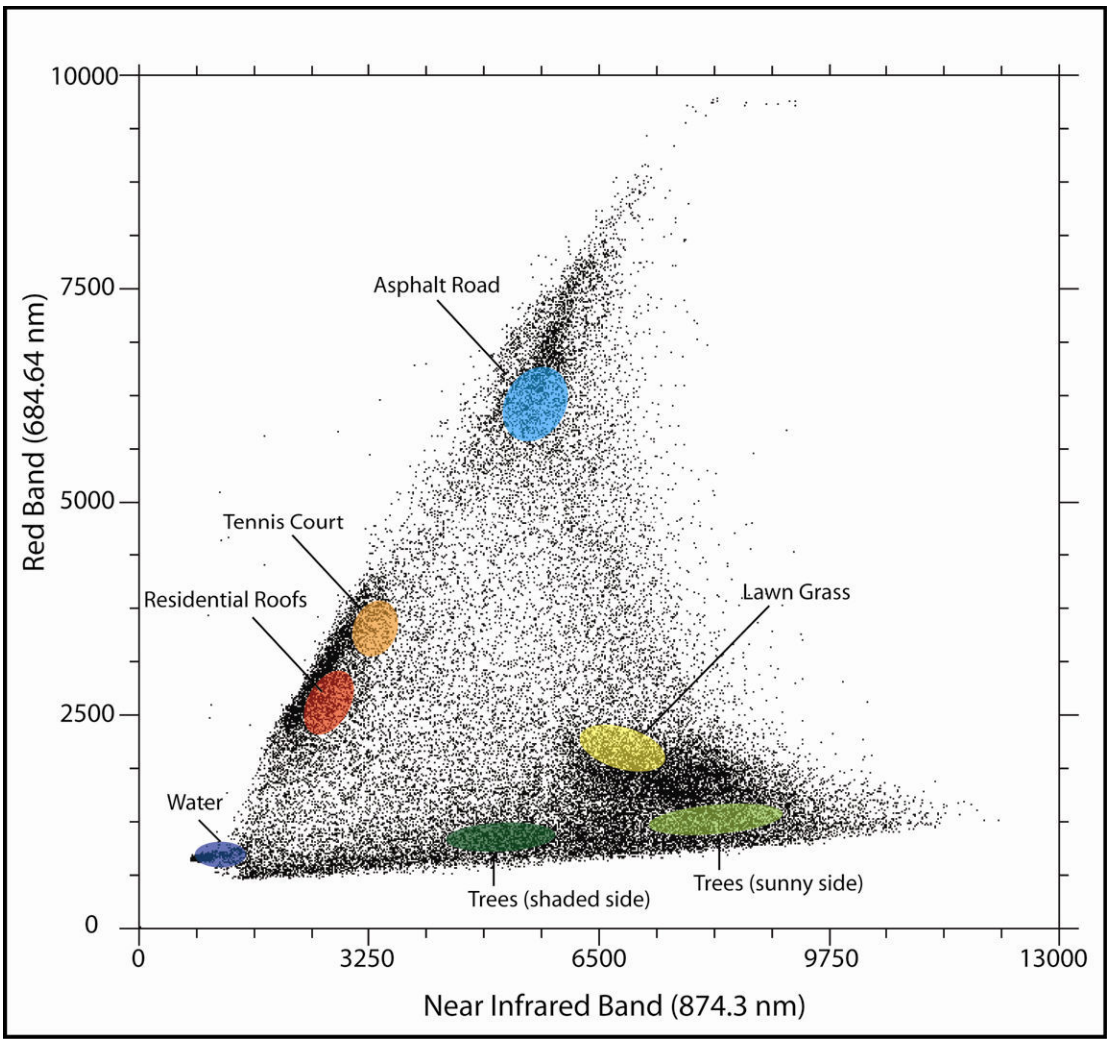

Figure 4. An example of distribution of pixel values in a two dimensional feature space (developed from AISA+ hyperspectral data).

Minimum Noise Fraction (MNF)

In hyperspectral remote sensing, another data reduction method called minimum noise fraction (MNF) transform is employed (Yang et al. 2007a, Yang et al. 2007b), as PCA sometimes is unable optimize for random noise in the data, and fails to capture variability of spectrally non-orthogonal small objects that are often found in hyperspectral data. MNF is a noise-adjusted PCA, which, instead of relying on the variance in data, produces images ordered by image quality based on signal to noise ratio. It is a two step process, called cascaded PCA, where the first transformation decorrelates and rescales noise in the data. Band to band correlation of noise is transformed so it has unit variance, thus 'whitening' it. A standard PCA is then performed to produce MNF data (Ifarraguerri et al. 2000, Jensen et al. 2003a).

Thematic Classification of Remote Sensor Data

In order to understand our environment, spatial scientists label and generalize the numerous variety of objects present in the environment into a manageable number of categories (Tso et al. 2001). For visual interpretation of orthographically represented earth data, certain methods that analyze colors, textures, patterns, shapes, size, and nature of neighboring features are employed to extract information (Jensen 2005). With advancements in digital information technology, earth features were represented in terms of numerical reflectance values. Information analysis advanced from using *image space* (visual) to the utilization of *spectral space* and *feature space*¸ although all three are indispensable. In spectral space (Figure 1), "spectral signature" of a feature is matched with known signatures for its identification and classification. Common to most computer classifiers, interpreting the feature space (Figure 4) involves N-dimensional analysis of vectors generated from plotting reflectance values of pixels in different spectral bands in multidimensional

space (Dias 2001, Landgrebe 1998). Numerical analysis of reflectance measurements can yield information that may not be possible by visual interpretation. However, it is important to note that numerical image classification still requires human analysts to understand the qualitative nature of underlying geographic area. Based on the purpose of research, detail of information required, and image data attributes, an analyst needs to formulate a classification scheme (Anderson et al. 1976). Sometimes when there is little qualitative information available, blind computer based statistical clustering is also performed, which is a vital tool in extracting thematic information from raw data (Shah et al. 2004). Typically, an analyst 'trains' an algorithm by providing it with a sample dataset for each pre-defined class (Foody et al. 2006). This approach is called supervised classification, as it requires an analyst's input based on his or her prior knowledge of the objects in the study area, and the spatial and spectral characteristics of those objects (Lu et al. 2007a, Lu et al. 2007b).

Supervised classification methods require an analyst to define and identify underlying land cover classes before selecting reference samples from a digital image. These reference samples, whose spectral signatures are indicative of each predefined class, are used to train a classification algorithm. Each algorithm uses a different approach to develop training samples to classify image data into a thematic map. The thematic map is evaluated for accuracy, and if the classification accuracy is unacceptable, the process may be repeated using new or additional training samples (Jensen 2005, Lu et al. 2007a).

Maximum Likelihood Classification (MLC)

MLC uses a probability based decision rule to classify a spatial dataset. It calculates the probability of every pixel to belong to each of an analyst defined classes. The pixel is then assigned to the class for which the probability is the highest.

The classifier assumes that the statistics for the training sample for each class is normally distributed (Gaussian). This assumption is generally reasonable for most common spectral response distributions, allowing for computing statistical probability of any given pixel belonging to a particular land cover class. To obtain probability information, the classifier uses statistics of a Gaussian probability density function model for each class. Unidentified pixels are classified by computing their probability of being members of each category (Lillesand et al. 2008).

Extraction and Classification of Homogeneous Objects (ECHO)

ECHO is a spatial-spectral classifier that is sensitive to texture or patterning of pixel groupings. It is a two stage process whereby pixels in the image data are first segmented into classes of statistically significant relatively homogeneous cells. Then maximum likelihood classification is applied on these pixel groupings rather than individual pixels. Segmentation is carried out in two stages. First the pixels are divided by a rectangular grid in to a small group of n x n 'cells' if they are homogeneous. Test for homogeneity is conducted by a distance to the center of the average value of the group. Any pixel that does not fall within a user designated percentage, say 98% of the Gaussian density function of an n x n group is cast as a 'singular cell'. In the second stage, an individual cell is compared to a contiguous 'field'. A field is a group of one or more cells that have already been merged. If two contiguous samples are statistically similar, the adjacent field is 'annexed' to form a new field (Kettig et al. 1976, Lu et al. 2004a, Lu et al. 2007a). Li et al. (1994) note that ECHO outperformed MLC by about 5 percent in agricultural areas, but consistently did better than per-pixel classifiers by almost 20% in tropical forest areas. Dell'Acqua et al. (2004) used ECHO in a comparative study of classifiers applied to DAIS hyperspectral data for urban features. They found ECHO to perform the best for overall accuracies.

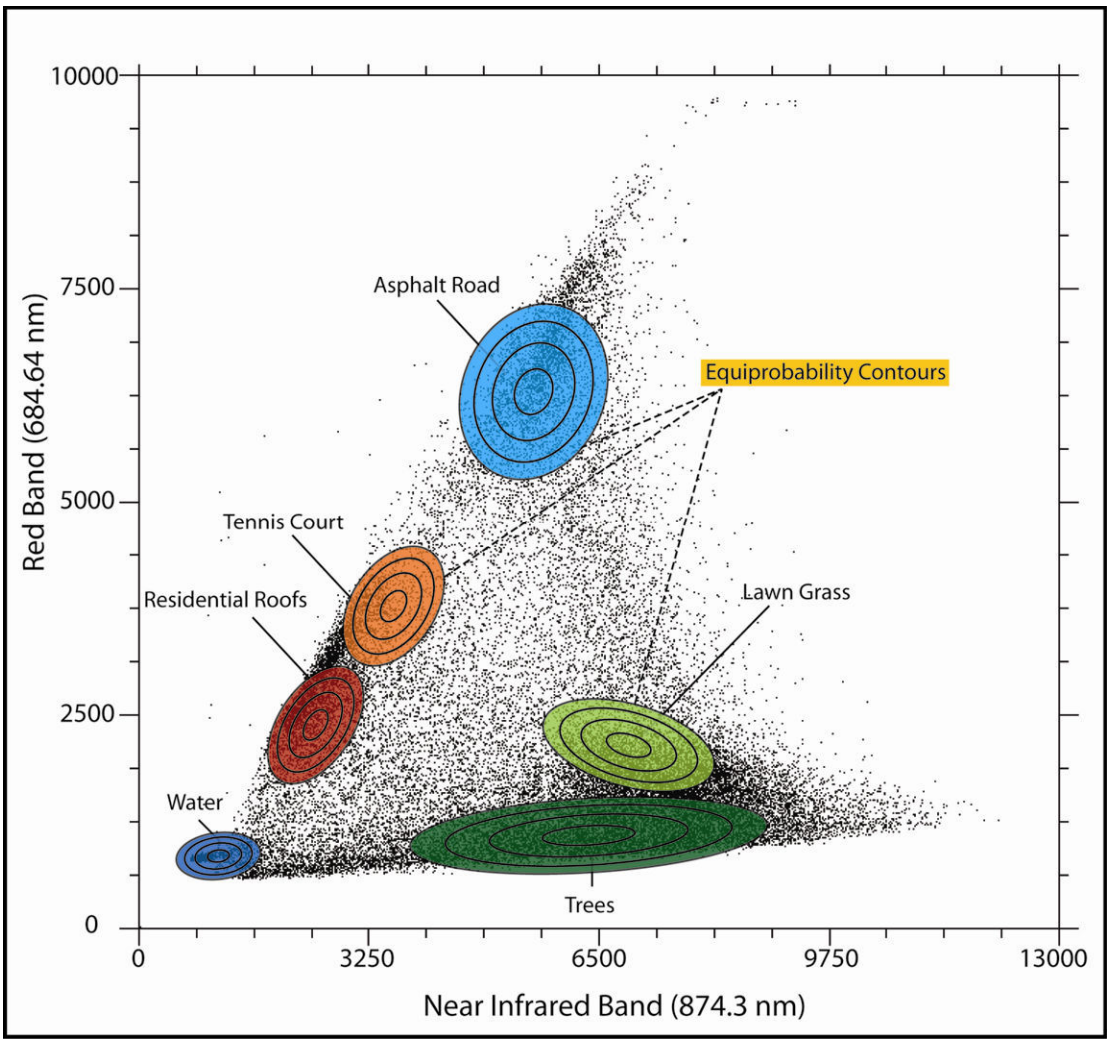

Figure 5. Equiprobability contours defined for urban features by maximum likelihood classifier (MLC) in a two band feature space (modified from Lillesand et al. 2008).

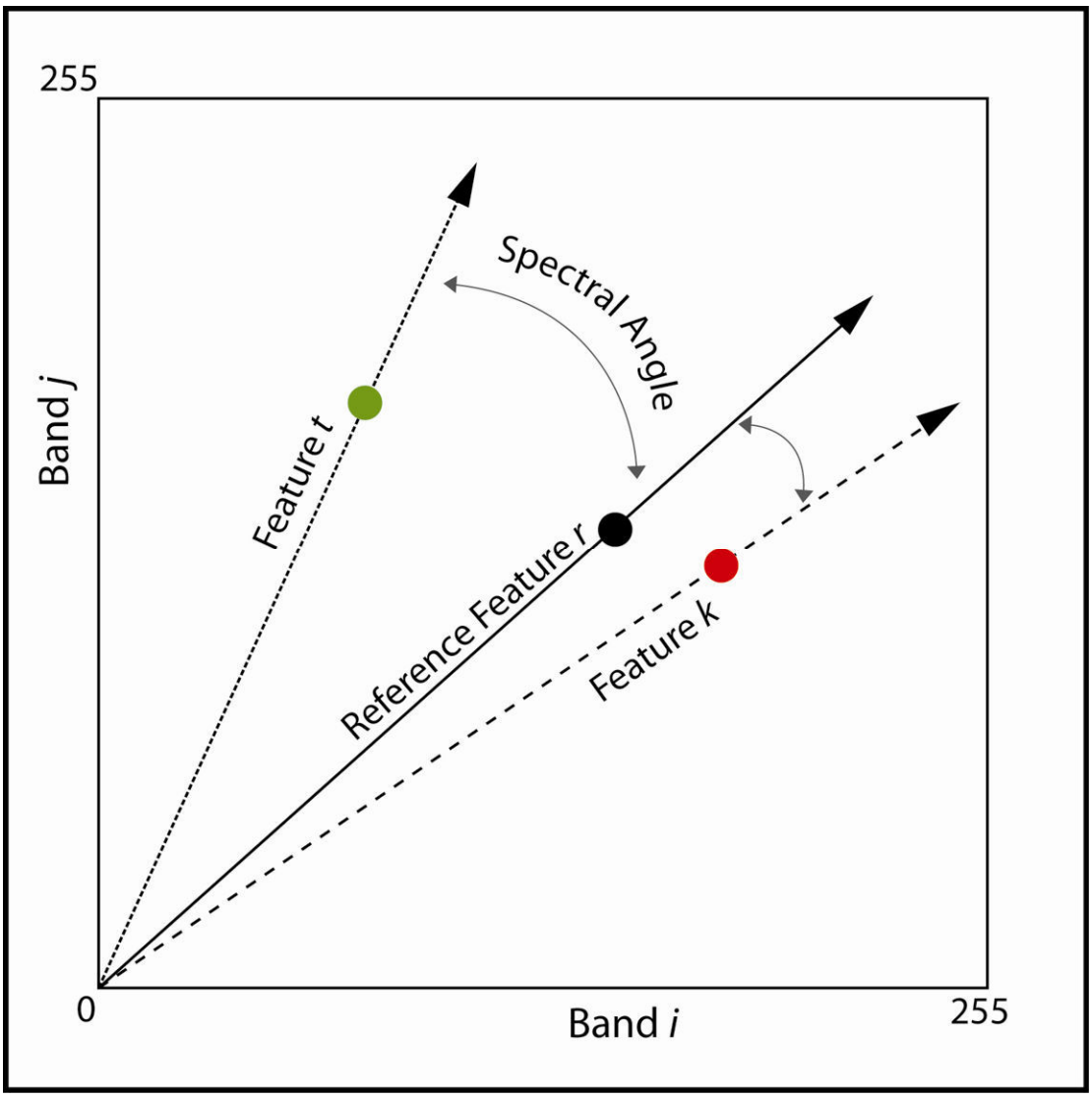

Figure 6. Two-band representation of classification approach used by SAM. Angle between reference *r* and feature *k* is smaller than feature *t* (modified from Jensen 2005, Shippert 2003).

Spectral Angle Mapper (SAM)

SAM is a spectral classifier that computes the similarity of an unknown spectrum to a reference spectrum or endmember spectrum. The similarity between pixel and endmember spectra is compared by calculating the angle between them. They are treated as vectors in space with dimensionality equal to the number of bands. The smaller between the unidentified pixel and the endmember pixel, the angle the closer the match found between them (Kruse et al. 1993). In a scatter plot of pixel values from band *i* and band *j*, vectors drawn from the origin through each feature will reveal angles between the endmember vector *r*, and image pixel vector *t* (Figure 6).

In addition to supervised classification techniques, information from remotely sensed data can also be extracted by automated grouping of pixels based on their spectral properties in feature space. This process requires no training input from an analyst, but requires posteriori class assignment for the clusters derived by the computer (Lu et al. 2007a, Sabins 1997).

Iterative Self Organizing Data Analysis Technique (ISODATA)

A commonly used clustering method is called ISODATA. Composed of a heuristic set of rules, this algorithm allows change in the number of clusters by merging, splitting, and deleting clusters as it moves from iteration to iteration. An analyst inputs the maximum number of clusters required, percentage threshold for unchanged pixels between iterations, and the maximum number of iterations for classifying pixels. Initially, the cluster centers determined by a single pass are used as cluster centers for ISODATA clustering. The algorithm then associates each pixel with cluster center with the smallest Euclidean distance. When one of the criteria input by an analyst is met, the iterations stop, and a cluster map is generated (Biehl et al. 2002, Landgrebe 2002, Landgrebe et al.

2001, Lillesand et al. 2008). Based on ancillary information and analyst's knowledge, these clusters may be merged post-classification to develop a final thematic map of the selected classes.

2.5 Accuracy Assessment

Thematic maps derived from remotely sensed data using different classification schemes and analysis methods represent the environment only to a certain degree of truth. This reality is magnified in complex urban environments. The usefulness of thematic maps is also limited by classification accuracy. Therefore, conducting and reporting accuracy assessment is standard practice in the remote sensing community (Foody 2002).

When human assisted computer classification is performed, an analyst provides the computer with known samples of predetermined classes, called training samples. These samples are usually randomly collected *in situ* using global position system (GPS) receiver to mark coordinates and note the LULC type. A field spectrometer is often used to collect field spectra for training purposes. DOQs, high resolution vertical and oblique aerial images can also be used as ancillary ground reference information sources. These samples can be used to match the corresponding pixels on the image data. The computer then compares the training samples with unknown areas in image space and produces a thematic map bearing the predetermined classes. Accuracy of the results depends on the ability of the classification algorithm to identify classes based on samples, the statistical closeness or difference between features in the image and number of available training samples. Accuracy is defined by deFries and Cheung-Wai Chan (2000) as the measure of percentage of pixels correctly classified. In other words it is the degree of correctness of a thematic map derived from classification (Foody 2002). Ground reference samples are used as test samples to calculate overall and per class percentage values to measure classification accuracy (Lu

et al. 2004b). A common method for classification accuracy assessment is through the use of an error matrix. Error matrix compares the relationship between the known reference data and corresponding classification results on a class by class basis. Classification performance can be assessed as error of omission (exclusion of an original land cover from its thematic class) and error of commission (inclusion of a land cover in a wrong class). It should be noted that since the accuracy is only measured from a set of test samples, however random their distribution, a percentage of correctness may occur simply by chance. KAPPA analysis is performed to derive KHAT statistic that measures the difference between the actual match and chance match between the reference samples and thematic classes (Lillesand et al. 2008, Congalton 1991). Yang et al. (2007b) provide a good example of accuracy assessment used in comparing different classification methods. The $\hat{k}$ (KHAT) is based on agreement between the results and ground reference is defined as:

$$\hat{k} = \frac{Observed - Chance}{1 - Chance}$$

KHAT ranges between 0 and 1. As KHAT approaches 1, it indicates higher confidence in the accuracy assessment.

CHAPTER 3

STUDY AREA AND DATA CHARACTERISTICS

3.1 Study Area

Terre Haute (39°27'N and 87°25' W) is located in Vigo County in west central Indiana. The 100 m wide Wabash River flows southward on the western edge of the city (Figure 7). The city population estimated in 2005-2007 was 57,585. The American Community Survey (ACS) estimate shows 26,552 housing units in the 80.9 square kilometer city with a median household income of $29,297 and median housing value of $73,300 (U.S.Census-Bureau 2009). Terre Haute lies in the glaciated Wabash lowlands ecoregion, mantled by pre-Wisconsinian loamy to sandy till or windblown silt and sand. The original vegetation is beech and oak-hickory forest interspersed by prairies. Currently, the generally fertile soils primarily support corn, soybean, wheat, and vegetable farming. In the surround regions, scattered deciduous woodlands and coals mines occur as well (Woods et al. 1998). The city displays a fairly flat topography both in the East-West and North-South directions. Its nearest neighboring large urban areas being St. Louis at about a road distance of 295 km to the southwest and Indianapolis at 124 km to the northeast .

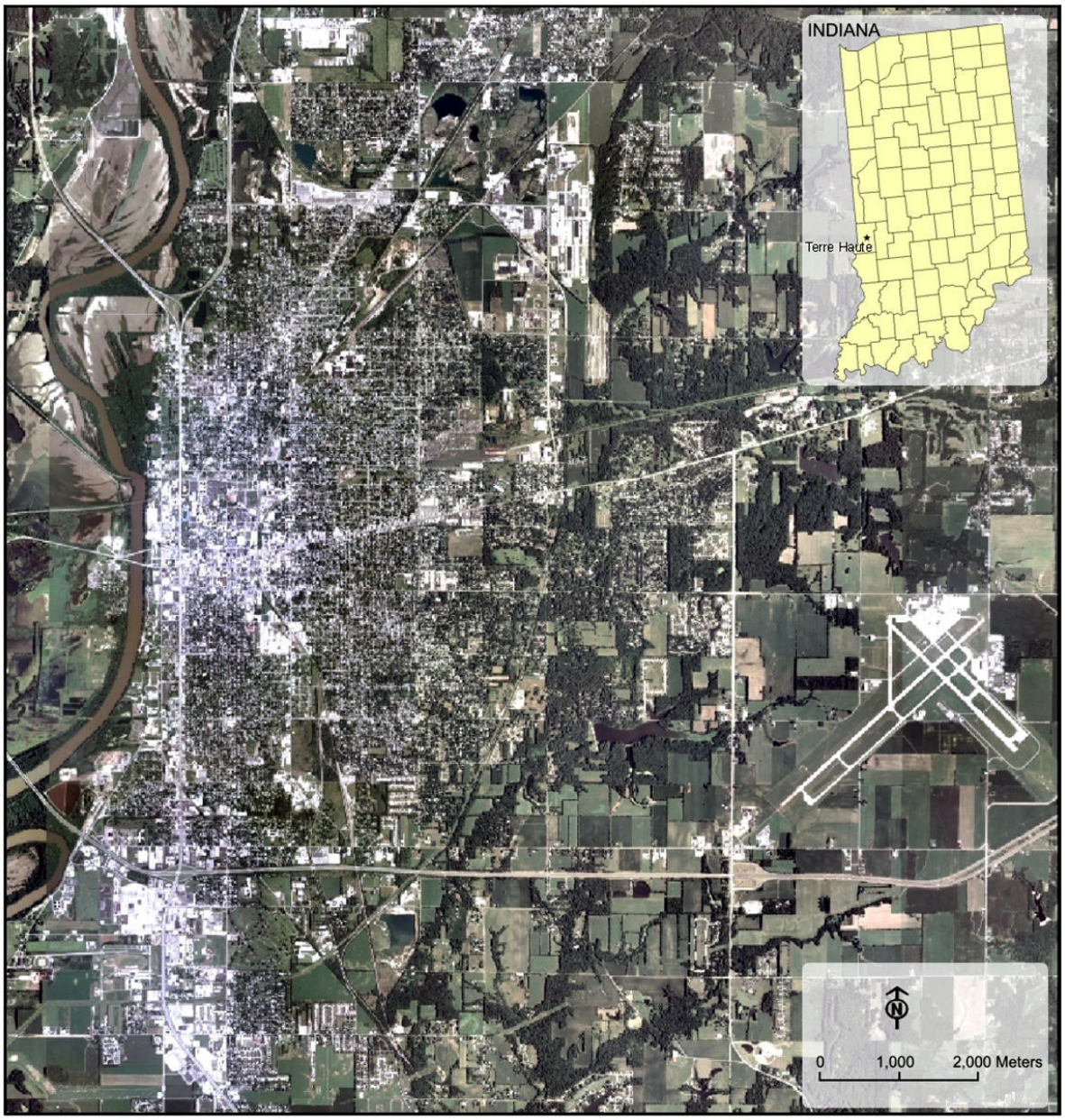

Figure 7. True color digital orthoquad (DOQ)[1] mosaic of Terre Haute, Indiana.

[1] Source: Indiana Spatial Data Portal. *http://www.indiana.edu/~gisdata/*

The specific areas selected for this study were six 163,216 m^2 area subsets. Subset categories include: commercial areas largely composed of parking lots, roads, large roofs (different shades of color), some grass and a few tree crowns (Figure 10 and Figure 11); residential areas composed of mixed trees, grass, multi colored rooftops, driveways, and water features (Figures 12 and 13); and recreational areas composed of some gravel and asphalt paths, parking areas, grass, water features, and continuous mixed woodlands with evergreen and deciduous trees (Figure 14 and Figure 15).

3.2 Data Characteristics

In Situ and Ancillary Data

Field samples were collected in July 2008 as part of a larger field campaign for urban leaf area index studies. Global positioning system (GPS) units were used to record location information and urban object and material characteristics. A total of 300 samples were collected throughout the city, out of which 15 - 25 samples fell within in each study area subset selected for this research. A large portion of additional sampling was conducted using 1 foot resolution DOQs. The Bird's eye feature in Microsoft's Bing Maps™ was extensively used to identify roof tops and other features inaccessible in the field. The street view feature in Google Maps™ was used for verifying ground features such as asphalt, concrete, and gravel (Figure 8).

AISA+ Hyperspectral Data

Data acquired using AISA+ hyperspectral sensor was used in this urban LULC research. The data was acquired by AISA+ sensor, collected over Terre Haute on 24 July 2006. The aircraft carrying the sensor was flown at a height of 1524 m at 200 km/hr groundspeed. Sensor pixel resolution was set to 2.1 m, and swath width per flight line was 1102 m (Jensen et al. 2009). Data

subsets were isolated from the flight lines (Figure 9), based on the characteristic of their qualitative composition, and geometric integrity. These subsets included commercial, residential and recreational areas, each composed of visually distinct proportions of features such as building rooftops, asphalt, concrete, gravel, soil, water, grass, and woody vegetation.

Table 3

AISA+ Bands and their corresponding wavelengths in the electromagnetic spectrum.

Bands	Wavelength (nm)	EM Spectrum
1 - 27	391.99 - 449.02	Violet + Indigo
28 - 49	451.26 - 498.30	Blue
50 - 80	500.61 - 568.50	Green
81 - 89	570.81 - 589.34	Yellow
90 - 97	591.67 - 607.94	Orange
98 - 136	610.26 - 698.62	Red
137 - 248	700.98 - 964.69	Near Infrared

AISA+ sensor data can be calibrated to record varying portions of the spectrum. At full spectral mode, it is capable of collecting 248 continuous spectral bands between 400 - 970 nm, with each band measuring a width of 2.3 nm. The data collected for this study was at full spectral mode, radiometrically corrected to at-sensor radiance using Specim's Caligeo software (SPECIM 2003, Jensen et al. 2009). The radiometric resolution of image data is 16 bits, allowing for recording 65,535 levels of brightness. Jensen et al. (2008) performed geometric correction using reference line correction method to remove error induced by aircraft roll. This corrected dataset was directly used during further enhancements and classification procedures. Due to a previously undetected fault on AISA+ sensor's GPS/INS correction system, several minor geometric anomalies exist in the data that remain uncorrected. In this research, since training samples are selected by visual inspection, these geometric errors did not affect the accuracy results. Since the scope of this research was to measure and compare feature accuracies, and not thematic mapping, these errors were tolerated.

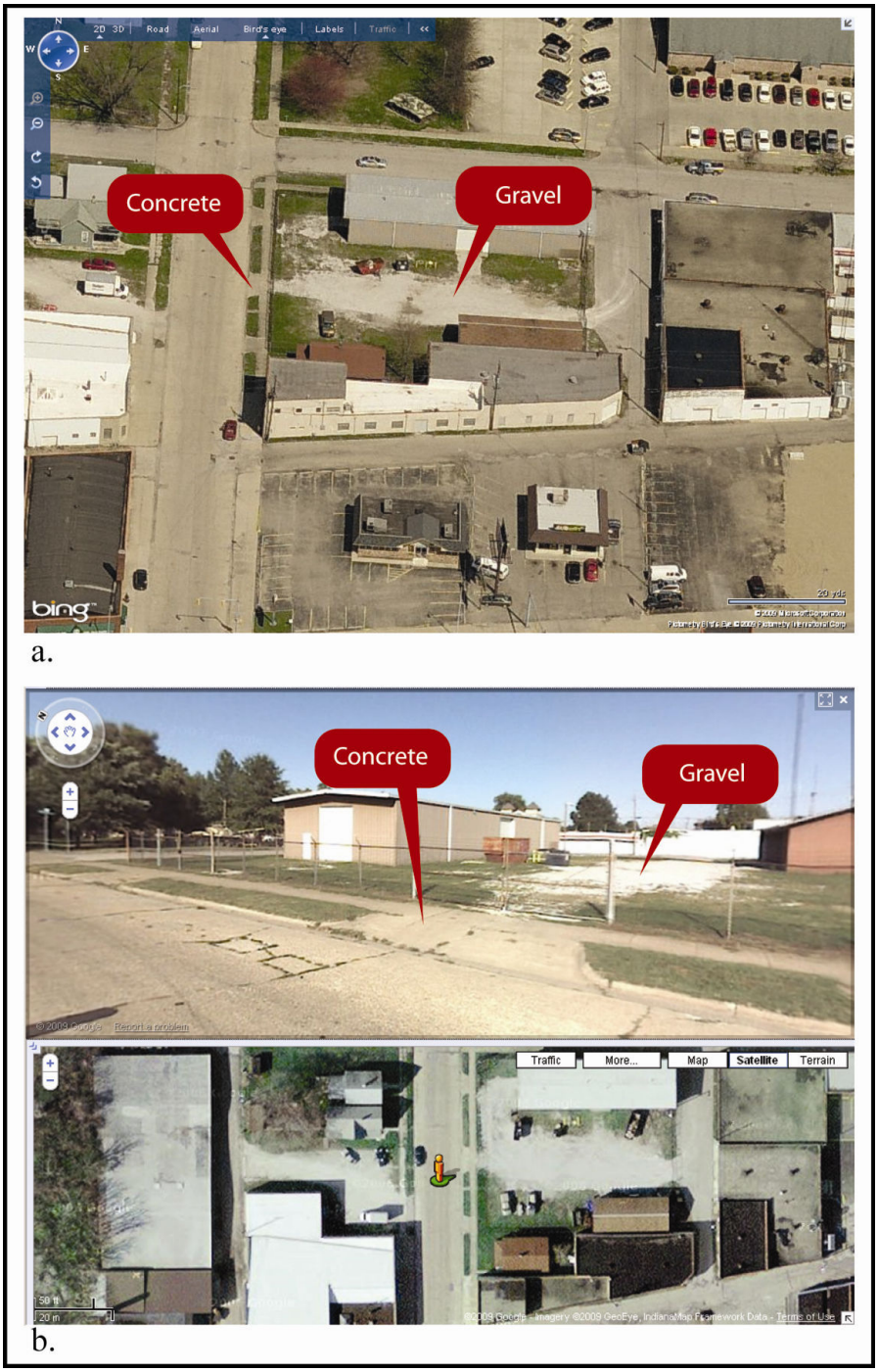

Figure 8. An example of validating sample feature from a location using a. Bing Maps™ Bird's Eye; b. Google Maps™ Street View.

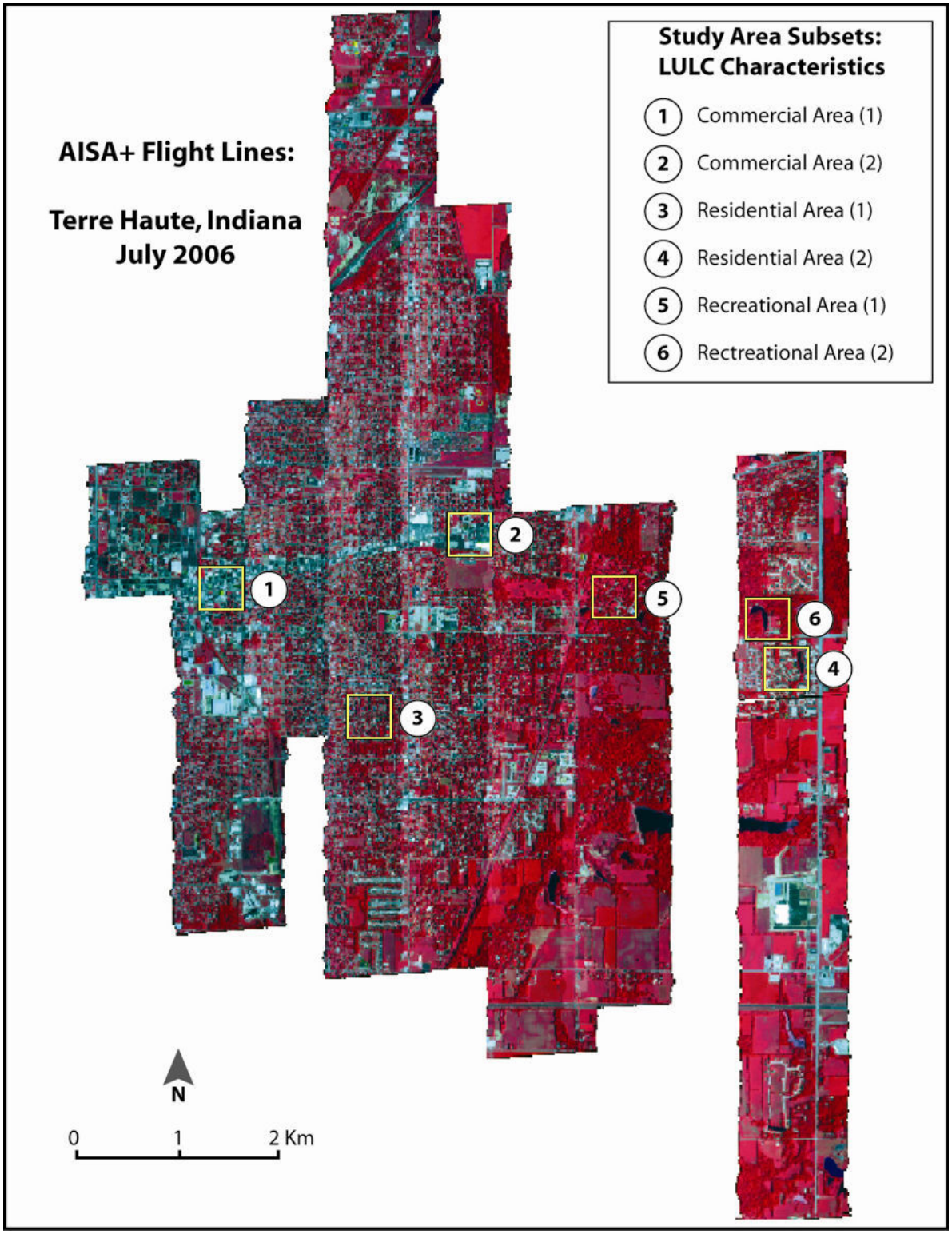

Figure 9. Study area subsets from AISA+ flight lines, July 2006.

Figure 10. Subset of a commercial area (1) (See 1 in Figure 9): a. AISA+ composite of (RGB 187, 125, 63)[2]; b. DOQ; c. High resolution oblique aerial view of a part of subset[3].

[2] NIR (819.65 nm), Red (673.02 nm), and Green (529.77 nm)
[3] Source: *http://www.bing.com/maps/*

Figure 11. Subset of a commercial area (2) (See 2 in Figure 9): a. AISA+ composite of (RGB 187, 125, 63); b. DOQ; c. High resolution oblique aerial view of a part of subset.

Figure 12. Subset of a residential area (1) with a spatially dense composition (See 3 in Figure 9): a. AISA+ composite of (RGB 187, 125, 63); b. DOQ; c. High resolution oblique aerial view of a part of subset.

Figure 13. Subset of a residential area (2) with spatially less dense composition (See 4 in Figure 9): a. AISA+ composite of (RGB 187, 125, 63); b. DOQ; c. High resolution oblique aerial view of a part of subset.

Figure 14. Subset of a recreational area (1) (See 5 in Figure 9): a. AISA+ composite of (RGB 187, 125, 63); b. DOQ; c. High resolution oblique aerial view of a part of subset.

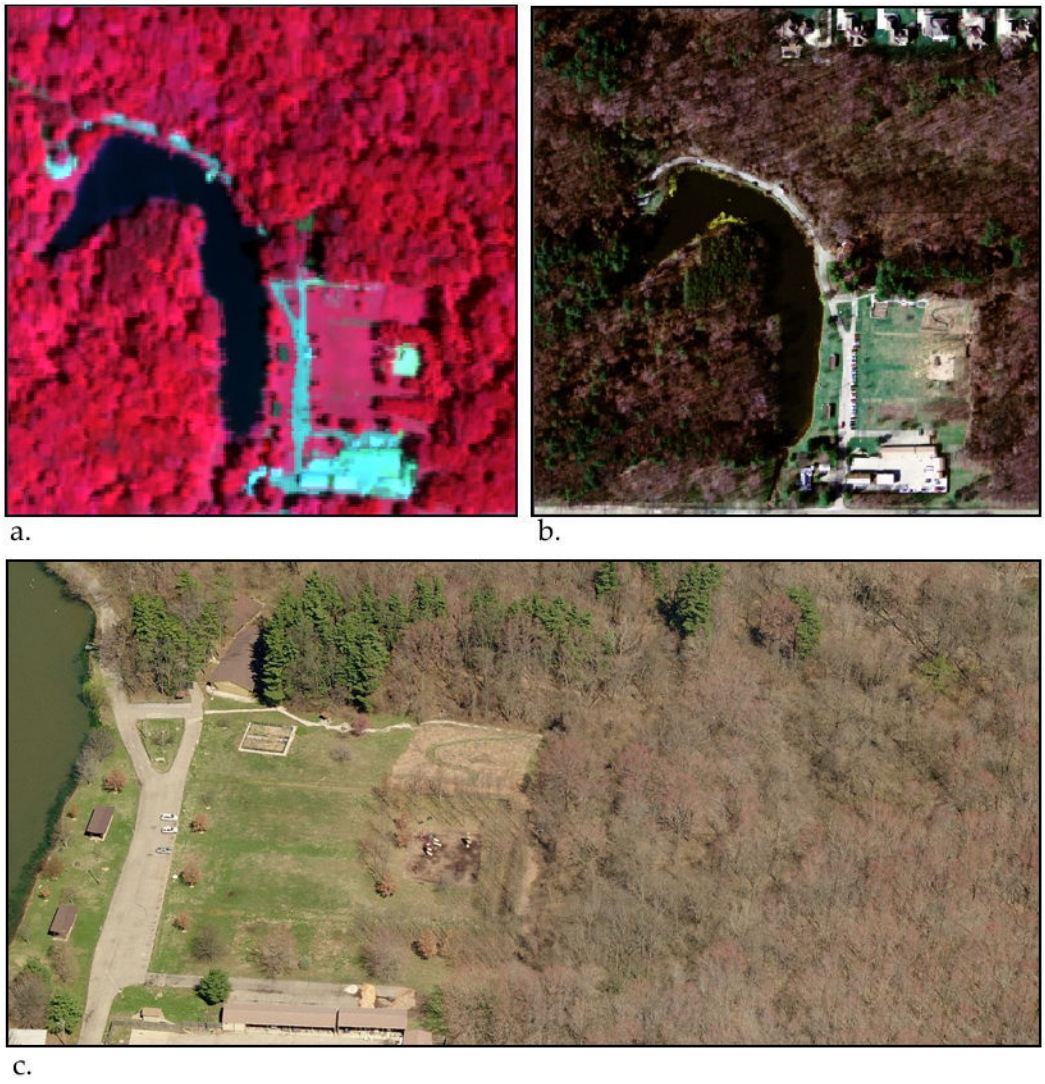

Figure 15. Subset of a recreational area (2) (See 6 in Figure 9): a. AISA+ composite of (RGB 187, 125, 63); b. DOQ; c. High resolution oblique aerial view of a part of subset.

CHAPTER 4

METHODOLOGY

4.1 Field Sampling and Ancillary Information

Six 0.16 km^2 (202 x 202 pixels x 248 bands) subsets were selected from the hyperspectral data flight lines acquired in 2006 using AISA+ sensor. The six areas included two subsets representing commercial areas, two subsets with residential areas, and two subsets representing recreational areas (parks). Study areas were selected from separate flight lines and areas of overlap were avoided to ensure spectral integrity within the subsets.

Field samples of ground features were recorded using GPS locations and associated feature description. Major urban features identified were water features, tree canopy, grass, asphalt, gravel, and concrete. A total of 15 to 20 samples per 0.16 km^2 study area subset were complied. Additionally, DOQs and oblique aerial photographs were used to compile training samples. Urban features identified using ancillary information included different colored rooftops including white, black, brown, beige, gray, and red. The color differences were emphasized because the reflectance characteristics of these rooftops were found to be distinct, especially in the visible regions of the spectrum. Inaccessible ground features within property boundaries such as swimming pools, gravel, and grass were also identified.

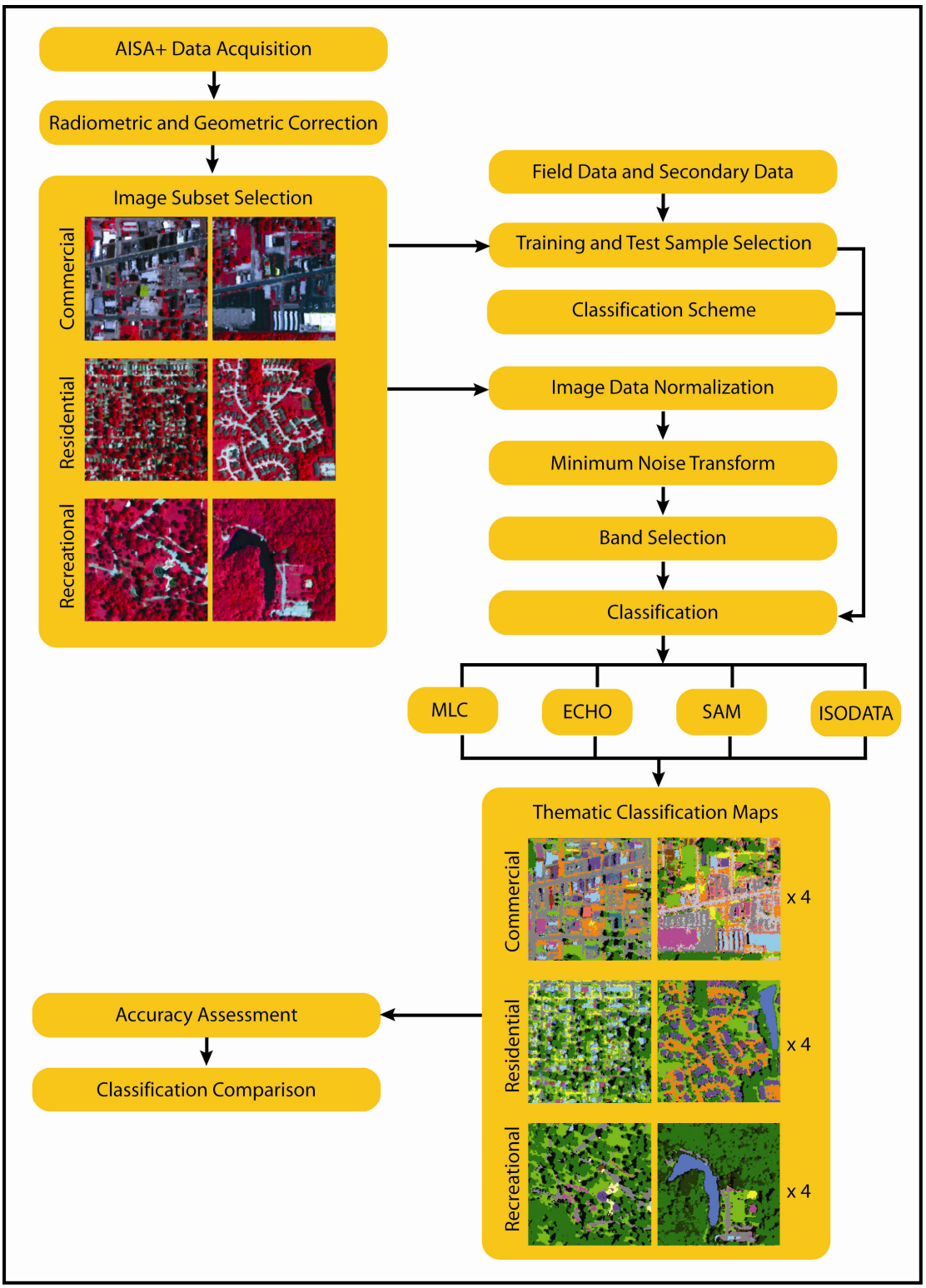

Figure 16. Research methodology.

In one of the study areas, recreational (2), due to its continuous occurrence, it was possible to distinguish between deciduous and evergreen tree canopies, both spectrally and by visual inspection of fall season DOQs and oblique photographs. Visual inspection of spectral signatures was used to distinguish between broader categories such as trees, grass, built-up features, and water features.

4.2 Land Use and Land Cover Classification Scheme

To ensure reconciliation with classification standards, a modified LULC classification schema was developed similar to Anderson's classification system (Anderson et al. 1976, Jensen 2007) using extensions specific to the study areas selected in this research (Table 4). Level III classes are especially modified to reflect the features identified and classified from the two meter hyperspectral data.

Built up Class

As mentioned previously, since it was not possible to ascertain roof material composition or texture, the classification scheme for this feature was based on visible color properties. It is likely that *black roof* areas were composed of asphalt shingles or tar. The two categories of *white roofs* A and B were possibly metallic and concrete respectively, but there was no ground truth evidence to support the assumption. The lightness and darkness in the two categories of *asphalt* may be either due to age, use, or composition - visual inspection of oblique images showed lighter tones belonging to heavily used transportation features, and darker toned asphalt occurring primarily in parking areas or drive through passages. The *concrete* category included concrete sidewalks, cemented platforms, and parking areas. In at least one study site, roads and driveways were completely composed of concrete material.

Table 4

Modified LULC classification scheme used in the six study areas (Anderson et al. 1976).

LEVEL I	LEVEL II	LEVEL III
Built up	Building/roofs	Red roof Brown roof White roof A White roof B Black roof Gray roof Beige roof
	Transportation areas	Dark asphalt Light asphalt Concrete
	Other Built up covers	Red pavement Gravel Tennis court Rubberized play area
Vegetation	Green natural/quasi-natural vegetation	Evergreen canopy Deciduous canopy Prairie vegetation Grassland
	Green urban vegetation	Trees and shrubs Urban grassland
Non-urban or non-vegetated bare surfaces	Bare Soil	
Water bodies	Natural/quasi-natural water bodies	
	Swimming pools	
Shadows		

Vegetation Class

In Level III vegetation class, *deciduous canopy* and *evergreen canopy* were separately classified. However, these two classes were distinctly discernible only in one of the study areas. Urban areas in which evergreen vegetation feature did not occur continuously, was classified into the *trees and shrubs* class. A land cover called *prairie vegetation*, a managed patch with a walking passage

maintained by Deming Park was identified. Although spectrally similar, two grassland types were distinguished in the classification scheme. The rationale was to differentiate lawn grass in residential and commercial areas from grasslands in the recreational areas. While this is acceptable in this study because of the independent treatment of each study area, in a continuous classification of the entire urban area, these distinctions may have to be redefined.

Non-Urban or Non-Vegetated Bare Surfaces, and Water Class

A few features in Level II *bare soil* category were identified in recreational (1), and commercial (1), study areas although their spatial extents were small. Residential area (1) contained several swimming pools. Residential (2) and recreational (2), contained continuous water features.

4.3 Data Processing

Spectral Normalization and Data Reduction

Each study area subset was acquired from a different flightline, and data analysis was conducted independently. Although the variation in overall brightness of each flightline was not expected to affect the results, the image data were normalized to minimize albedo variations and topographic effects in the spectrum (Figure 17). Pixel albedo, especially in airborne sensors, is affected by sensor look angle and local topographic effects. A normalization algorithm was applied using ERDAS Imagine (ERDAS 1999) software to minimize the differences in average luminance across scenes by shifting each pixel spectrum to the same overall average brightness (Zamudio et al. 1990).

Forward minimum noise transformation (MNF) (Green et al. 1988) was applied on the normalized dataset using ENVI image processing software. In this cascaded principal components

procedure, the transformation decorrelates and rescales the noise in the data based on an estimated noise covariance matrix. Eigenvalues that result from the transformation indicate the information and noise content of the data. The assumption is that each pixel contains both signal and noise, but adjacent pixels contain the same signal but different noise. It performs a "shift difference" on the data by differencing adjacent pixels to the right and above each pixel and averaging the results to obtain the noise value to assign to the pixel being processed (ENVI 2009). The inherent dimensionality of the data was determined by examination of eigenvalues and the associated images. As the size of the covariance matrix for hyperspectral data is large (248 x 248 matrix), the software allows for selecting the bands with the highest variation during the MNF analysis (Figure 18). A 25 x 25 band portion of the covariance matrix generated from MNF transform of commercial area (1) has been shown in Table 32 (Appendix B).

The bands with large eigenvalues show image coherence. Bands with near-unit eigenvalues show noise dominated images. The degree to which noise was separated from data containing useful information was determined by examining the eigenvalues and through visual inspection of image coherence. The noise bands were eliminated, and in each study subset, 20 to 30 bands were selected for further consideration (Table 33). Although the first 20 principal components (Figures 19 to 24) in none of the study subsets reached unit variance, deterioration of coherence was evident from the images and the associated eigenvalue graph. The position on the eigenvalue graph where the break in the slope occurs is indicative of deterioration of image coherence from that point forward. From the MNF principal components that were initially developed, further reduction of bands was conducted during classification stage, based on maximum variance or spatial coherence of image data. The eigenvalues of the top 25 bands from each study subset is listed in Appendix C.

Sampling

Training sample selection was done using MultiSpec© software (Biehl et al. 2002). Using the field data, ancillary information from DOQs and oblique photographs (see Figure 8), and visual inspection of spectral signatures (Figure 25), training samples were developed for each study subset independently (Table 5).

Table 5

The number of pixels used in training LULC classes across the study subsets is shown.

Classes/ Study Area	Com-1	Com-2	Res-1	Res-2	Rec-1	Rec-2
Tree canopy	196	80	287	242	1285	x
Deciduous canopy	x	x	x	x	x	632
Evergreen canopy	x	x	x	x	x	180
Grass	202	71	87	232	497	331
Prairie vegetation	x	x	x	x	x	51
Open soil	22	x	x	x	49	42
Shadow	67	25	83	40	146	35
Water features	x	x	16	154	x	224
Asphalt	373	250	118	x	208	122
Concrete	182	111	x	144	47	x
Gravel	50	50	28	x	19	x
Red roof/Red pavement	97	60	x	x	x	x
Brown roof	91	57	45	44	25	19
White roof	275	117	58	x	30	x
Black roof	117	26	x	x	x	x
Gray roof	92	x	x	x	245	x
Beige roof	x	x	40	42	42	x
Tennis court	x	x	x	72	x	x
Play area (rubberized material)	x	x	x	x	46	x
Total pixels	1764	847	762	970	2639	1636

Note: Com - Commercial; Res - Residential; Rec - Recreational

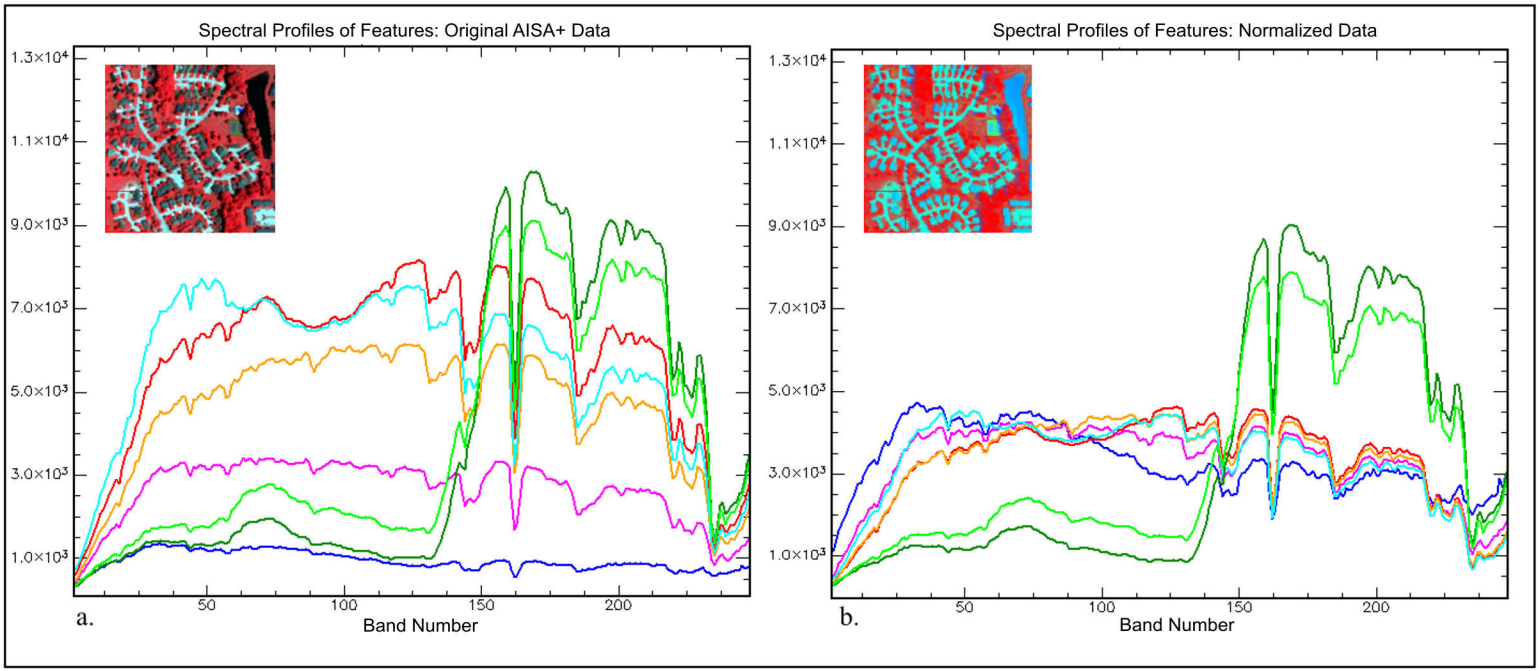

Figure 17. A comparison between spectral curves developed from a. original data, and b. normalized data. AISA+ false color image is shown in RGB 210, 130, 70 band combination. See Figure 25 for signature legend.

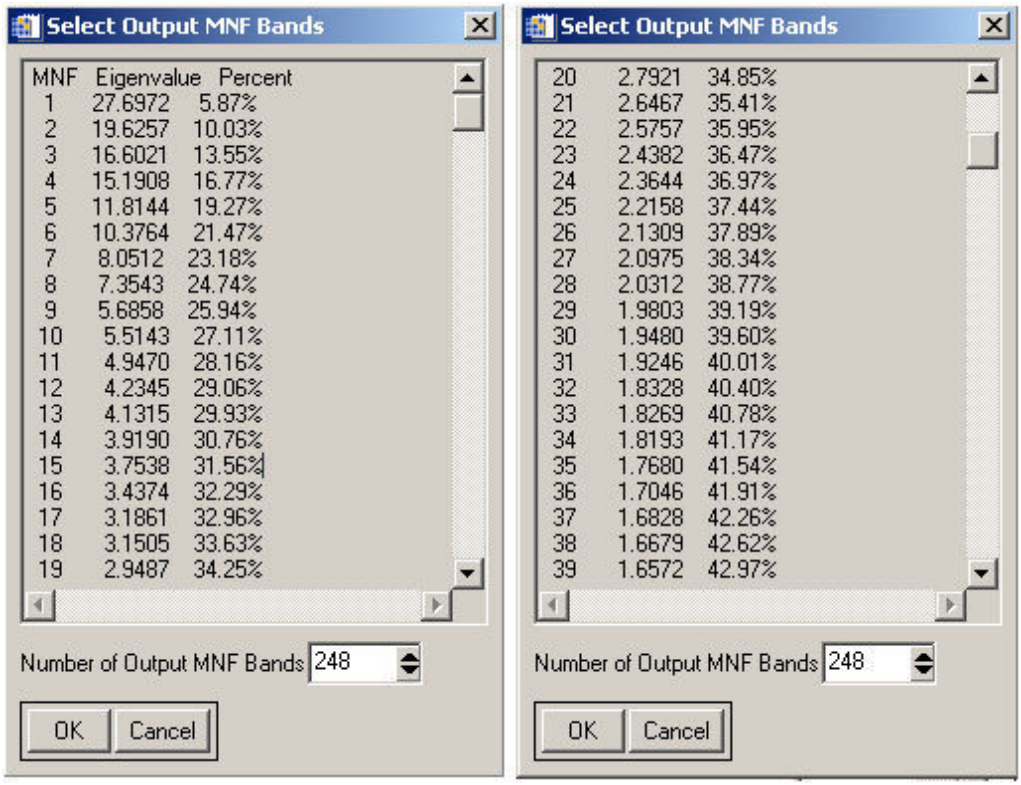

Figure 18. ENVI software interface for selecting MNF bands with highest variance.

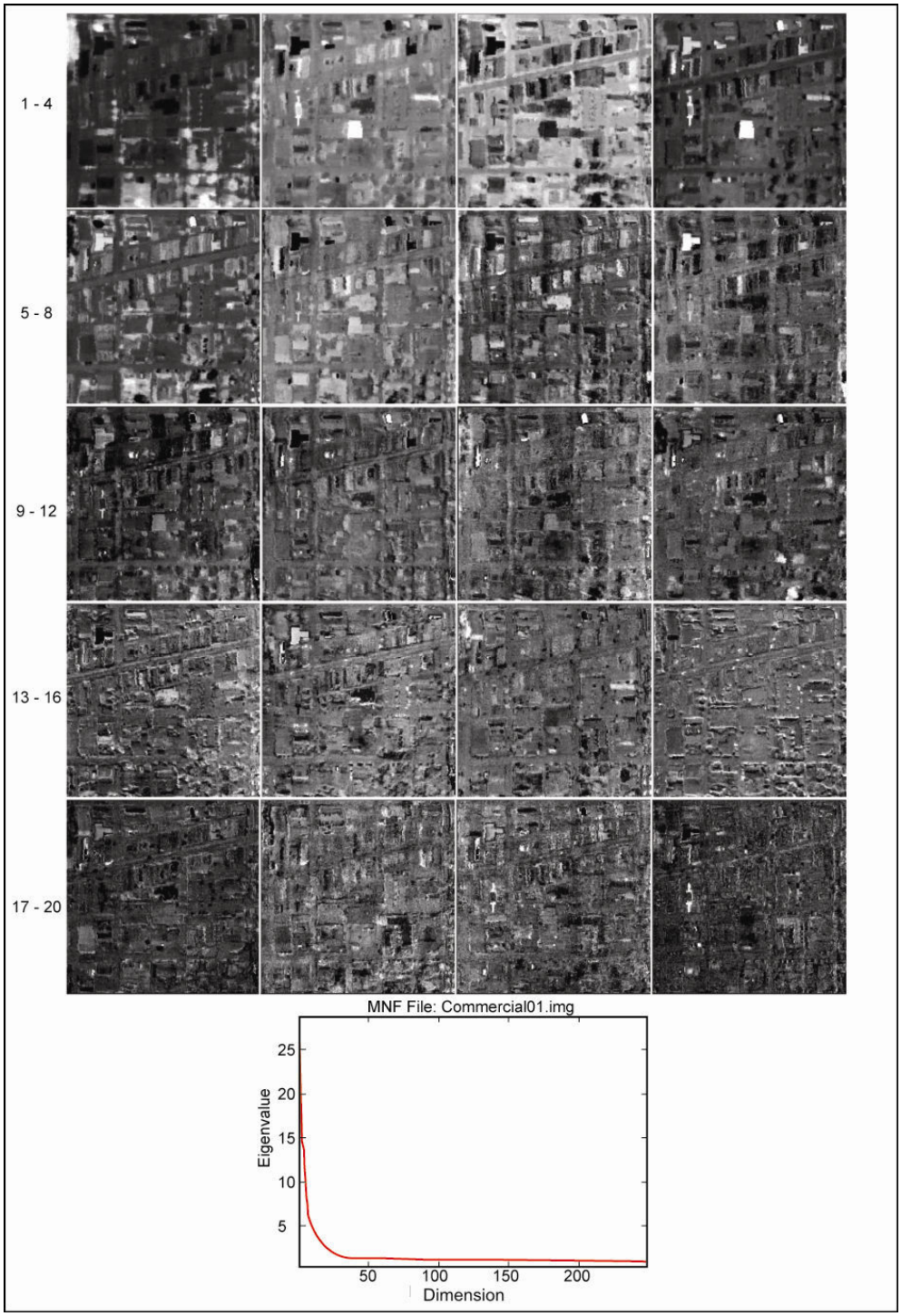

Figure 19. The first 20 principal component images from a Minimum Noise Fraction (MNF) transformation of commercial area (1).

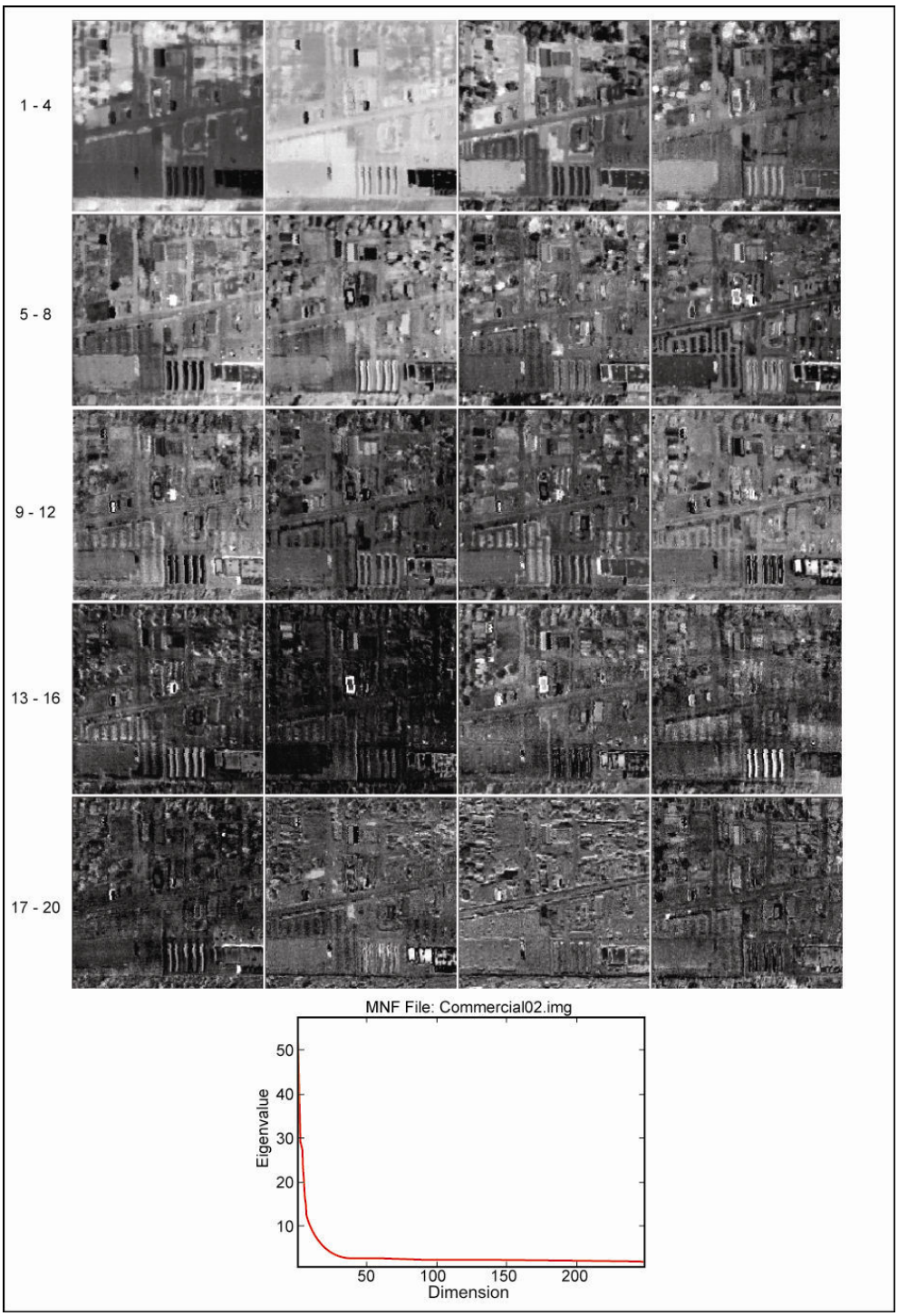

Figure 20. The first 20 principal component images from a Minimum Noise Fraction (MNF) transformation of a commercial area (2).

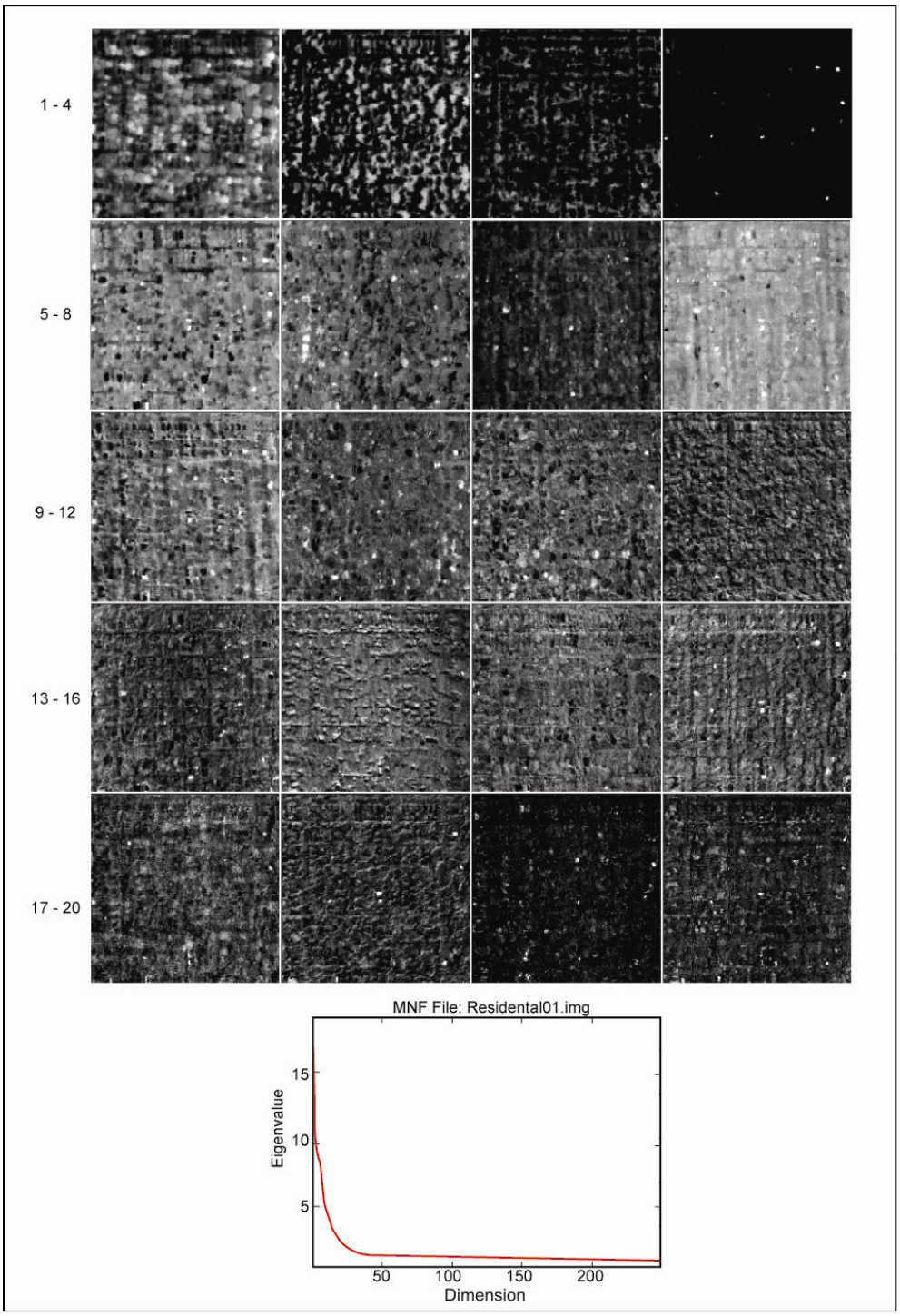

Figure 21. The first 20 principal component images from a Minimum Noise Fraction (MNF) transformation of a residential area (1).

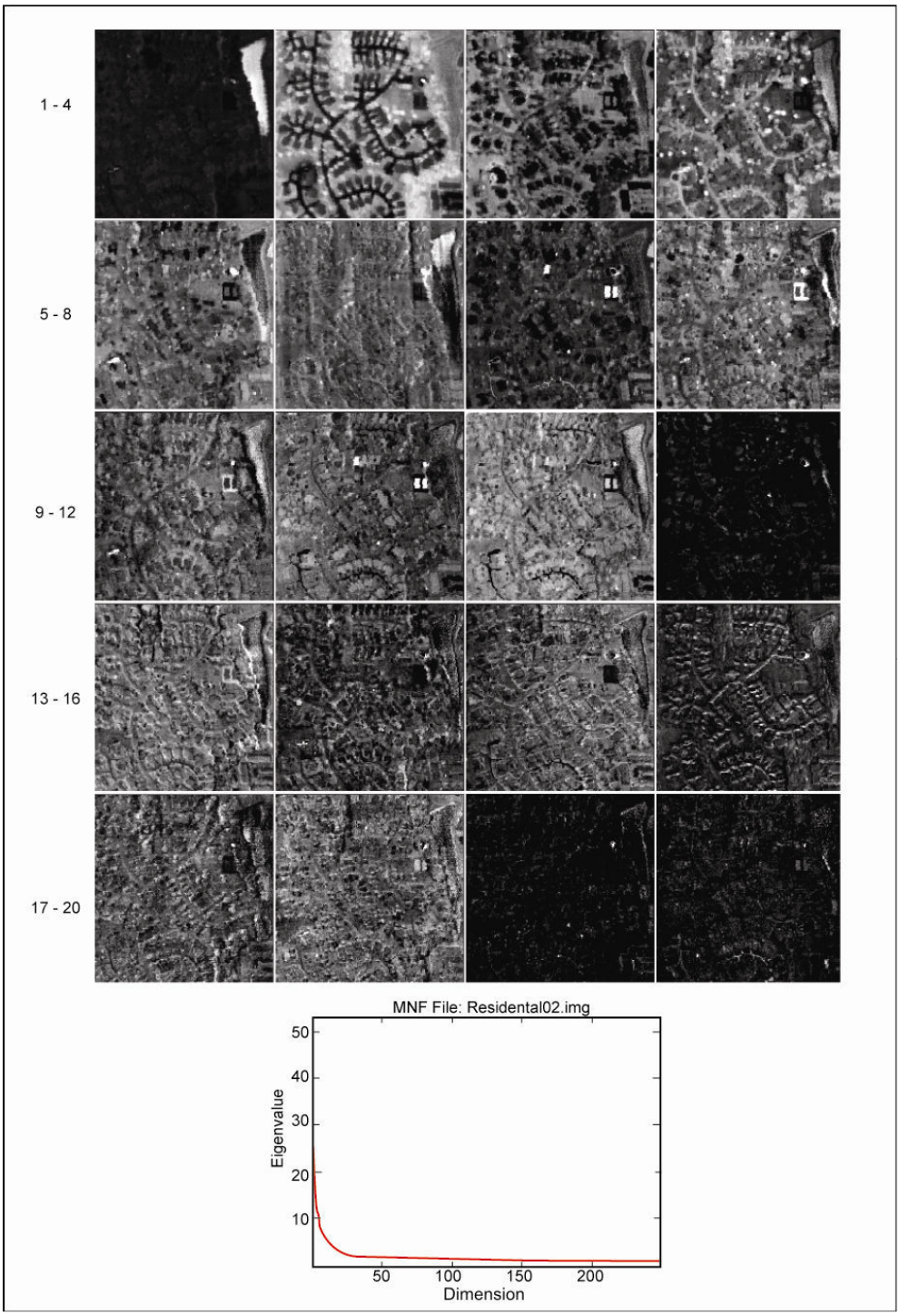

Figure 22. The first 20 principal component images from a Minimum Noise Fraction (MNF) transformation of a residential area (2).

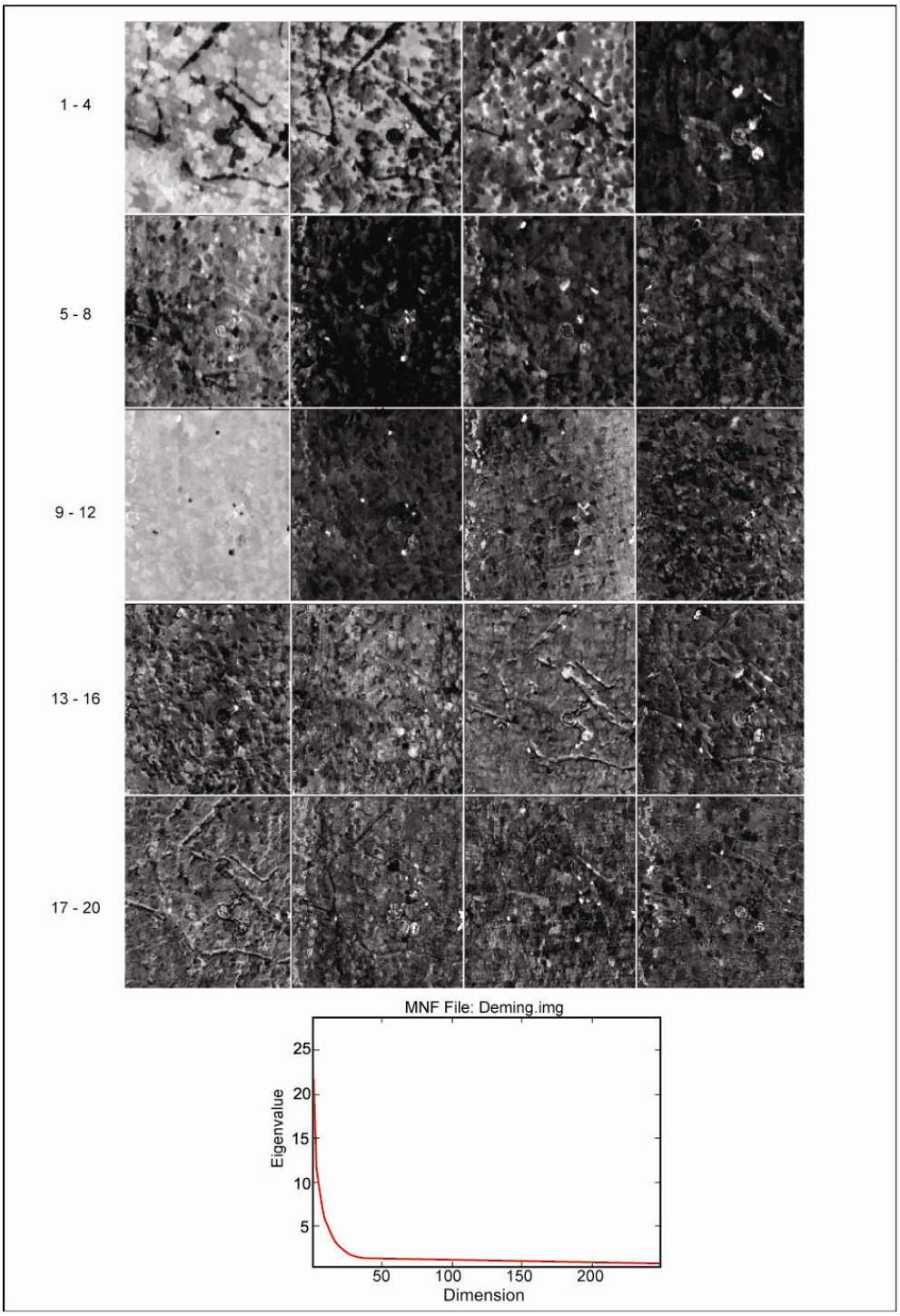

Figure 23. The first 20 principal component images from a Minimum Noise Fraction (MNF) transformation of a recreational area (1).

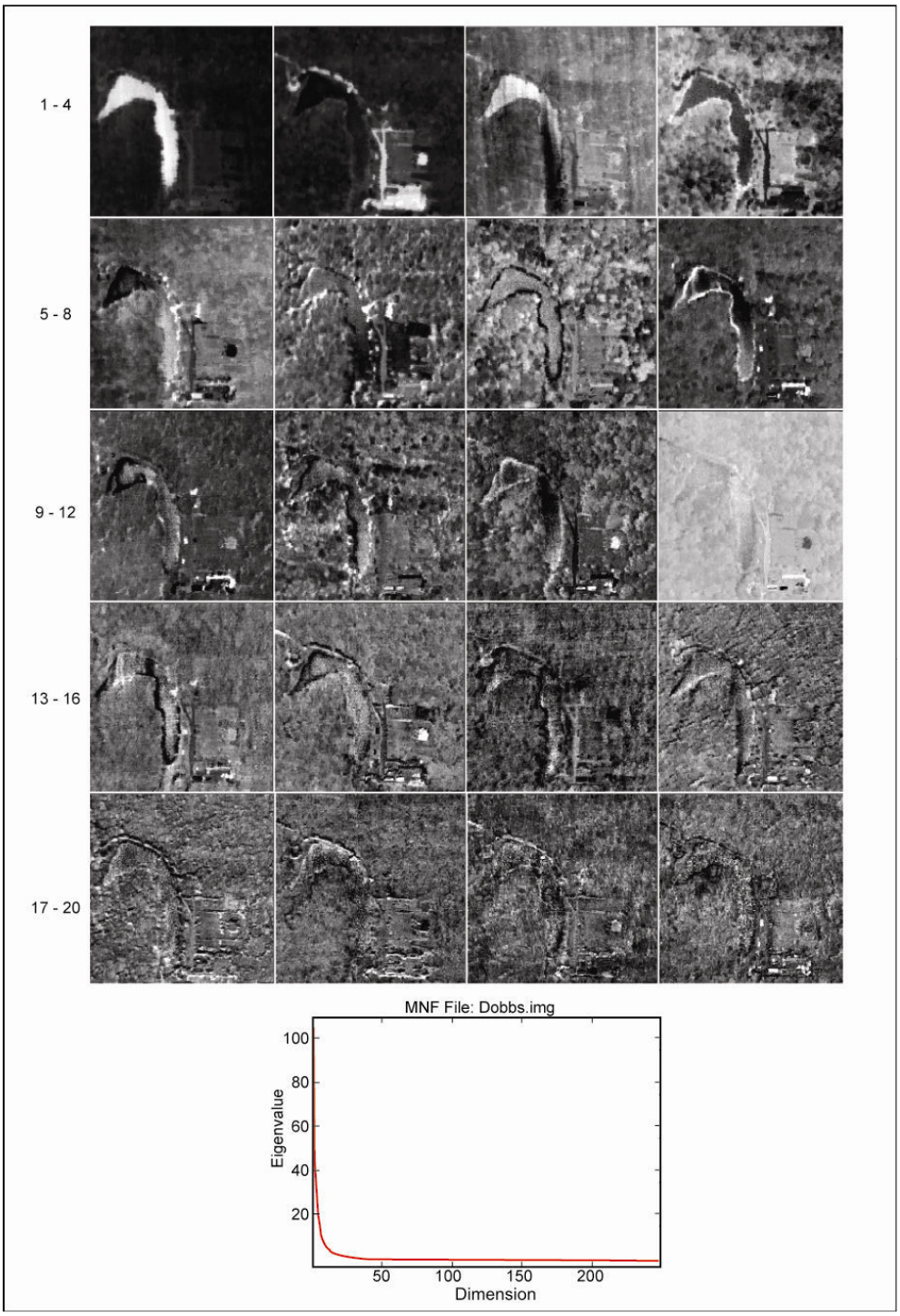

Figure 24. The first 20 principal component images from a Minimum Noise Fraction (MNF) transformation of a recreational area (2).

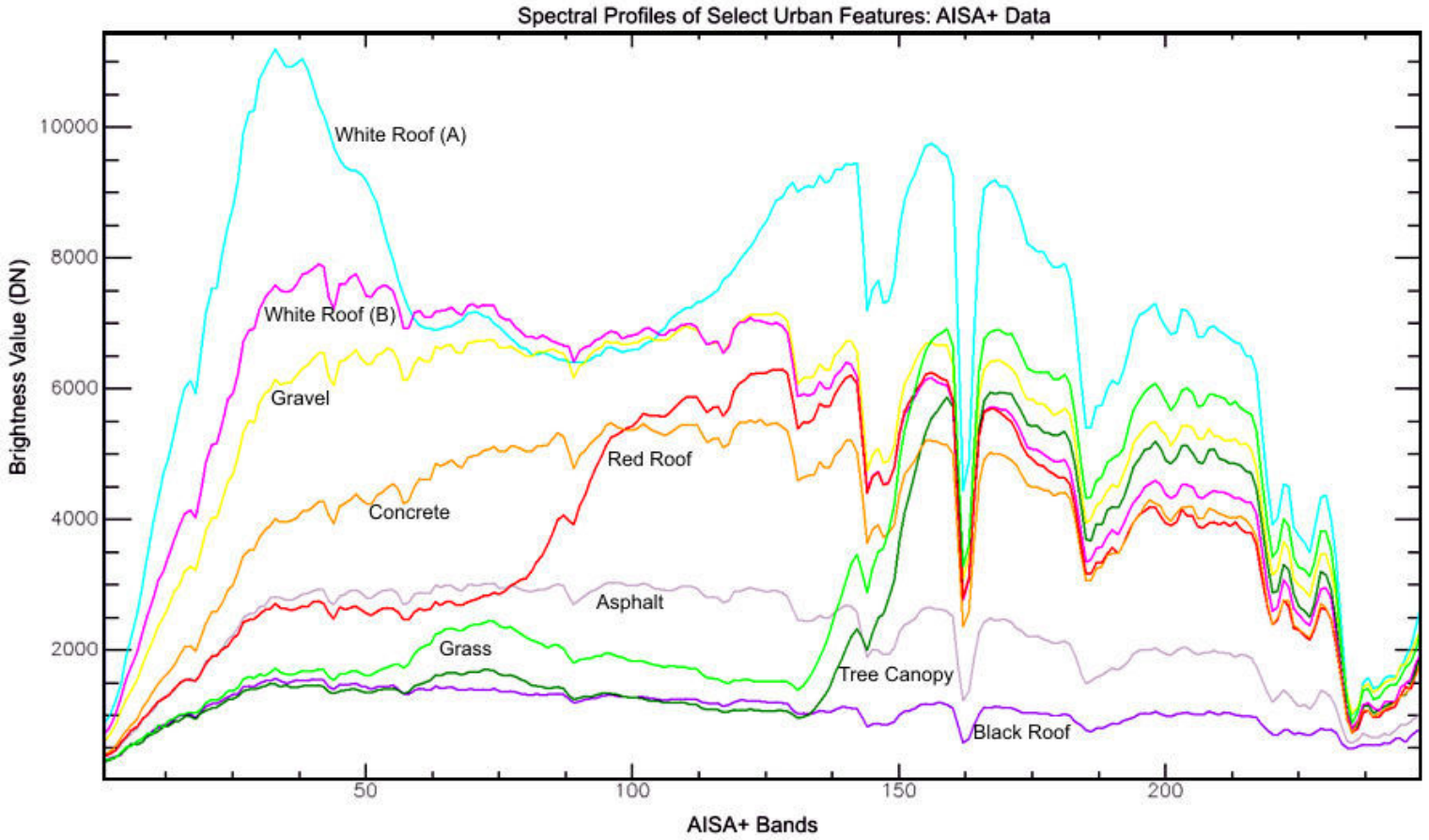

Figure 25. Spectral profiles of select urban features in AISA+ spectral feature space.

Some of the features shown in Table 4 were consolidated. For example, there were two kinds of white roofs as evident from cyan and magenta colored signatures in Figure 25. Similarly, two colors dominated the 'tennis court' class, but were consolidated in the table as a single class for convenience. However, these were considered as separate classes during classification. The samples selected for each study area were saved and used repeatedly for all three kinds of supervised classification methods.

4.4 Data Analysis

Unsupervised ISODATA clustering was performed on each study subset to generate maximum of 30 clusters at 98% convergence threshold and minimum cluster size set to 5. Clusters were merged into their appropriate classes based on comparison with ground reference information.

Supervised classification was conducted using three classifiers, MLC, ECHO, and SAM using the same set of training and test samples in the respective image subsets. For every image subset, the same MNF bands were used during each classification method, although these varied from subset to subset according to the reflectance characteristics of each area. ECHO classification was performed with cell size, homogeneous cell threshold, and annexation threshold set to 2 cells (Biehl 2001). A larger number would make the algorithm faster, but render the results blocky. This may be desirable for large moderate resolution datasets, but in a high resolution image larger values may sacrifice detail and accuracy. Post annexation classification was set to a quadratic maximum likelihood method. This procedure was repeated for all six image subsets.

Accuracy Assessment

Classes in the thematic maps were compared to their geographically corresponding ground referenced data. It is impractical to test every pixel of a classified image using ground reference. A set of randomly selected sample reference pixels is usually used to test the classification accuracy.

Test samples were generated simultaneously with training samples and classifications were conducted using test areas "hold out" procedure. This ensured that test samples were not used for training purposes, and the training samples were excluded during the generation of the classification error matrix. The number of reference pixels used in accuracy assessment is an important factor in determining the accuracy of the classification. Ideally, more than 250 reference pixels are needed to estimate within ± 5% of the mean accuracy of a class (Congalton 1991). A multinomial distribution is typically used to determine the number of test samples per class necessary to perform reliable accuracy assessment. However, given the small extent (404 m x 404 m) of the study area, the general rule of thumb to collect at least 50 samples per class was closely followed (Jensen 2005). For some of the classes with small proportion of pixels, even this rule could not be applied. Again, owing to the small study area extent, for particularly small class proportions, lower number of test samples was allowed. Care was taken to collect samples in approximately equal proportions for all classes so that an unbiased representative sample could be generated. For example, in a study area with a large water feature, which typically has low variability, fewer number of test samples were taken.

Error matrices were generated for each classification on the six study areas. Overall accuracy and kappa statistics were derived for every case. The kappa coefficient indicates the measure of agreement between the remote sensing classification and the reference data. A value of 0.93, for instance, means that 93 percent of the errors were avoided by the classification that a completely

random classification generates. Typically, kappa values more than 80% represent strong agreement between classification map and ground reference information. A value between 40% - 80% indicates moderate agreement, and less than 40% indicates poor agreement (Jensen 2005).

CHAPTER 5

RESULTS AND DISCUSSION

5.1 Thematic Classification

Four thematic maps were generated for each of the six study areas. The results for each of the study areas are discussed in the following subsections.

Commercial Areas

Commercial area (1) subset (Figure 26) was largely composed of impervious surface materials such as asphalt, concrete, and building structures. A relatively small proportion of tree canopy and grass was also observed in this area.

Apart from a distinctive red colored roof top, large proportions of roofs were either black or white. Two visibly white yet distinct roof tops were identified. The variation in their reflectance was likely influenced by their material character, but the reason is unknown. All four classifiers performed most poorly in this study area (Figure 33). Despite multiple iterations of training and reclassification efforts, SAM especially performed with least success with 66.7% accuracy. Most misclassification occurred primarily between asphalt, concrete, and gravel features. To a lesser extent, misclassification was seen between roofs and asphalt as well. This is likely because some of the roofs may be composed of asphalt shingles, but there was no clear evidence available.

Visual examination of thematic maps showed that SAM seemed to resemble ISODATA more than the others. It cannot be ruled out that in terms of spectral characteristics alone SAM was likely performing better, but it could not generalize on the basis of the training samples. This was especially evident in the 'gray roof' class seen in the lower right quadrant of the thematic map. While MLC and ECHO followed the object boundary, SAM meticulously differentiated areas with the slightest shadow and those of 'gray roof' reflectance. That being said, there was clear misclassification between spectrally unambiguous classes such as open soil and asphalt as evident in the lower part of the thematic map. The same errors were observed between concrete and gravel as evident in the area south of the large red roof. ECHO classifier performed the best in this study area with 83.6% overall accuracy, with MLC closely following it. The largest commission error (17%) was of shadows included into black roof class. The most ambiguous classes asphalt and concrete were best classified by ECHO. Overall, this study area was classified with the least accuracy by all the classifiers. In commercial area (2) (Figure 27), both MLC and ECHO performed significantly better with 94.3% and 95.4% respective overall accuracies. SAM and ISODATA performance improved, but were still low with 75.8% and 78.4% overall accuracy.

Two classes of spectrally distinct asphalt classes were identified (Figure 28). Both ISODATA and SAM had considerable misclassification between these two classes and those of concrete and gravel classes. The largest error between classes derived using SAM were between asphalt, concrete, and white roof B class. It was likely that some of the white roofs were composed of concrete, but there was not clear evidence to support it. ECHO performed the best with about 94% overall accuracy. The availability of additional reference information on the roof material may be useful in abating such problems. Speckling was observed on asphalt and concrete classes, which may be from parked or moving vehicles.

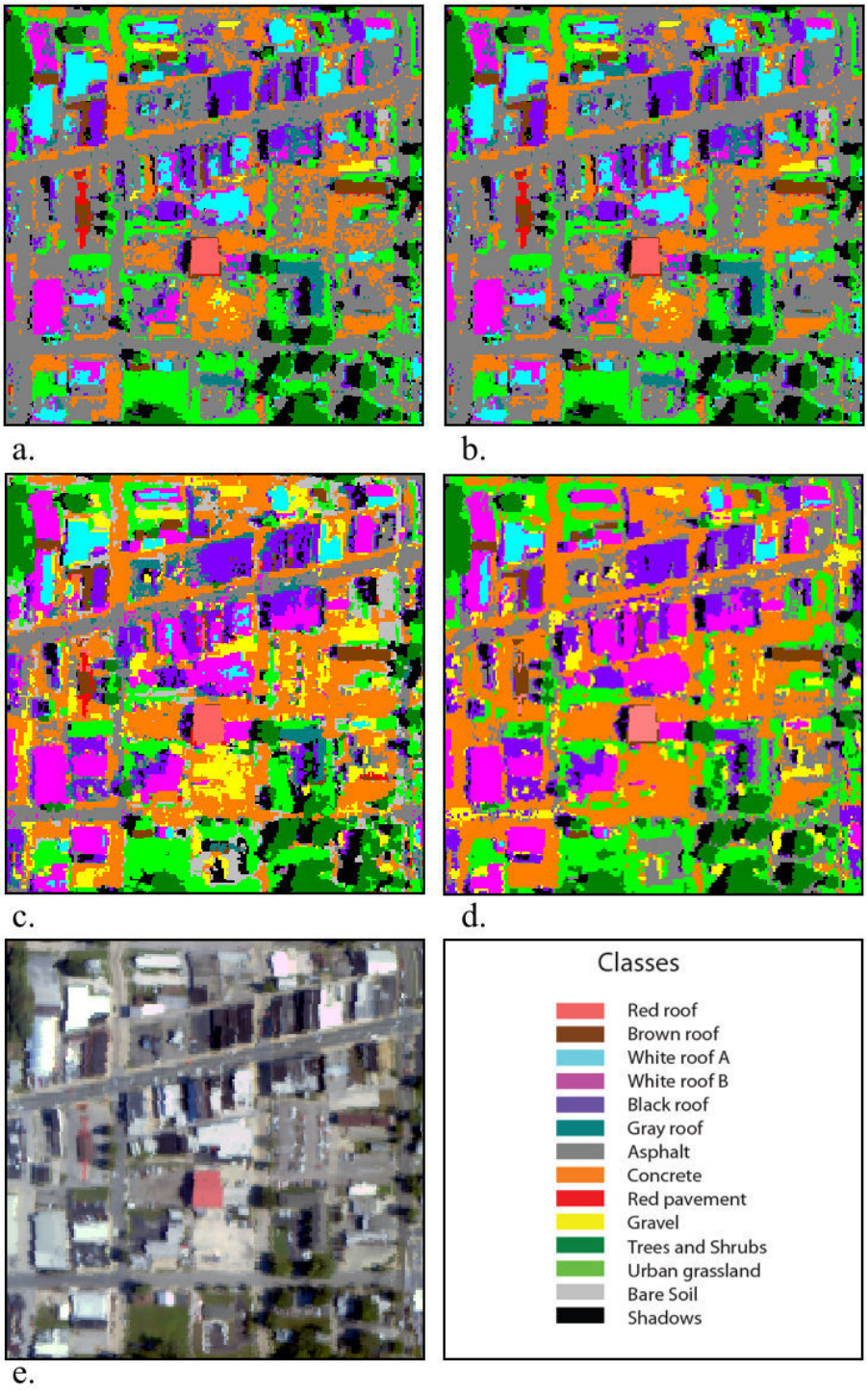

Figure 26. Classification results of commercial area (1) with a. MLC, b. ECHO, c. SAM, d. ISODATA, and e. Original data are displayed in true color (RGB 135, 75, 25).

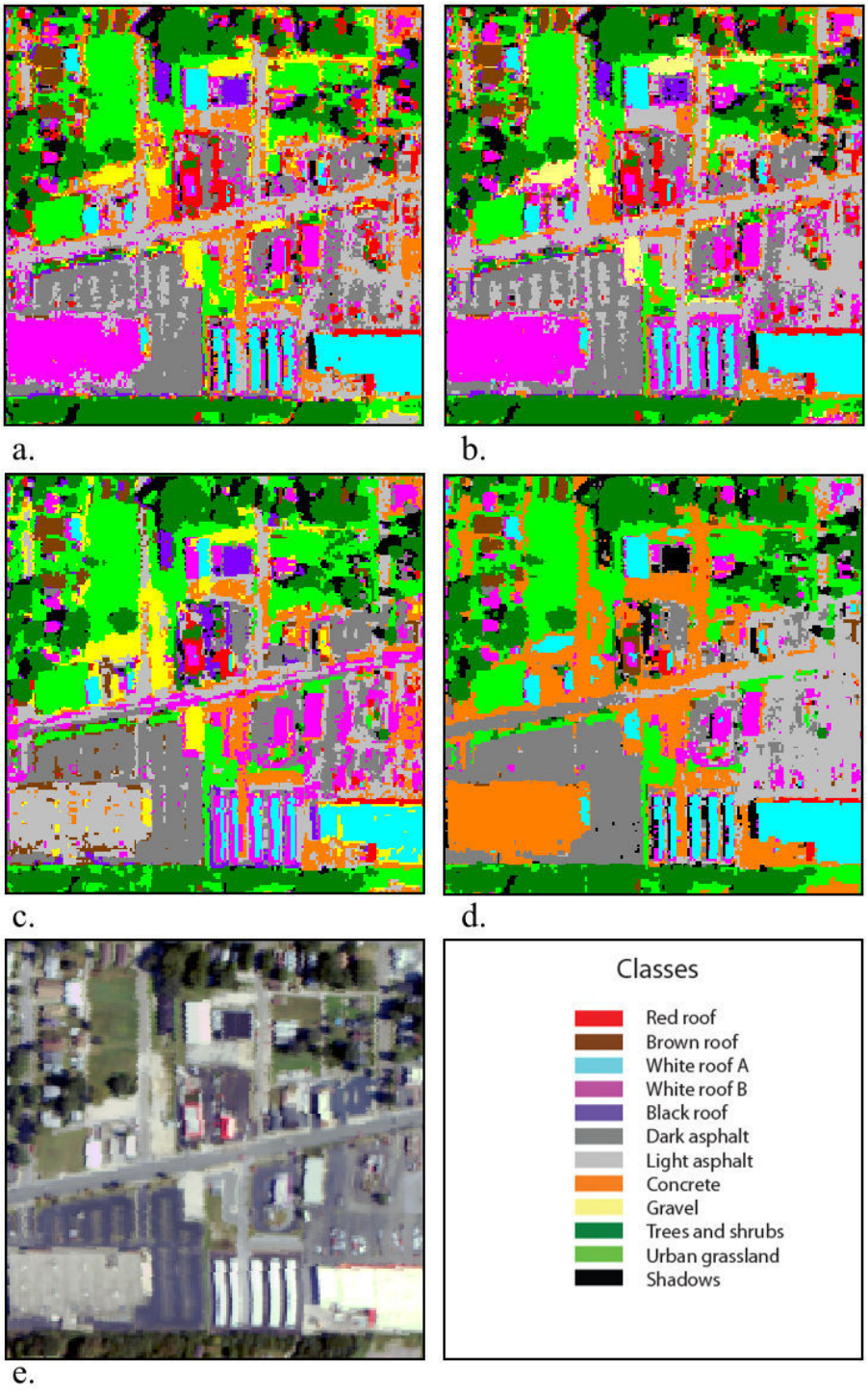

Figure 27. Classification results of commercial area (2) with a. MLC, b. ECHO, c. SAM, d. ISODATA, and e. Original AISA+ data are displayed in true color (RGB 135, 75, 25).

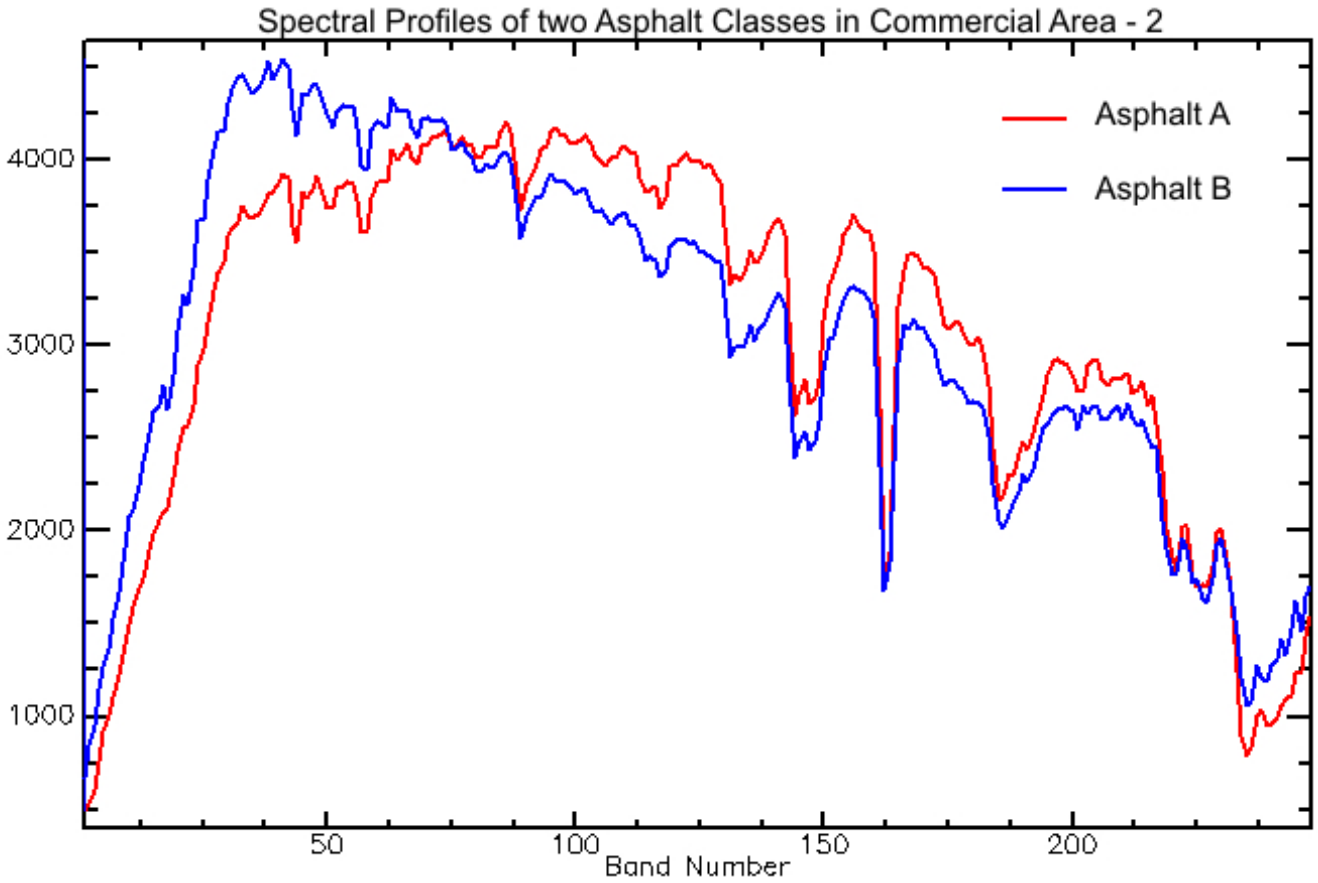

Figure 28. Spectral curves of two different asphalt classes.

Residential Areas

The spatial arrangement of residential area (1) was the most complex with a high level of neighborhood pixel variance. In other words, the spatial makeup of this study area was heterogeneous. ECHO performed the best amongst all the classifiers with about 91% accuracy. Tree canopy and grass were the most misclassified by ECHO. The thematic map produced by SAM was the most visually coherent, but its percentage accuracy was 5% lower than ECHO.

While it is likely that even more rigorous test sampling may improve SAM accuracy, the classes that most contribute towards misclassification error are tree canopy, grass, and shadow, which are prone to inter-class mixing due to sun angle influence. Collection of spectral signatures from these classes using field spectrometers and incorporating them in the analyses will need to be explored in future research.

Both SAM and ISODATA performed their best in residential area (2) with 92% and 94% accuracy respectively. This was the only study area where all classifiers achieved more than 90% accuracy. Apart from misclassification between tree canopy, grass, and shadow classes, the most error was between gray and brown roof colors. Several roofs fell under no clear color category, creating a certain level of ambiguity. The overall high accuracy in this study area is likely due to relatively less ambiguity of the majority of classes. Larger roof sizes and wider roads may pose less mixed pixel problems at two meter resolution, allowing for better training and classification. The number of spectrally similar classes was relatively low in this study area as well.

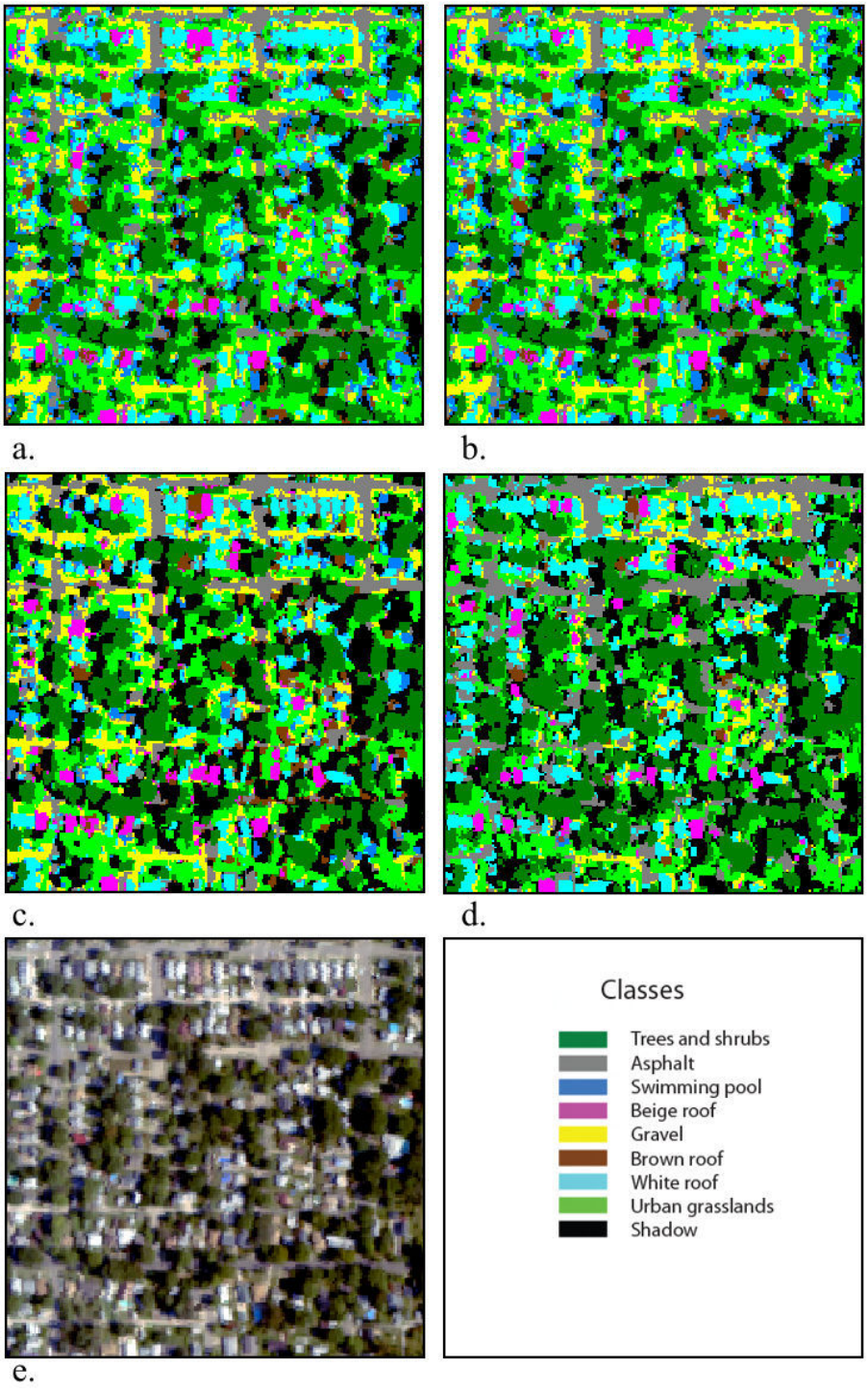

Figure 29. Classification results of residential area (1) with a. MLC, b. ECHO, c. SAM, d. ISODATA, and e. Original AISA+ data are displayed in true color (RGB 135, 75, 25).

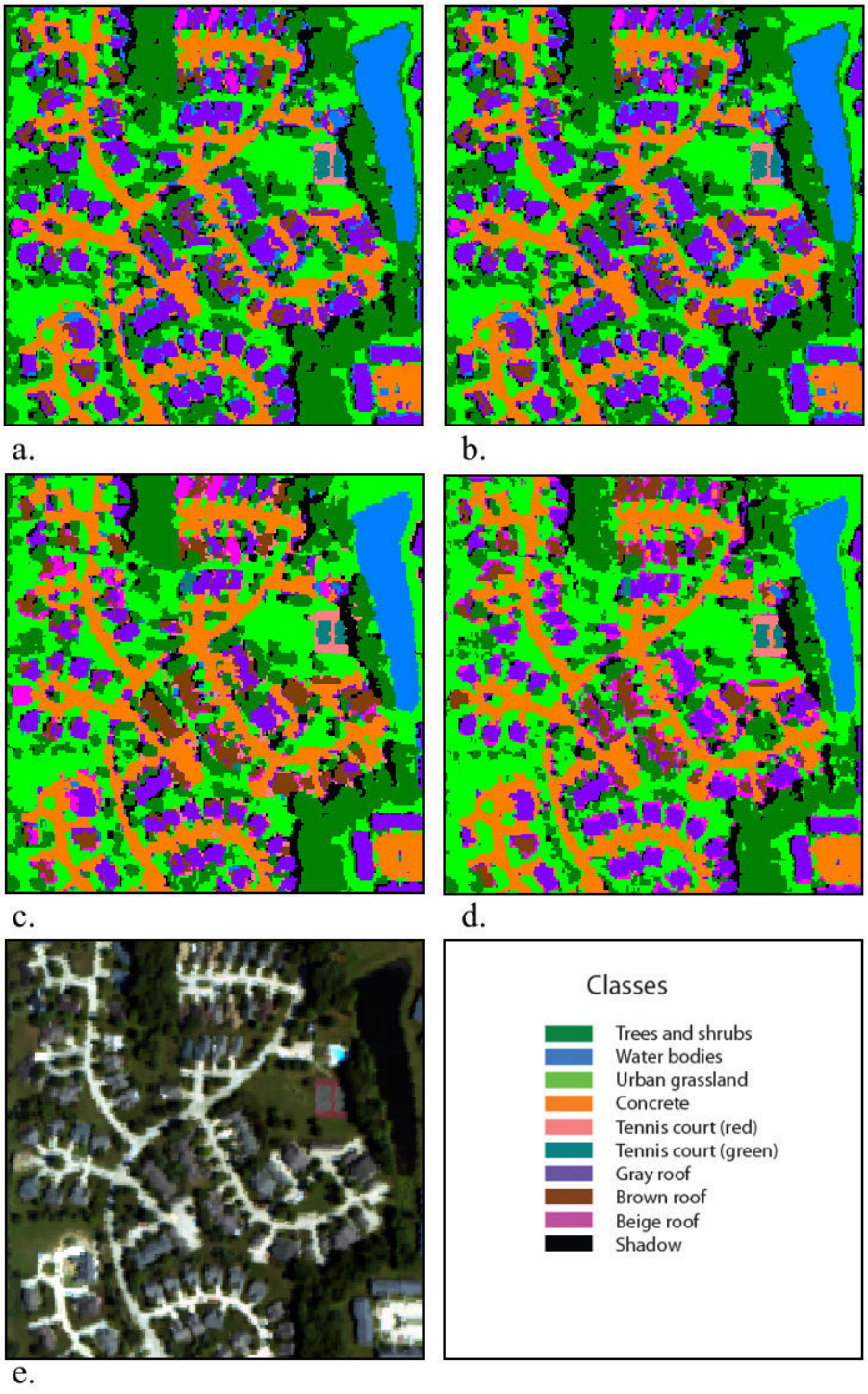

Figure 30. Classification results of residential area (2) with a. MLC, b. ECHO, c. SAM, d. ISODATA, and e. Original AISA+ data are displayed in true color (RGB 135, 75, 25).

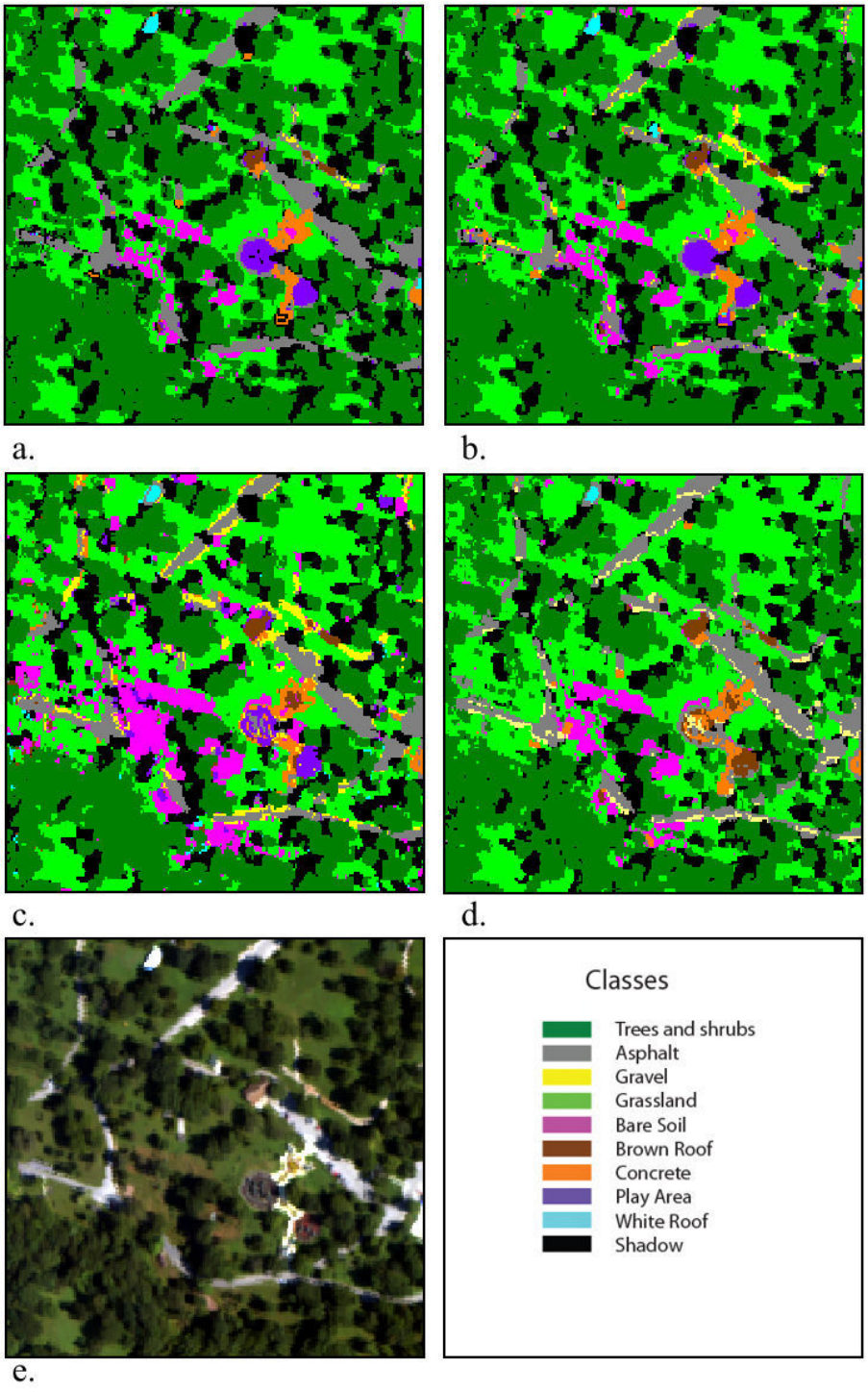

Figure 31. Classification results of recreational area (1) with a. MLC, b. ECHO, c. SAM, d. ISODATA, and e. Original AISA+ data are displayed in true color (RGB 135, 75, 25).

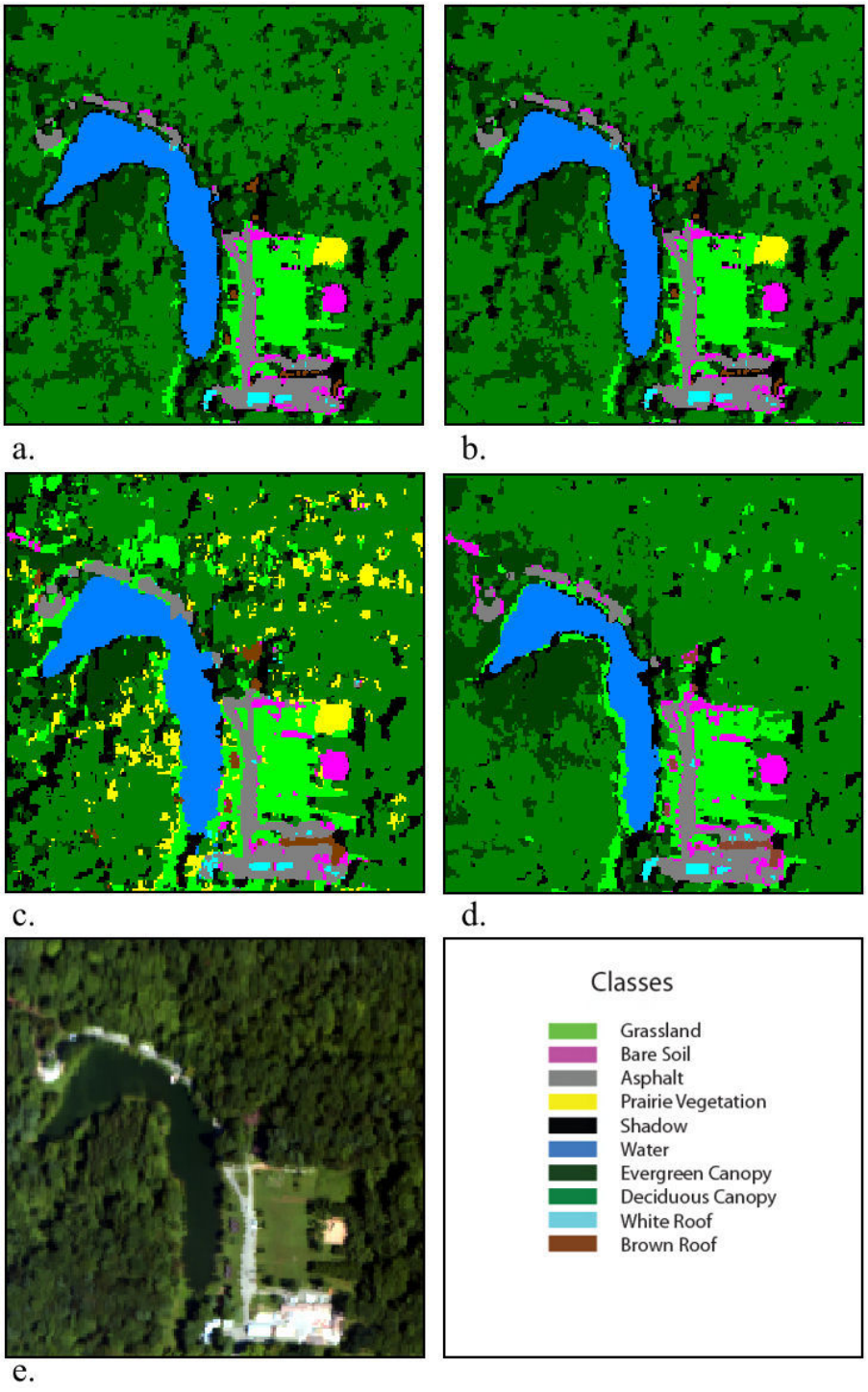

Figure 32. Classification results of recreational area (2) with a. MLC, b. ECHO, c. SAM, d. ISODATA, and e. Original AISA+ data are displayed in true color (RGB 135, 75, 25).

Recreational Areas

Recreational area (1) was a part of Deming Park in Terre Haute, Indiana. MLC and ECHO performed exceedingly well with overall accuracies of 97.6% and 98.6% respectively. Due to unusual success, which is often unlikely, multiple efforts at sampling and reclassification were undertaken, but the results were similar. SAM misclassified tree canopy, grass, and open soils and achieved 85.7% accuracy. ISODATA failed to separate gravel and asphalt, but achieved 90% overall accuracy because of its superior classification of tree canopy, grass, and open soils which are dominant in the scene. Two unique rubberized play areas were visible in the lower right quadrant of the scene that were classified correctly by the three supervised methods, but ISODATA misclassified it as asphalt, concrete, and gravel. Also, the gravel on the railroad track was too narrow for 2 m spatial resolution, and those pixels mixed with neighboring grass pixels, creating ambiguity.

Recreational area (2) was a part of Dobbs Park in Terre Haute, Indiana, with a large continuously wooded area, an open water body, and other smaller features. The clumped spatial arrangement of evergreen and deciduous canopies allowed for distinguishing their canopies into two separate classes. ECHO performed with the highest accuracy (88%), and SAM achieved the lowest accuracy (84.7%). Although ISODATA failed to classify prairie vegetation class, its overall accuracy was higher than SAM, because SAM misclassified several younger deciduous and evergreen trees as prairie vegetation. In strictly spectral terms SAM may not be inaccurate, but ground truth nevertheless does not match the thematic class, and hence has lower accuracy. Overall, in terms of classification accuracies derived from the test areas, MLC and ECHO were the most successful in all study areas. SAM performed with least success. ECHO performed with the

most success in commercial (1), commercial (2), and residential (1) scenes that were the most heterogeneous.

5.2 Classification Accuracies

Evaluation of Overall Accuracies and Classification Significance

Overall classification accuracies of each classifier in the six study areas are reported in Table 6. These values represent the total number of pixels correctly classified out of the total number of test sample pixels. The kappa statistic indicates the percentage of error avoided by the classification process that a completely random classification would generate. In other words, it is a measure of significance of the classification process.

Table 6

Comparison of overall classification accuracies.

Study Areas	MLC Accuracy		ECHO Accuracy		SAM Accuracy		ISODATA Accuracy	
	(%)	Kappa	(%)	Kappa	(%)	Kappa	(%)	Kappa
Com (1)	82.2	79.6	83.6	81.2	63.9	59.2	74.8	70.4
Com (2)	94.3	93.7	95.4	94.0	75.8	73.2	80.1	80.0
Res (1)	85.9	78.1	91.1	85.0	85.1	76.9	84.4	80.1
Res (2)	95.4	94.3	94.4	93.2	92.0	90.3	95.0	91.2
Rec (1)	97.6	96.4	96.8	96.1	85.7	79.6	90.1	88.5
Rec (2)	86.5	76.0	88.0	78.2	84.7	68.3	87.6	80.4

Note: Com - Commercial; Res - Residential, Rec – Recreational

The lowest of any classification accuracy is 63.9% attained by SAM classifier on recreational area (2). The lowest kappa value is 59.2%, which means that there is 40.8% possibility that 63.9% overall accuracy could have been achieved just by chance. By this measure, the most significantly accurate classification was achieved by MLC and ECHO on three study areas, commercial (2),

residential (2), and recreational (1). Accuracy of SAM had high agreement only in residential area (2). ISODATA classified with high agreement in residential (2), and recreational (1). The relationship is shown in Figure 33.

It is evident from Figure 34 that commercial area (1) was the least accurately classified by all the classifiers. The more complex residential area (1) was classified with high accuracy by ECHO, the less complex residential area (2) and recreational area (2) were classified relatively consistently by all classifiers. Both the commercial areas classified by SAM and ISODATA did not meet the hypothesized accuracy of 80%.

In addition to overall accuracy, individual class accuracies are reported in the following subsections. Both user's accuracy (error of commission) and producer's accuracy (error of omission) are reported. The measure for producer's accuracy indicates the probability of a reference pixel being classified correctly. User's accuracy, also called reliability, indicates probability that a pixel classified in the map actually represents that class on the ground. A user of the imagery who is particularly interested in a class might wish to know what proportion of pixels assigned to that class was correctly assigned.

Evaluation of Per Class Accuracies for Commercial Areas

Homogeneous classes with small spatial proportions, *red roof* and *brown roof*, were classified most accurately across all the classifiers. *Gravel* class had commission error between *white roof B* and concrete. *White roof B* class had a moderate amount of omission error with *gray roof* class. In general urban materials, unless significantly distinct, were misclassified the most by the classifiers used in this research on AISA+ VNIR bands.

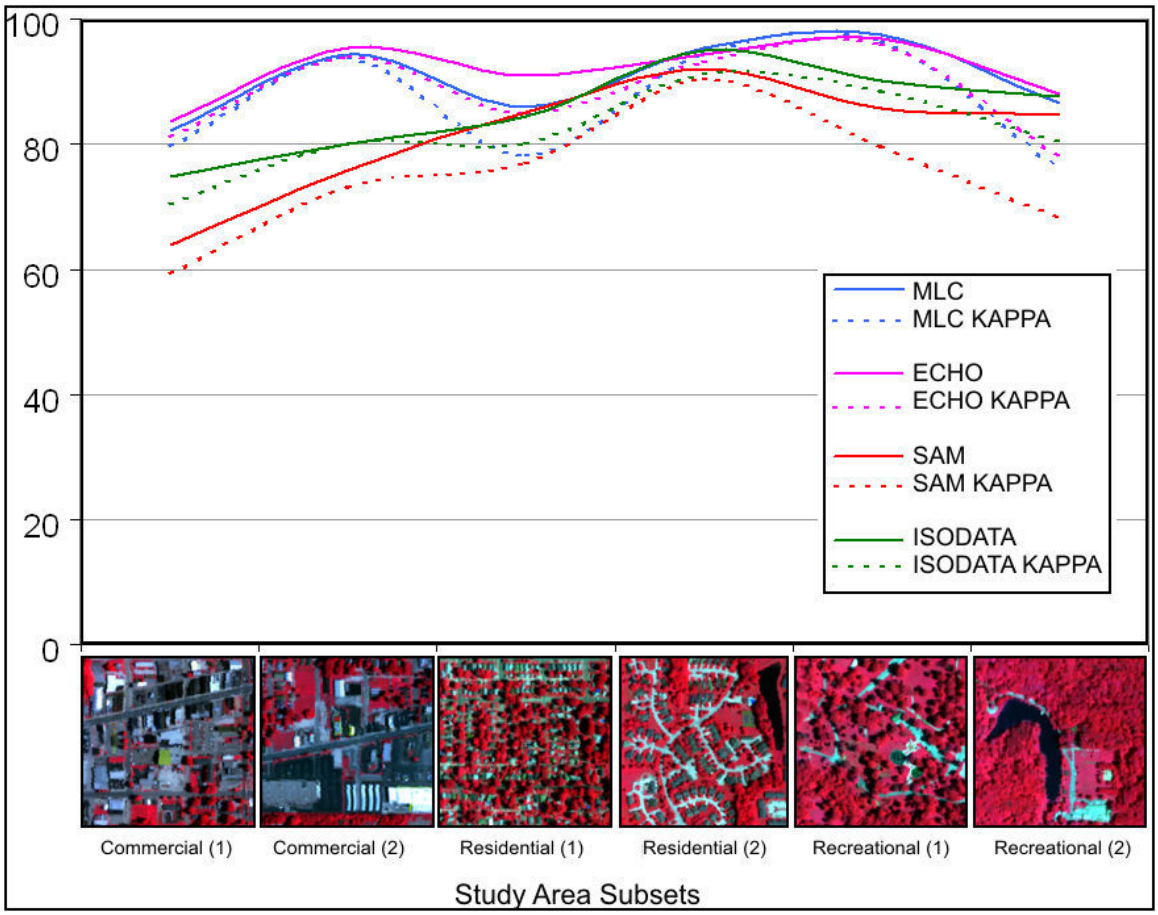

Figure 33. Comparison of overall accuracies of four classifiers over six urban study areas.

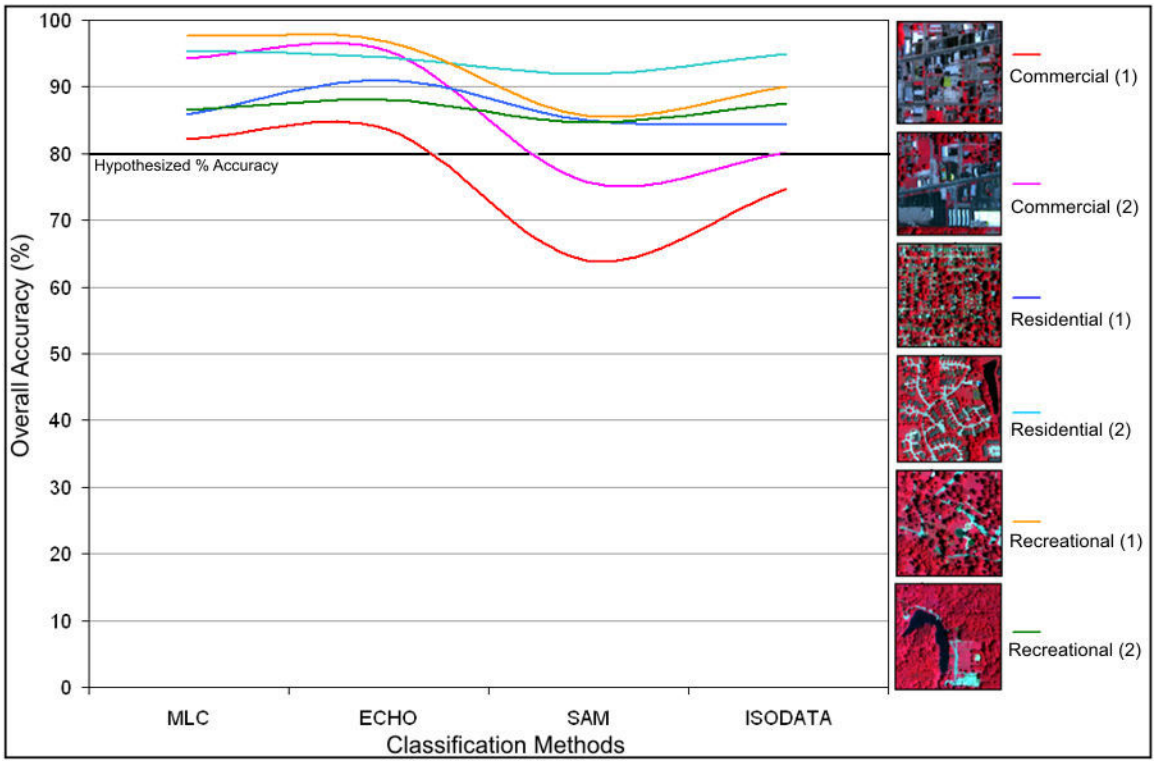

Figure 34. Comparison between classification methods when applied to the six study areas.

Table 7

Individual class accuracies (%) for commercial area (1).

CLASSES	MLC		ECHO		SAM		ISODATA	
	PA	UA	PA	UA	PA	UA	PA	UA
Red roof	100.0	100.0	100.0	100.0	100.0	100.0	100.0	100.0
Brown roof	100.0	100.0	100.0	100.0	100.0	100.0	100.0	100.0
White roof A	100.0	60.6	100.0	60.1	75.6	60.6	78.4	90.1
White roof B	42.8	99.0	41.9	99.0	66.5	99.0	69.1	80.3
Black roof	78.6	97.1	78.6	97.1	87.3	97.1	90.6	97.6
Gray roof	90.0	69.2	90.0	70.3	74.0	69.2	18.0	11.4
Asphalt	83.8	84.1	90.7	85.3	22.1	84.1	23.0	72.3
Concrete	87.6	82.0	87.9	86.5	58.2	82.0	60.0	86.0
Red pavement	100.0	100.0	100.0	100.0	100.0	100.0	8.0	7.8
Gravel	43.6	26.6	43.6	26.6	69.2	26.6	79.0	72.0
Trees and Shrubs	98.5	92.8	98.5	97.0	72.3	92.8	95.4	95.8
Urban grassland	97.9	98.7	99.1	98.7	100.0	98.7	96.3	98.4
Bare Soil	100.0	70.0	70.0	100.0	97.5	100.0	7.9	7.0
Shadows	63.0	100.0	100.0	63.0	87.0	63.0	69.0	72.1

Note: PA - Producer's Accuracy; UA - User's Accuracy

Table 8

Individual class accuracies (%) for commercial area (2).

CLASSES	MLC		ECHO		SAM		ISODATA	
	PA	UA	PA	UA	PA	UA	PA	UA
Red roof	100.0	87.8	100.0	97.3	94.4	100.0	86.9	92.4
Brown roof	100.0	100.0	100.0	100.0	65.2	100.0	65.2	100.0
White roof A	98.7	100.0	98.7	100.0	75.5	100.0	92.1	100.0
White roof B	94.3	81.1	95.0	85.8	39.0	38.5	68.0	91.4
Black roof	100.0	100.0	84.8	97.5	87.0	69.0	42.0	40.1
Dark asphalt	94.0	100.0	82.7	98.9	92.6	92.2	88.0	71.8
Light asphalt	94.9	64.0	98.6	81.1	63.5	50.0	86.1	72.5
Concrete	82.0	87.1	74.1	97.6	72.9	83.3	81.4	94.3
Gravel	100.0	92.3	99.0	94.1	100.0	81.4	26.6	26.0
Trees and shrubs	98.9	93.2	99.4	95.2	92.8	89.8	91.4	89.4
Urban grassland	100.0	95.2	96.7	100.0	93.0	95.4	93.0	93.7
Shadows	100.0	93.5	84.8	78.0	65.2	83.3	64.8	71.9

The amount of misclassification in commercial area (2), between *concrete* class and *white roof B* class may be indicative that *white roof B* class was composed of concrete. The *concrete* class may have to be redefined in the classification scheme to accommodate for concrete roofs. Although spectrally distinct from each other, there is also much error between *dark* asphalt and *light asphalt* classes. In some of the dark asphalt areas, at 2 m resolution, yellow paint from on parking lots created spectral mixing. More cautious classification redefinition will be useful in including such variations, but at Level III, some amount of generalization of classes is necessary.

Evaluation of Per Class Accuracies for Residential Areas

In residential area (1), there is considerable commission of *trees and shrubs* class into the *urban grasslands* and *shadow* class. High intra class variability and interclass spectral similarities, especially on the extreme sunny and shady sides of trees were the reasons for the poor classification. Overall ECHO performed best in such classes, due to its segmentation and assimilation of homogeneous pixels before the classification procedure.

Residential area (2) was different from residential area (1) in many ways. The scene was less complex, and the classes had spatial continuity and relatively low intra-class variability. For example, the water, urban grass, and trees and shrubs classes in this area had a high level of continuity and relatively clearly defined edges. Most errors occurred in the classification of roof types that were more discontinuous as well as smaller in extent. It is likely that classification based on detailed analysis of roof materials may improve accuracies. Information on roofing materials can be compared to spectral libraries to obtain better results in these classes. Reliability in other classes was consistently high.

Table 9

Individual class accuracies (%) for residential area (1).

CLASSES	MLC		ECHO		SAM		ISODATA	
	PA	UA	PA	UA	PA	UA	PA	UA
Trees and shrubs	81.0	98.7	93.4	97.8	80.5	98.5	80.5	98.5
Asphalt	98.9	96.4	100.0	95.4	98.9	97.4	89.6	94.8
Swimming pool	78.7	92.5	12.8	100.0	68.1	64.0	22.0	14.0
Beige roof	100.0	100.0	100.0	55.3	100.0	100.0	99.0	100.0
Gravel	86.3	78.6	82.4	84.0	86.3	73.3	74.8	73.3
Brown roof	100	92.5	81.6	85.1	98.0	96.0	98.0	96.0
White roof	96.7	97.5	94.3	85.9	95.9	95.2	91.4	95.2
Urban grasslands	89.2	45.0	84.3	61.9	87.0	45.4	89.0	57.0
Shadow	97.5	68.6	94.1	99.1	97.5	66.7	96.5	72.0

Table 10

Individual class accuracies (%) for residential area (2).

CLASSES	MLC		ECHO		SAM		ISODATA	
	PA	UA	PA	UA	PA	UA	PA	UA
Trees and shrubs	97.1	95.6	94.9	98.5	91.6	97.6	96.5	90.6
Water bodies	99.9	97.3	99.6	99.5	99.6	99.5	99.6	97.0
Urban grassland	92.4	100.0	99.3	93.0	97.2	94.6	93.0	86.8
Concrete	95.6	99.2	98.9	99.4	99.0	99.6	98.0	98.9
Tennis court (red)	94.0	100.0	100.0	98.0	100.0	92.6	100.0	97.0
Tennis court (green)	100.0	95.9	97.9	100.0	97.9	97.9	98.0	100.0
Gray roof	91.1	96.4	76.6	99.5	66.3	98.9	94.1	95.0
Brown roof	100.0	32.4	100.0	16.2	87.5	11.3	84.6	78.0
Beige roof	52.0	100.0	86.0	100.0	100.0	82.0	61.0	62.2
Shadow	98.2	78.7	90.8	84.6	93.6	65.8	97.2	87.0

Evaluation of Per Class Accuracies for Recreational Areas

Recreational area (1) subset contained classes in disproportionate amounts. *Trees and shrubs* class was dominant, followed by *grasslands* class. Unsupervised ISODATA did not differentiate the rubberized *play area* from concrete, and asphalt classes. Both SAM and ISODATA performed poorly in gravel likely due to the spectral mixing caused by its spatially narrow/linear arrangement. Overall, all classes were classified with more than 80% user's accuracy by MLC and ECHO.

Table 11

Individual class accuracies (%) for recreational area (1).

CLASSES	MLC		ECHO		SAM		ISODATA	
	PA	UA	PA	UA	PA	UA	PA	UA
Trees and shrubs	99.0	98.7	99.4	99.6	76.0	99.5	96.0	82.4
Asphalt	96.9	86.1	95.3	96.8	93.8	89.6	82.1	86.0
Gravel	38.5	100.0	84.6	91.7	100.0	56.5	89.5	72.8
Grassland	98.3	100.0	99.4	100.0	97.1	80.4	98.0	83.9
Bare Soil	100.0	100.0	100.0	100.0	85.7	47.4	97.7	96.5
Brown Roof	91.3	100.0	91.3	100.0	82.6	95.0	89.7	92.4
Concrete	95.7	100.0	95.7	95.7	87.0	90.9	97.8	87.1
Play Area	100.0	88.5	100.0	82.1	78.3	81.8	3.7	2.5
White Roof	100.0	88.9	100.0	88.9	87.5	63.6	99.6	82.6
Shadow	95.2	90.9	96.8	95.3	95.2	69.0	95.3	89.2

Table 12

Individual class accuracies (%) for recreational area (2).

CLASSES	MLC		ECHO		SAM		ISODATA	
	PA	UA	PA	UA	PA	UA	PA	UA
Grassland	100.0	94.5	100.0	94.5	100.0	72.9	100.0	70.5
Bare Soil	100.0	97.3	100.0	97.3	100.0	100.0	100.0	96.8
Asphalt	98.7	100.0	98.7	100.0	100.0	100.0	99.7	100.0
Prairie Vegetation	89.6	100.0	89.6	100.0	93.8	15.8	0.0	0.0
Shadow	100.0	66.7	100.0	66.7	100.0	37.5	100.0	62.4
Water	100.0	100.0	100.0	100.0	100.0	100.0	100.0	100.0
Evergreen Canopy	88.9	21.2	91.7	23.7	70.8	44.7	69	44.7
Deciduous Canopy	82.1	99.3	83.9	99.5	81.6	98.9	81.3	89.8
White Roof	100.0	100.0	100.0	100.0	100.0	100.0	89.5	94.6
Brown Roof	100.0	100.0	100.0	100.0	100.0	100.0	100.0	100.0

Recreational area (2) contained a large proportion of continuous vegetation. *Evergreen cano*py was classified with poor reliability by all classifiers. ISODATA was unable to distinguish between *prairie vegetation* and *grassland* classes. SAM classified the sunny sides of several deciduous tree crowns as prairie grass.

CHAPTER 6

CONCLUSIONS

The objective of this study was to understand the usefulness of hyperspectral VNIR bands in classifying urban features. Twenty four LULC maps were derived from six study areas and four classification methods. Two hypotheses were developed for this research. The first hypothesis was the following:

Spectral information from AISA+ sensor's VNIR bands can be utilized to classify urban LULC from Level I through Level III, of a modified Anderson's classification, with accuracy of 80% or greater.

Based on the training and test samples used in this study, the first hypothesis is accepted except in commercial areas that contained a large proportion of artificial features with mixed spatial arrangement. All the study areas except commercial, using SAM and ISODATA, were classified with more than 80% overall accuracy for Level I through Level III urban LULC. MLC and ECHO consistently achieved more than the hypothesized accuracy for all study areas. However, the confidence in the accuracy values, as indicated by kappa statistic, ranged from 76% - 96%. More than 80% kappa value usually indicates high reliability of classification, and ECHO was the only classifier that was successful (> 80%) for both accuracy and kappa values in all the study areas except recreational area (2).

Lower accuracy of Level III classes in most study areas was particularly evident. At two meter spatial resolution, it was found that several Level III classes such as cement sidewalks or

gravel paths were resolved neither entirely within a single pixel nor occupied two pixels. Especially in scenes where object boundaries occurred frequently, there was a mixing of Level III classes in the boundary pixels. Overall, VNIR bands from AISA+ hyperspectral data can be utilized for LULC classification for most Level I through Level III LULC classes. However, more advanced techniques such as object oriented classification or neural network classification will be explored in future research to address deficiencies.

Table 13

Percentage difference between classifiers in terms of overall accuracy.

Classifier	Com (1)	Com (2)	Res (1)	Res (2)	Rec (1)	Rec (2)
Most Accurate	1.4	1.1	5.2	0.4	0.8	0.4
	7.4	14.2	0.8	0.6	6.7	1.1
Least Accurate	10.9	4.3	0.7	2.4	4.4	1.8
Range	19.7	19.6	6.7	3.4	11.9	3.3

The second hypothesis that was developed for this research was:

ISODATA, ECHO, MLC, and SAM will perform differently when classifying complex urban scenes but will perform in similar manner when classifying homogeneous scenes.

A scene was considered complex if pixel to pixel (neighboring pixels) class variability was high. By this definition, commercial area (1) and residential area (1) were considered most complex and residential area (2) and recreational area (2) were considered least complex.

As evident from Figure 33 and Table 6, between the classifiers, the overall classification accuracies were similar for residential area (2) and recreational area (2). This is indicated by the distance between classifiers in Table 13, where the least complex study areas show ranges of 3.4% and 3.3% respectively, with small inter-classifier difference in accuracy. By this analysis, the second part of the hypothesis that the classifiers will perform similarly in homogeneous scenes is validated.

However, while the inter-classifier difference and range between lowest and highest accuracies are large in commercial area (1), they are moderate in residential area (1). The first part of the hypothesis that the classifiers will perform differently in complex scenes, is accepted with caution, pending replication of analysis on other urban study areas. From this research it is evident that Level I through Level III urban LULC classification using AISA+ data produces measurable results that may be expanded to include the complete extent of Terre Haute, Indiana. Further analysis of hyperspectral data will be required to identify feature specific "best bands" that can be used for targeted classification of urban features.

6.1 Need for Hyperspectral Remote Sensing

Remote sensing technology allows geographers to monitor earth objects and understand the spatial relationships between those objects. Due to increasing urbanization in the U.S. (Auch et al. 2004), there is a need for efficient, repetitive, and inexpensive monitoring of urban areas. For example, we are pressed to answer questions such as: Where are the locations of damaged infrastructure? What materials are they made up of? Is the vegetation near residential areas fire prone? Where are energy inefficient buildings located? Where are the sources of pollution? How much area has impervious surface materials leading to rainwater runoff and loss that also contributes to damage by flooding? What neighborhoods have excessive water usage in lawn care? Identification, classification, and mapping of urban features are the first steps towards answering such questions.

Human created urban landscapes are complex, owing to the variation in types of materials and the intimate spatial arrangement of objects. Moderate and low resolution sensors are able to differentiate LULC at a general extent that cover Anderson's (1976) Level I and Level II classes.

High resolution data are needed for urban mapping, as most LULC objects have relatively small extents. Currently the United States Department of Agriculture (USDA), through its National Agricultural Imagery Program (NAIP), acquires one meter VNIR imagery in four bands during the agricultural growing season every year. NAIP's total cost for Indiana was $480,522.00 in 2008. Both Indiana Department of Transportation (INDOT) and Farm Service Agency (FSA) contributed towards the program's expenditure. This data is freely available for public use (ISDP 2009).

Hyperspectral sensors are expensive and processing and storing statewide hyperspectral data is impractical. However, hyperspectral data can be extremely useful in identifying subtle variations between features in specific wavelengths that is especially useful in urban environments. Bands that explain the most variation can be identified through PCA or MNF processing of hyperspectral data. Large eigenvalues can be used to indicate high variation, allowing for the selection of the best individual bands. Relatively inexpensive filters for specific narrow hyperspectral wavelengths bands can be used with aerial photography for targeted acquisition of features, or in combination with the NAIP color infrared (CIR) photographs. This practice has been pioneered by the Agricultural Research Service (ARS-USDA) scientists in Weslaco, Texas (Yang et al. 2008) for vegetation related studies, and should be repeated in modified form for urban LULC studies.

This LULC research showed that hyperspectral data contain information for accurate classification of many urban features. However, for Level IV classes, meter or sub-meter spatial resolution will be needed. This was evident from classes such as cement sidewalks in residential neighborhoods, which, by virtue of being one meter wide, did not classify with the spatial coherence that is required for useful mapping. It is also observed that features in the lowest layer such as lawns, sidewalks, and roads were obscured by tree canopy or shadow. For LULC mapping,

and generation of multilayered GIS, it will be essential to acquire data both in summer and "leaf-off" seasons. However, hyperspectral remote sensing will be most effective if used to identify best bands for classifying features of interest that may be used most effectively in combination with aerial photography or high resolution satellite data. Much research needs to be conducted in improving the extraction of urban information from hyperspectral data. Some future research questions are discussed in the next section.

6.2 Future Research and Recommendations

Classification Scheme

USGS (Anderson et al. 1976) LULC classification scheme for use with remote sensor data has been most widely used in LULC research, as the classification standard. With the availability of high resolution data, more classification is conducted at Level III and Level IV. Cautious modifications using extensions are often made to suit the underlying environment. However, this classification schema is mostly based on function, as indicated by the underlying feature. With hyperspectral data, it is possible to distinguish objects based on their material composition. For example, a shingle roof class under the USGS classification will need expansion on the basis of material type. Therefore, development of new or modified urban classification schema for hyperspectral data will need exploration.

Remote Sensing of Urban Features

This research has raised several questions in relation to optimum spatial resolution for urban features. Better spectral resolution alone does not improve LULC classification. The two meter spatial resolution used in this research was ideal for classes with tree crowns and rooftops.

However, urban features such as narrow gravel paths, sidewalks, and vehicular traffic neither resolved nor could they be excluded. Future research needs to entail a thorough research on identifying optimum spatial resolution for urban features, using both field measurements and sub-meter orthophotgraphs. It is also recommended that data acquisition be coincidental with annual NAIP flight campaign both in the summer and early spring seasons. It is further recommended that best bands for specific features be identified and documented for use in application specific urban studies.

Urban Spectral Libraries

The next step for this research will be to select best bands for specific urban features from AISA+ data, and create a library. More widely, it will be useful to develop field and sensor based spectral libraries for urban features in general, and maintain a shared database. Since urban materials are varied, a nationwide initiative is needed where institutions such as universities can, based on certain standards, add spectral signatures of materials to the library. This will allow long term cost reduction in monitoring and mapping of urban areas by administrative agencies.

Classification Methods

In this research, the usefulness of segment based classification method such as ECHO was highlighted. Under the conditions SAM performed relatively poorly. However, it was evident from inspecting the classification results that more research needs to be conducted using SAM. Rigorous identification and use of pure endmembers for application in SAM will be needed. As mentioned previously, the development of spectral libraries will be valuable for fully utilizing the potential of such classification methods.

REFERENCES

Aardt J. A. N. and R. H. Wynne. (2007). Examining pine spectral separability using hyperspectral data from an airborne sensor: An extension of field-based results. *International Journal of Remote Sensing,* 28**,** 431-436.

Land-Based Classification Standards. Online, *http://www.planning.org/LBCS*. American Planning Association: Chicago, Illinois.

Anderson J. R., E. E. Hardy, J. T. Roach and R. E. Witmer. (1976). A land use and land cover classification system for use with remote sensor data. In *USGS Paper 964*, 28. Washington.

Artigas F. J. and J. S. Yang. (2005). Hyperspectral remote sensing of marsh species and plant vigour gradient in the New Jersey Meadowlands. *International Journal of Remote Sensing,* 26**,** 5209-5220.

Auch R., J. Taylor and W. Acecedo. (2004). Urban growth in American cities: glimpses of U. S. urbanization. *USGS Circular,* 1252.

Bajcsy P. and P. Groves. (2004). Methodology of hyperspectral band selection. *Journal of Photogrammetry and Remote Sensing,* 70**,** 793-802.

Bakker W. H. and K. S. Schmidt. (2002). Hyperspectral edge filtering for measuring homogeneity of surface cover types. *Journal of Photogrammetry and Remote Sensing,* 56**,** 246-256.

Bassani C., R. M. Cavalli, F. Cavalcante, V. Cuomo, A. Palombo, S. Pascicci and S. Pignatti. (2007). Deterioration status of asbestos-cement roofing sheets assessed by analyzing hyperspectral data. *Remote Sensing of Environment,* 109**,** 361-378.

Ben-Dor E., R. Lugassi, R. Richter, H. Saaroni and A. Muller. (2001). Quantitative approach for monitoring the urban heat island effects, using hyperspectral remote sensing. In *IEEE International Geoscience and Remote Sensing Symposium (IGARSS '01)*, 2541-2546.

Biehl L. (2001). MultiSpec. 5.2001, Purdue Research Foundation, West Lafayette, Indiana.

Biehl L. and D. Landgrebe. (2002). MultiSpec - a tool for multispectral-hyperspectral image data analysis. *Computers and Geosciences,* 28**,** 1153-1159.

Buddenbaum H., M. Schlerf and J. Hill. (2005). Classification of coniferous tree species and age classes using hyperspectral data and geostatistical methods. *International Journal of Remote Sensing,* 26**,** 5453-5465.

Carlson T. (2003). Applications of remote sensing to urban problems. *Remote Sensing of Environment,* 86**,** 273-274.

Cavalli R. M., L. Fusilli, S. Pascucci, S. Pignatti and F. Santini. (2008). Hyperspectral sensor data capability for retrieving complex urban land cover in comparison with multispectral data: Venice City case study (Italy). *Sensors,* 8**,** 3299-3320.

Cidell J. (2009). Building Green: The Emerging Geography of LEED-Certified Buildings and Professionals. In *Professional Geographer*, 200-215.

Clapham Jr. W. B. (2003). Continuum-based classification of remotely sensed imagery to describe urban sprawl on a watershed scale. *Remote Sensing of Environment,* 86**,** 322-340.

Congalton R. G. (1991). A review of assessing the accuracy of classifications of remotely sensed data. *Remote Sensing of Environment,* 37**,** 35-46.

Cowen D. J. and J. R. Jensen. (1998). Extraction and modeling of urban attributes using remote sensing technology. In *People and Pixels: Linking Remote Sensing and Social Science,* eds. D. Liverman, E. F. Moran, R. R. Rindfuss & P. C. Stern. Washington D. C.: National Academy Press.

DeFries R. S. and J. Cheung-Wai Chan. (2000). Multiple criteria for evaluating machine learning algorithms for land cover classification from satellite data. *Remote Sensing of Environment,* 74**,** 503-515.

Dell'Acqua F., P. Gamba, V. Casella, F. Zucca, J. A. Benediktsson, G. Wilkinson, A. Galli, E. S. Maliverni, G. Jones, D. Greenhill and L. Ripke. (2006). HySenS data exploitation for urban land cover analysis. *Annals of Geophysics,* 49**,** 311-318.

Dell'Acqua F., P. Gamba, A. Ferrari, J. A. Palmason, J. A. Benediktsson and K. Arnason. (2004). Exploiting spectral and spatial information in hyperspectral urban data with high resolution. *IEEE Geoscience and Remote Sensing Letters,* 1**,** 322-326.

Dell'Acqua F., P. Gamba and G. Lisini. (2005). Urban land cover mapping using hyperspectral and multispectral VHR sensors: spatial versus spectral resolution. In *ISPRS Joint Conferences 3rd International Symposium Remote Sensing and Data Fusion Over Urban Areas (URBAN 2005) / 5th International Symposium Remote Sensing of Urban Areas (URS 2005),* eds. M. Moeller & E. Wentz.

Dias Nelson. (2001). Forest structure and biomass estimates derived from red edge and water absorption geometry using AVIRIS data. In *Dept. of Geography, Geology, and Anthropology*, 116. Terre Haute, Indiana: Indiana State University.

Ehlers M. (2005). Urban remote sensing: new developments and trends. In *Proceedings of International Symposium Remote Sensing and Data Fusion Over Urban Areas,* eds. M. Moeller & E. Wentz.

ENVI. (2009). ENVI User's Guide. 4.x.

ERDAS. (1999). ERDAS field guide. Atlanta, GA.

Fesenmaier D. R., M. F. Goodchild and S. Morrison. (1979). The spatial structure of the rural urban fringe. *Canadian Geographer,* 23**,** 255-265.

Fisher J. I. and S. J. Goetz. (2001). Considerations in the use of high spatial resolution imagery: an applications research assessment. In *American Society for Photogrammetry and Remote Sensing (ASPRS) Conference Proceedings*. St. Louis, MO.

Foody G. M. (2002). Status of land cover classification accuracy assessment. *Remote Sensing of Environment,* 80**,** 185-201.

Foody G. M, I. M. J. Sargent, P. M. Atkinson and J. W. Williams. (2004). Thematic labelling from hyperspectral remotely sensed imagery: trade-offs in image properties. *International Journal of Remote Sensing,* 25**,** 2337-2363.

Gatrell J. D. and R. R. Jensen. (2008). Sociospatial applications of remote sensing in urban environments. *Geography Compass,* 2**,** 728-743.

Gong P. and P. J. Howarth. (1990). The use of structural information for improving land-cover classification accuracies at the rural-urban fringe. *Photogrammetric Engineering and Remote Sensing,* 56**,** 67-73.

Goodchild M. F. (1997). Towards a geography of geographic informaton in a digital world. *Computers, Environment and Urban Systems,* 21**,** 377-391.

Goodchild M. F. (2001). The digital city: inventory and prospect. In *Geoinformatics: 2001 International Conference Proceedings,* 248–257. Wuhan: Publishing House of Surveying and Mapping.

Green A. A., M. Berman, P. Switzer and M. D. Craig. (1988). A transformation for ordering multispectral data in terms of image quality with implications for noise removal. *IEEE Transactions on Geoscience and Remote Sensing,* 26**,** 65-74.

Guo B., R. I. Damber, S. R. Gunn and J. D. B. Nelson. (2008). A fast separability-based feature-selection method for high dimensional remotely sensed image classification. *Pattern Recognition,* 41**,** 4653-4662.

Hardin P. J. and R. R. Jensen. (2007). The effect of urban leaf area on summertime urban surface kinetic temperatures: A Terre Haute case study. *Urban Forestry and Urban Greening,* 6**,** 63-72.

Heiden U., K. Segl, S. Roessner and Hermann Kauffman. (2007). Determination of robust spectral features for identification of urban surface materials in hyperspectral remote sensing data. *Remote Sensing of Environment,* 111**,** 537-552.

Herold M. (2003). The spatiotemporal form of urban growth: measurement, analysis and modeling. *Remote Sensing of Environment,* 86**,** 286-302.

Herold M., M. E. Gardner, B. C. Hadley and D. A. Roberts. (2002). The spectral dimension in urban land cover mapping from high resolution optical remote sensing data. In *Proceedings of the 3rd Symposium on Remote Sensing of Urban Areas*. Istanbul, Turkey.

Herold M., M. E. Gardner and D. A. Roberts. (2003a). Spectral resolution requirements for urban mapping areas. *IEEE Transactions on Geoscience and Remote Sensing,* 41**,** 1907-1919.

Herold M., N. C. Goldstein and K. C. Clarke. (2003b). The spatiotemporal form of urban growth: measurement, analysis, and modeling. *Remote Sensing of Environment,* 86**,** 286-302.

Herold M., D. A. Roberts, M. E. Gardner and P. E. Dennison. (2004). Spectrometry for urban area remote sensing - development and analysis of a spectral library from 350 to 2400 nm. *Remote Sensing of Environment,* 91**,** 304-319.

Ifarraguerri A. and C. Chang. (2000). Unsupervised hyperspectral image analysis with projection pursuit. *IEEE Transactions on Geoscience and Remote Sensing,* 38**,** 2529-2538.

Irwin E. G., N. E. Bockstael and H. J. Cho. (2006). Measuring and modeling urban sprawl: data, scale, and spatial dependencies. In *Proceesings of 53rd Annual North American Regional Science Association Meetings of the Regional Science Association International*. Toronto, Canada.

ISDP. (2009). *2008 National Agriculture Imagery Program* Indiana Spatial Data Portal, Indiana University. *http://www.indiana.edu/~gisdata/statewide/08naip.html*.

Jeer S. (1999). Land-Based Classification Standards - Federal role. In *APA National Planning Conference,* ed. American Planning Association.

Jeer S. (2006). Land-Based Classification Standards. *http://myapa.planning.org/LBCS*.

Jensen J. R. (2005). *Introductory Digital Image Processing - A Remote Sensing Perspective*. Upper Saddle River, New Jersey: Prentice Hall.

Jensen J. R. (2007). *Remote Sensing of Environment: An Earth Resource Perspective*. New Jersey: Prentice Hall.

Jensen J. R. and D. J. Cowen. (1999). Remote sensing of urban/suburban infrastructure and socio-economic attributes. *Photogrammetric Engineering and Remote Sensing,* 65**,** 611-622.

Jensen J. R., B. C. Hadley, J. A. Tullis, J. Gladden, E. Nelson, S. Riley, T. Fillippi and M. Pendergast. (2003a). Hyperspectral analysis of hazardous waste sites on the Savannah River site in 2002. *Westinghouse Savannah River Company: Aiken, WSRC-TR-2003-00275*.

Jensen J. R., M. W. Jackson and V. Lulla. (2008). Single line correction method to remove aircraft roll errors in hyperspectral imagery. *Journal of Applied Remote Sensing,* 2**,** 1-10.

Jensen J. R. and D. L. Toll. (1982). Detecting residential land use development at the urban fringe. *Photogrammetric Engineering and Remote Sensing,* 48**,** 629-643.

Jensen R. R. (2000). Measurement, comparison, and use of remotely derived leaf area index predictors. In *Department of Geography*. Gainsville: University of Florida.

Jensen R. R., J. R. Boulton and B. T. Harper. (2003b). The relationship between urban leaf area and household energy usage in Terre Haute, Indiana, U.S. *Journal of Arboriculture,* 29**,** 226-230.

Jensen R. R., J. R. Boulton and B. T. Harper. (2005). The relationship between urban leaf area and summertime household energy use. In *Geo-spatial Technologies in Urban Environments,* eds. R. R. Jensen, J. D. Gatrell & D. McLean. Springer.

Jensen R. R., P. J. Hardin, M. Bekker, D. A. Farnes, V. Lulla and A. Hardin. (2009). Modeling urban leaf area index with AISA+ hyperspectral data. *Applied Geography,* 29**,** 320-332.

Jensen R. R., P. Mausel, N. Dias, R. Gonser, C. Yang, J. H. Everitt and R. S. Fletcher. (2007). Spectral analysis of coastal vegetation and land cover using AISA+ hyperspectral data. *Geocarto International,* 22**,** 17-28.

Keshava N. (2001). Best bands selection for detection in hyperspectral processing. In *Proceedings of IEEE International Conference on Acoustics, Speech and Signal Processing*, 3149-3152. Salt Lake City, UT: ICASSP'01.

Kettig R. L. and D. Landgrebe. (1976). Classification of multispectral image data by extraction and classification of homogeneous objects. *IEEE Transactions on Geoscience and Electronics,* GE-14**,** 19-26.

Kontoes C. C. and V. Raptis. (2000). The potential of kernel classification techniques for land use mapping in urban areas using 5m spatial resolution IRS-1C imagery. *International Journal of Remote Sensing,* 21**,** 3145-3151.

Koponen S., J. Pulliainen, K. Kallio and M. Hallikainen. (2002). Lake water quality classification with airborne hyperspectral spectrometer and simulated MERIS data. *Remote Sensing of Environment,* 79**,** 51-59.

Landgrebe D. (1998). Information extraction principles and methods for multispectral and hyperspectral image data. In *Information Processing for Remote Sensing,* ed. C. H. Chen. River Edge, New Jersey: World Scientific Publishing Co.

Landgrebe D. (1999). Some fundamentals and methods for hyperspectral image data analysis. In *SPIE Photonics*. San Jose, California.

Landgrebe D. (2002). Hyperspectral image data analysis as a high dimensional signal problem. *IEEE Signal Processing Magazine,* 19**,** 17-28.

Landgrebe D. and L. Biehl. (2001). An introduction to MultiSpec. Purdue University.

Li G. and Q. Weng. (2005). Using Landsat ETM+ imagery to measure population density in Indianapolis, Indiana, USA. *Photogrammetric Engineering and Remote Sensing,* 71**,** 947-958.

Li Y., P. Mausel, Y. Wu, E. Moran and E. Brondizio. (1994). Discrimination between advanced secondary forest succession and mature moist forest near Altamira, Brazil using Landsat TM data. In *Proceedings of the American Society for Photogrammetry and Remote Sensing*. Reno, Nevada.

Lillesand T. M., R. W. Kiefer and J. W. Chipman. (2008). *Remote sensing and Image Interpretation*. John Wiley and Sons, Inc.

Lo C. P. and E. Noble. (1990). Detailed urban land-use and land-cover mapping using large format camera photographs: an evaluation. *Photogrammetric Engineering and Remote Sensing,* 56**,** 197-206.

Lo C. P., D. A. Quattrochi and J. C. Luvall. (1997). Application of high-resolution thermal infrared remote sensing and GIS to assess the urban heat island effect *International Journal of Remote Sensing,* 18**,** 287-304.

Lu D., P. Mausel, M. Batistella and E. Moran. (2004a). Comparison of land cover classification methods in the Brazilian Amazon basin. *Photogrammetric Engineering and Remote Sensing,* 70**,** 723-731.

Lu D. and Q. Weng. (2004b). Spectral mixture analysis of the urban landscape in Indianapolis with Landsat ETM+ imagery. *Photogrammetric Engineering and Remote Sensing,* 70**,** 1053-1062.

Lu D. and Q. Weng. (2005). Urban classification using full spectral information of Landsat ETM+ imagery in Marion County, Indiana. *Photogrammetric Engineering and Remote Sensing,* 71**,** 1275-1284.

Lu D. and Q. Weng. (2006). Use of impervious surface in urban land use classification. *Remote Sensing of Environment,* 102**,** 146-160.

Lu D. and Q. Weng. (2007a). A survey of image classification methods and techniques for improving classification performance. *International Journal of Remote Sensing,* 28**,** 823-870.

Lu S., K. Oki, Y Shimizu and K. Omasa. (2007b). Comparison between several feature extraction/classification methods for mapping complicated agricultural land use patches using airborne hyperspectral data *International Journal of Remote Sensing,* 28**,** 963-984.

Lulla V. (2009). Hyperspectral applications in urban geography. In *Geotechnologies and the Environment: Socioeconomic and Planning Applications,* eds. J. D. Gatrell & R. R. Jensen. Heidelberg: Springer-Verlag.

Mäkisara K., M. Meinander and M. Rantasuo. (1993). Airborne Imaging Spectrometer for Applications (AISA). In *International Geoscience and Remote Sensing Symposium (IGRASS '93)*, 479-481.

Masser I. (2000). Managing our urban future - communication. *Journal of Geography,* 2**,** 216-222.

Mausel P., R. R. Jensen, N. Dias, Y. Chenghai, J. H. Everitt, R. S. Fletcher, D. Hockaday and H. DeYoe. (2005). Preliminary spectral assessment of Laguna Madre water features using AISA+ hyperspectral data. In *20th Biennial Workshop on Aerial Photography, Videography, and High Resolution Digital Imagery for Resource Assessment*. Weslaco, Texas.

Mausel P. W., W. J. Kramber and J. K. Lee. (1990). Optimum band selection for supervised classification of multispectral data. *Photogrammetric Engineering and Remote Sensing,* 56**,** 55-60.

Medina M. (2000). Effects of shingle absorptivity, radiant barrier emmissivity, attic ventilation flowrate, and roof slope on performance of radiant barriers. *International Journal of Energy Research,* 24**,** 665-678.

Meinel G., R. Lippold and M. Netzband. (1998). The potential use of new high resolution satellite data for urban and regional planning. In *ISPRS Commission IV Symposium on GIS - Between Visions and Applications,* eds. D. Fritsch, M. Englich & M. Sester, 375-381. Suttgart, Germany.

Moeller M. S. (2005). Remote sensing for the monitoring of urban growth patterns. In *Proceedings of International Symposium Remote Sensing and Data Fusion Over Urban Areas,* eds. M. Moeller & E. Wentz. Tempe, Arizona: ISPRS.

Pal M. and P. Mather. (2003). An assessment of the effectiveness of decision tree methods for land cover classification. *Remote Sensing of Environment,* 86**,** 554-565.

Pekkarinen A. (2002a). Image segment-based spectral features in the estimation of timber volume. *Remote Sensing of Environment,* 82**,** 349-359.

Pekkarinen A. (2002b). A method for the segmentation of very high spatial resolution images of forested landscapes. *International Journal of Remote Sensing,* 23**,** 2817-2836.

Pozzi F. and C. Small. (2001). Exploratory analysis of suburban land cover and population density in the U.S.A. In *Proceedings of the IEEE/ISPRS Joint Workshop on Remote Sensing and Data Fusion over Urban Area*. Rome, Italy.

Priestall G., J. Jaafar and A. Duncan. (2000). Extracting urban features from LiDAR digital surface models. *Computers, Environment and Urban Systems,* 24**,** 65-78.

Radeloff V. C., R. B. Hammer and S. I. Stewart. (2005). Rural and suburban sprawl in the U.S. Midwest from 1940 to 2000 and its relation to forest fragmentation. *Conservation Biology,* 19**,** 793-805.

Ridd M. K. (1995). Exploring a V-I-S (vegetation-impervious surface-soil) model for urban ecosystem analysis through remote sensing: comparative anatomy for cities. *International Journal of Remote Sensing,* 16**,** 2165-2185.

Roberts D. A. and M. Herold. (2004). Imaging spectroscopy of urban materials. In *Infrared Spectroscopy in Geochemistry, Exploration and Remote Sensing,* eds. P. King, M. S. Ramsey & G. Swayze, 155-181. London, Ontario: Mineral Association of Canada, Short Course Series.

Sabins F. F. (1997). *Remote Sensing: Principles and Interpretation*. Long Grove, Illinois: Waveland Press Inc.

Segl K., S. Roessner, U. Heiden and H. Kauffman. (2003). Fusion of spectral and shape features for identification of urban surface cover types using reflective and thermal hyperspectral data. *Journal of Photogrammetry and Remote Sensing,* 58**,** 99-112.

Shaban M. A. and O. Dikshit. (2002). Evaluation of the emerging SPOT multispectral and panchromatic data for classification of an urban environment. *International Journal of Remote Sensing,* 23**,** 249-262.

Shah C. A., M. K. Arora and P. K. Varshney. (2004). Unsupervised classification of hyperspectral data: an ICA mixture mode based approach. *International Journal of Remote Sensing,* 25**,** 481-487.

Shippert P. (2003). Introduction to hyperspectral image analysis. *Online Journal of Space Communication, http://satjournal.tcom.ohiou.edu/pdf/shippert.pdf*

Small C. (2002). Multitemporal analysis of urban reflectance. *Remote Sensing of Environment,* 81**,** 427-442.

Small C. (2006). Comparitive analysis of urban reflectance and surface temperature. *Remote Sensing of Environment,* 104**,** 168-189.

Small C. and R. B. Miller. (1999). Monitoring the urban environment from space. In *Proceedings of International Society of Photogrammetry and Remote Sensing,* eds. M. Moeller & E. Wentz. Tempe, Arizona.

SPECIM. (2003). AISA Bandage User's Manual.

Tso B. and P. Mather. (2001). *Classification Methods for Remotely Sensed Data*. New York: Taylor and Francis Ltd.

U.S.Census-Bureau. (2009). Online, *http://quickfacts.census.gov/qfd/states/18/1875428.html.* State and County QuickFacts, US Government Database.

USDC. (1965). Standard land use coding manual, a standard system for identifying and coding land use activities. Urban Renewal Administration, Dept. of Commerce. Washington D.C.

Vaiphasa C. (2006). Consideration of smoothing techniques for hyperspectral remote sensing. *Journal of Photogrammetry and Remote Sensing,* 60**,** 91-99.

Voogt J. A. and T. R Oke. (2003). Thermal remote sensing of urban climates. *Remote Sensing of Environment,* 86**,** 370-384.

Voss M. and R. Sugumaran. (2008). Seasonal effects on tree species classification in an urban environment using hyperspectral data, LiDAR, and an object oriented approach. *Sensors,* 8**,** 3020-3036.

Wiegand N., D. Patterson, N. Zhou, S. Ventura and I. F. Cruz. (2002). Querying heterogeneous land use data: problems and potential. In *National Conference for Digital Government Research*.

Woods Alan J., James M. Omernik, C. Scott Brockman, Timothy D. Gerber, William D. Hosteter and Sandra H. Azevedo. (1998). Ecoregions of Indiana and Ohio. (Map poster and Supplementary Text). U.S. Geological Survey, Reston, VA.

Yang C. C., S. O. Prasher, P. Enright, C. Madramootoo, M. Burgess, P. Goel and I. Callum. (2003). Application of decision tree technology for image classification using remote sensing data. *Agricultural Systems,* 76**,** 1101-1117.

Yang C. and J. H. Everitt. (2007a). Mapping waterhyacinth infestations usnig airborne hyperspectral imagery. In *21st Binennial Workshop on Aerial Photography, Videography, and High Resolution Digital Imagery for Resource Assessment*. Terre Haute, Indiana.

Yang C., J. H. Everitt and J. M. Bradford. (2008). Yield estimation from hyperspectral imagery using spectral angle mapper. *American Society of Agricultural and Biological Engineers,* 51**,** 729-737.

Yang C., J. H. Everitt, R. S. Fletcher, R. R. Jensen and P. Mausel. (2007b). Mapping black mangrove along the south Texas gulf coast using AISA+ hyperspectral imagery. In *21st Biennial Workshop on Aerial Photography, Videography, and High Resolution Digital Imagery for Resource Assessment*. Terre Haute, Indiana.

Ye X., K. Sakai, L. O. Garciano, S. Asada and A. Sasao. (2006). Estimation of citrus yield from airborne hyperspectral images using neural network model. *Ecological Modelling,* 198**,** 426-432.

Zamudio J. A. and W. W. Atkinson. (1990). Analysis of AVIRIS data for spectral discrimination of geologic materials in the Dolly Varden mountains. In *Proceedings of the Second AVIRIS Conference*, 162-66. NASA JPL.

Zhang W. and G. M Foody. (2001). Fully-fuzzy supervised classification of suburban land cover from remotely sensed imagery: statistical and artificial neural network approaches. *International Journal of Remote Sensing,* 22**,** 615-628.

Zhang Y. (1999). A new merging method and its spectral and spatial effects. *International Journal of Remote Sensing,* 20**,** 2003-2014.

Zhang Y. (2001). Detection of urban housing development by fusing multisensor satellite data and performing spatial feature post-classification. *International Journal of Remote Sensing,* 22**,** 3339-3355.

Zhou B. (2007). Application of hyperspectral remote sensing in detecting and mapping Sericea Lespedeza in Missouri. In *Department of Geography*, 81. Columbia: University of Missouri-Columbia.

Zhu M., N. Jiang, J. Li, J. Xu and Y. Fan. (2006). The effects of sensor spatial resolution and changing grain size on fragmentation indices in urban landscape. *International Journal of Remote Sensing,* 27**,** 4791-4805.

APPENDIX A: ERROR MATRICES

The following tables contain error matrices resulting from accuracy assessment conducted on six study areas. PA is producer's accuracy, reliability accuracy is also known as user's accuracy, and kappa statistic indicates the confidence in the accuracy assessment.

Table 14

Commercial (1) error matrix for MLC classification results.

Class Name	PA (%)	Tree Canopy	Grass	Asphalt	Concrete	Gravel	Red Roof	Brown Roof	White Roof A	White Roof B	Black Roof	Gray Roof	Shadow	Red Pavement	Open Soil
Tree Canopy	98.5	64	1	0	0	0	0	0	0	0	0	0	0	0	0
Grass	97.9	5	228	0	0	0	0	0	0	0	0	0	0	0	0
Asphalt	83.8	0	0	269	49	0	0	0	0	0	0	3	0	0	0
Concrete	87.6	0	0	17	333	26	0	0	4	0	0	0	0	0	0
Gravel	43.6	0	0	9	13	17	0	0	0	0	0	0	0	0	0
Red Roof	100.0	0	0	0	0	0	24	0	0	0	0	0	0	0	0
Brown Roof	100.0	0	0	0	0	0	0	31	0	0	0	0	0	0	0
White Roof A	100.0	0	0	0	0	0	0	0	131	0	0	0	0	0	0
White Roof B	42.8	0	0	10	6	21	0	0	81	101	0	17	0	0	0
Black Roof	78.6	0	0	10	0	0	0	0	0	0	136	0	27	0	0
Gray Roof	90.0	0	0	2	0	0	0	0	0	1	2	45	0	0	0
Shadow	100.0	0	0	0	0	0	0	0	0	0	0	0	46	0	0
Red Pavement	100.0	0	0	0	0	0	0	0	0	0	0	0	0	8	0
Open Soil	70.0	0	2	3	5	0	0	0	0	0	2	0	0	0	28
TOTAL		69	231	320	406	64	24	31	216	102	140	65	73	8	28
Reliability Accuracy (%)		92.8	98.7	84.1	82.0	26.6	100.0	100.0	60.6	99.0	97.1	69.2	63.0	100.0	100.0
OVERALL CLASS PERFORMANCE = 82.2%															
Kappa Statistic (X100) = 79.6%. Kappa Variance = 0.000106															

Table 15

Commercial (1) error matrix for ECHO classification results.

Class Name	PA (%)	Tree Canopy	Grass	Asphalt	Concrete	Gravel	Red Roof	Brown Roof	White Roof A	White Roof B	Black Roof	Gray Roof	Shadow	Red Pavement	Open Soil
Tree Canopy	98.5	64	1	0	0	0	0	0	0	0	0	0	0	0	0
Grass	99.1	2	231	0	0	0	0	0	0	0	0	0	0	0	0
Asphalt	90.7	0	0	291	28	0	0	0	0	0	0	2	0	0	0
Concrete	87.9	0	0	16	334	26	0	0	4	0	0	0	0	0	0
Gravel	43.6	0	0	9	13	17	0	0	0	0	0	0	0	0	0
Red Roof	100.0	0	0	0	0	0	24	0	0	0	0	0	0	0	0
Brown Roof	100.0	0	0	0	0	0	0	31	0	0	0	0	0	0	0
White Roof A	100.0	0	0	0	0	0	0	0	131	0	0	0	0	0	0
White Roof B	41.9	0	0	10	6	21	0	0	83	99	0	17	0	0	0
Black Roof	78.6	0	0	10	0	0	0	0	0	0	136	0	27	0	0
Gray Roof	90.0	0	0	2	0	0	0	0	0	1	2	45	0	0	0
Shadow	100.0	0	0	0	0	0	0	0	0	0	0	0	46	0	0
Red Pavement	100.0	0	0	0	0	0	0	0	0	0	0	0	0	8	0
Open Soil	70.0	0	2	3	5	0	0	0	0	0	2	0	0	0	28
TOTAL		66	234	341	386	64	24	31	218	100	140	64	73	8	28
Reliability Accuracy (%)		97.0	98.7	85.3	86.5	26.6	100.0	100.0	60.1	99.0	97.1	70.3	63.0	100.0	100.0
OVERALL CLASS PERFORMANCE = 83.6%															
Kappa Statistic (X100) = 81.2%. Kappa Variance = 0.000099															

Table 16

Commercial (1) error matrix for SAM classification results.

Class Name	PA (%)	Tree Canopy	Grass	Asphalt	Concrete	Gravel	Red Roof	Brown Roof	White Roof A	White Roof B	Black Roof	Gray Roof	Shadow	Red Pavement	Open Soil
Tree Canopy	72.3	47	18	0	0	0	0	0	0	0	0	0	0	0	0
Grass	100.0	0	233	0	0	0	0	0	0	0	0	0	0	0	0
Asphalt	22.1	0	0	71	157	32	0	0	0	3	8	14	27	0	9
Concrete	58.2	0	0	9	221	146	0	0	0	0	0	0	0	0	4
Gravel	69.2	0	0	0	12	27	0	0	0	0	0	0	0	0	0
Red Roof	100.0	0	0	0	0	0	24	0	0	0	0	0	0	0	0
Brown Roof	100.0	0	0	0	0	0	0	31	0	0	0	0	0	0	0
White Roof A	75.6	0	0	0	0	0	0	0	99	32	0	0	0	0	0
White Roof B	66.5	0	0	2	0	33	1	0	43	157	0	0	0	0	0
Black Roof	87.3	0	0	0	0	0	0	0	0	0	151	0	22	0	0
Gray Roof	74.0	0	0	0	0	0	0	0	0	12	0	37	1	0	0
Shadow	87.0	3	0	0	0	0	0	0	0	0	3	0	40	0	0
Red Pavement	100.0	0	0	0	0	0	0	0	0	0	0	0	0	8	0
Open Soil	97.5	0	0	0	1	0	0	0	0	0	0	0	0	0	39
TOTAL		50	251	82	391	238	25	31	142	204	162	51	90	8	52
Reliability Accuracy (%)		94.0	92.8	86.6	56.5	11.3	96.0	100.0	69.7	77.0	93.2	72.5	44.4	100.0	75.0
OVERALL CLASS PERFORMANCE = 66.7%															
Kappa Statistic (X100) = 62.5%. Kappa Variance = 0.000156															

Table 17

Commercial (2) error matrix for MLC classification results.

Class Name	PA (%)	Tree Canopy	Grass	Asphalt A	Asphalt B	Cement	Gravel	White Roof A	White Roof B	Black Roof	Shadow	Red Roof	Brown Roof
Tree Canopy	98.9	178	0	0	0	0	0	0	0	0	1	1	0
Grass	95.2	13	257	0	0	0	0	0	0	0	0	0	0
Asphalt A	89.4	0	0	169	0	17	0	0	3	0	0	0	0
Asphalt B	80.6	0	0	36	195	0	0	0	11	0	0	0	0
Cement	64.6	0	0	59	0	155	8	0	18	0	0	0	0
Gravel	100.0	0	0	0	0	0	96	0	0	0	0	0	0
White Roof A	98.7	0	0	0	0	1	0	149	0	0	1	0	0
White Roof B	94.3	0	0	0	0	5	0	0	150	0	0	4	0
Black Roof	100.0	0	0	0	0	0	0	0	0	46	0	0	0
Shadow	93.5	0	0	0	0	0	0	0	3	0	43	0	0
Red Roof	100.0	0	0	0	0	0	0	0	0	0	0	36	0
Brown Roof	100.0	0	0	0	0	0	0	0	0	0	0	0	23
TOTAL		191	257	264	195	178	104	149	185	46	45	41	23
Reliability Accuracy (%)		93.2	100.0	64.0	100.0	87.1	92.3	100.0	81.1	100.0	95.6	87.8	100.0
OVERALL CLASS PERFORMANCE = 89.2%													
Kappa Statistic (X100) = 87.9%. Kappa Variance = 0.000073													

Table 18

Commercial (2) error matrix for ECHO classification results.

Class Name	PA (%)	Tree Canopy	Grass	Asphalt A	Asphalt B	Cement	Gravel	White Roof A	White Roof B	Black Roof	Shadow	Red Roof	Brown Roof
Tree Canopy	99.4	179	0	0	0	0	0	0	0	1	0	0	0
Grass	96.7	9	261	0	0	0	0	0	0	0	0	0	0
Asphalt A	98.6	0	0	137	0	0	0	0	2	0	0	0	0
Asphalt B	82.7	0	0	26	177	0	0	0	11	0	0	0	0
Cement	74.1	0	0	4	0	40	6	0	4	0	0	0	0
Gravel	99.0	0	0	0	0	0	95	0	1	0	0	0	0
White Roof A	98.7	0	0	0	0	0	0	149	1	0	1	0	0
White Roof B	95.0	0	0	2	0	1	0	0	151	0	4	1	0
Black Roof	84.8	0	0	0	1	0	0	0	0	39	6	0	0
Shadow	84.8	0	0	0	1	0	0	0	6	0	39	0	0
Red Roof	100.0	0	0	0	0	0	0	0	0	0	0	36	0
Brown Roof	100.0	0	0	0	0	0	0	0	0	0	0	0	23
TOTAL		188	261	169	179	41	101	149	176	40	50	37	23
Reliability Accuracy (%)		95.2	100.0	81.1	98.9	97.6	94.1	100.0	85.8	97.5	78.0	97.3	100.0
OVERALL CLASS PERFORMANCE = 93.8%													
Kappa Statistic (X100) = 92.9%. Kappa Variance = 0.000053													

Table 19

Commercial (2) error matrix for SAM classification results.

Class Name	PA (%)	Tree Canopy	Grass	Asphalt A	Asphalt B	Cement	Gravel	White Roof A	White Roof B	Black Roof	Shadow	Red Roof	Brown Roof
Tree Canopy	92.8	167	12	0	0	0	0	0	0	0	1	0	0
Grass	93.0	19	251	0	0	0	0	0	0	0	0	0	0
Asphalt A	63.5	0	0	120	5	32	0	0	32	0	0	0	0
Asphalt B	92.6	0	0	3	224	0	0	0	10	5	0	0	0
Cement	72.9	0	0	23	0	175	12	0	30	0	0	0	0
Gravel	100.0	0	0	0	0	0	96	0	0	0	0	0	0
White Roof A	75.5	0	0	0	0	0	10	114	27	0	0	0	0
White Roof B	39.0	0	0	94	0	3	0	0	62	0	0	0	0
Black Roof	87.0	0	0	0	1	0	0	0	0	40	5	0	0
Shadow	65.2	0	0	0	13	0	0	0	0	3	30	0	0
Red Roof	94.4	0	0	0	0	0	0	0	0	2	0	34	0
Brown Roof	65.2	0	0	0	0	0	0	0	0	8	0	0	15
TOTAL		186	263	240	243	210	118	114	161	58	36	34	15
Reliability Accuracy (%)		89.8	95.4	50.0	92.2	83.3	81.4	100.0	38.5	69.0	83.3	100.0	100.0

OVERALL CLASS PERFORMANCE = 79.1%

Kappa Statistic (X100) = 76.5%. Kappa Variance = 0.000124

Table 20

Residential (1) error matrix for MLC classification results.

Class Name	PA (%)	Tree Canopy	Asphalt	Water (pool)	Beige Roof	Gravel	Brown Roof	White Roof	Grass	Shadow
Tree Canopy	81.0	1074	0	2	0	2	3	0	199	46
Asphalt	98.9	0	185	0	0	1	0	0	0	1
Water (pool)	78.7	0	0	37	0	0	1	3	0	6
Beige Roof	100.0	0	0	0	26	0	0	0	0	0
Gravel	86.3	0	4	0	0	44	0	0	3	0
Brown Roof	100.0	0	0	0	0	0	49	0	0	0
White Roof	96.7	0	2	1	0	1	0	119	0	0
Grass	89.2	11	1	0	0	8	0	0	165	0
Shadow	97.5	3	0	0	0	0	0	0	0	116
TOTAL		1088	192	40	26	56	53	122	367	169
Reliability Accuracy (%)		98.7	96.4	92.5	100.0	78.6	92.5	97.5	45.0	68.6
OVERALL CLASS PERFORMANCE = 85.9%										
Kappa Statistic (X100) = 78.1%. Kappa Variance = 0.000139										

Table 21

Residential (1) error matrix for ECHO classification results.

Class Name	PA (%)	Tree Canopy	Asphalt	Water (pool)	Beige Roof	Gravel	Brown Roof	White Roof	Grass	Shadow
Tree Canopy	93.4	1239	0	0	0	0	0	0	86	1
Asphalt	100.0	0	187	0	0	0	0	0	0	0
Water (pool)	12.8	0	0	6	16	0	7	18	0	0
Beige Roof	100.0	0	0	0	26	0	0	0	0	0
Gravel	82.4	0	3	0	0	42	0	1	5	0
Brown Roof	81.6	0	0	0	4	0	40	0	5	0
White Roof	94.3	0	6	0	1	0	0	116	0	0
Grass	84.3	21	0	0	0	8	0	0	156	0
Shadow	94.1	7	0	0	0	0	0	0	0	112
TOTAL		1267	196	6	47	50	47	135	252	113
Reliability Accuracy (%)		97.8	95.4	100.0	55.3	84.0	85.1	85.9	61.9	99.1
OVERALL CLASS PERFORMANCE = 91.1%										
Kappa Statistic (X100) = 85.0%. Kappa Variance = 0.000104										

Table 22

Residential (1) error matrix for SAM classification results.

Class Name	PA (%)	Tree Canopy	Asphalt	Water (pool)	Beige Roof	Gravel	Brown Roof	White Roof	Grass	Shadow
Tree Canopy	93.4	1239	0	0	0	0	0	0	86	1
Asphalt	100.0	0	187	0	0	0	0	0	0	0
Water (pool)	12.8	0	0	6	16	0	7	18	0	0
Beige Roof	100.0	0	0	0	26	0	0	0	0	0
Gravel	82.4	0	3	0	0	42	0	1	5	0
Brown Roof	81.6	0	0	0	4	0	40	0	5	0
White Roof	94.3	0	6	0	1	0	0	116	0	0
Grass	84.3	21	0	0	0	8	0	0	156	0
Shadow	94.1	7	0	0	0	0	0	0	0	112
TOTAL		1084	190	50	26	60	50	124	355	174
Reliability Accuracy (%)		98.5	97.4	64.0	100.0	73.3	96.0	95.2	45.4	66.7
OVERALL CLASS PERFORMANCE = 85.1%										
Kappa Statistic (X100) = 76.9%. Kappa Variance = 0.000144										

Table 23

Residential (2) error matrix for MLC classification results.

Class Name	PA (%)	Tree Canopy	Water	Grass	Cement	Tennis Court	Tennis Court	Gray Roof	Brown Roof	Beige Roof	Shadow
Tree Canopy	97.1	963	0	0	0	0	0	0	0	0	29
Water	99.9	1	828	0	0	0	0	0	0	0	0
Grass	92.4	41	0	495	0	0	0	0	0	0	0
Cement	95.6	0	22	0	501	0	0	1	0	0	0
Tennis Court (Red)	94.0	0	0	0	0	47	2	0	1	0	0
Tennis Court (Green)	100.0	0	0	0	0	0	47	0	0	0	0
Gray Roof	91.1	0	1	0	0	0	0	484	46	0	0
Brown Roof	100.0	0	0	0	0	0	0	0	24	0	0
Beige Roof	52.0	0	0	0	4	0	0	17	3	26	0
Shadow	98.2	2	0	0	0	0	0	0	0	0	107
TOTAL		1007	851	495	505	47	49	502	74	26	136
Reliability Accuracy (%)		95.6	97.3	100.0	99.2	100.0	95.9	96.4	32.4	100.0	78.7
OVERALL CLASS PERFORMANCE = 95.4%											
Kappa Statistic (X100) = 94.3%. Kappa Variance = 0.000018											

Table 24

Residential (2) error matrix for ECHO classification results.

Class Name	PA (%)	Tree Canopy	Water	Grass	Cement	Tennis Court	Tennis Court	Gray Roof	Brown Roof	Beige Roof	Shadow
Tree Canopy	94.9	941	0	33	0	0	0	0	0	0	18
Water	99.6	0	826	1	0	0	0	2	0	0	0
Grass	99.3	4	0	532	0	0	0	0	0	0	0
Cement	98.9	0	4	2	518	0	0	0	0	0	0
Tennis Court (Red)	100.0	0	0	0	0	50	0	0	0	0	0
Tennis Court (Green)	97.9	0	0	0	0	1	46	0	0	0	0
Gray Roof	76.6	0	0	0	0	0	0	407	124	0	0
Brown Roof	100.0	0	0	0	0	0	0	0	24	0	0
Beige Roof	86.0	0	0	4	3	0	0	0	0	43	0
Shadow	90.8	10	0	0	0	0	0	0	0	0	99
TOTAL		955	830	572	521	51	46	409	148	43	117
Reliability Accuracy (%)		98.5	99.5	93.0	99.4	98.0	100.0	99.5	16.2	100.0	84.6

OVERALL CLASS PERFORMANCE = 94.4%

Kappa Statistic (X100) = 93.2%. Kappa Variance = 0.000021

Table 25

Residential (2) error matrix for SAM classification results.

Class Name	PA (%)	Tree Canopy	Water	Grass	Cement	Tennis Court	Tennis Court	Gray Roof	Brown Roof	Beige Roof	Shadow
Tree Canopy	91.6	909	0	30	0	0	0	0	0	0	53
Water	99.6	0	826	0	0	0	0	3	0	0	0
Grass	97.2	15	0	521	0	0	0	0	0	0	0
Cement	99.0	0	4	0	519	0	0	1	0	0	0
Tennis Court (Red)	100.0	0	0	0	0	50	0	0	0	0	0
Tennis Court (Green)	97.9	0	0	0	0	1	46	0	0	0	0
Gray Roof	66.3	0	0	0	2	0	1	352	165	11	0
Brown Roof	87.5	0	0	0	0	3	0	0	21	0	0
Beige Roof	100.0	0	0	0	0	0	0	0	0	50	0
Shadow	93.6	7	0	0	0	0	0	0	0	0	102
TOTAL		931	830	551	521	54	47	356	186	61	155
Reliability Accuracy (%)		97.6	99.5	94.6	99.6	92.6	97.9	98.9	11.3	82.0	65.8
OVERALL CLASS PERFORMANCE = 92.0%											
Kappa Statistic (X100) = 90.3%. Kappa Variance = 0.000029											

Table 26

Recreational (1) error matrix for MLC classification results.

Class Name	PA (%)	Tree Canopy	Asphalt	Gravel	Grass	Open Soil	Brown Roof	Cement	Play Area	White Roof	Shadow
Tree Canopy	99.0	521	0	0	0	0	0	0	0	0	5
Asphalt	96.9	0	62	0	0	0	0	0	1	1	0
Gravel	38.5	0	8	5	0	0	0	0	0	0	0
Grass	98.3	6	0	0	340	0	0	0	0	0	0
Open Soil	100.0	0	0	0	0	21	0	0	0	0	0
Brown Roof	91.3	0	0	0	0	0	21	0	2	0	0
Cement	95.7	0	0	0	0	0	0	22	0	0	1
Play Area	100.0	0	0	0	0	0	0	0	23	0	0
White Roof	100.0	0	0	0	0	0	0	0	0	8	0
Shadow	95.2	1	2	0	0	0	0	0	0	0	60
TOTAL		528	72	5	340	21	21	22	26	9	66
Reliability Accuracy (%)		98.7	86.1	100.0	100.0	100.0	100.0	100.0	88.5	88.9	90.9
OVERALL CLASS PERFORMANCE = 97.6%											
Kappa Statistic (X100) = 96.4%. Kappa Variance = 0.000047											

Table 27

Recreational (1) error matrix for ECHO classification results.

Class Name	PA (%)	Tree Canopy	Asphalt	Gravel	Grass	Open Soil	Brown Roof	Cement	Play Area	White Roof	Shadow
Tree Canopy	99.4	523	0	0	0	0	0	0	0	0	3
Asphalt	95.3	0	61	1	0	0	0	1	0	1	0
Gravel	84.6	0	2	11	0	0	0	0	0	0	0
Grass	99.4	2	0	0	344	0	0	0	0	0	0
Open Soil	100.0	0	0	0	0	21	0	0	0	0	0
Brown Roof	91.3	0	0	0	0	0	21	0	2	0	0
Cement	95.7	0	0	0	0	0	0	22	1	0	0
Play Area	100.0	0	0	0	0	0	0	0	23	0	0
White Roof	100.0	0	0	0	0	0	0	0	0	8	0
Shadow	96.8	0	0	0	0	0	0	0	2	0	61
TOTAL		525	63	12	344	21	21	23	28	9	64
Reliability Accuracy (%)		99.6	96.8	91.7	100.0	100.0	100.0	95.7	82.1	88.9	95.3
OVERALL CLASS PERFORMANCE = 98.6%											
Kappa Statistic (X100) = 98.0%. Kappa Variance = 0.000026											

Table 28

Recreational (1) error matrix for SAM classification results.

Class Name	PA (%)	Tree Canopy	Asphalt	Gravel	Grass	Open Soil	Brown Roof	Cement	Play Area	White Roof	Shadow
Tree Canopy	76.0	400	0	0	82	12	1	0	0	4	27
Asphalt	93.8	0	60	3	0	0	0	1	0	0	0
Gravel	100.0	0	0	13	0	0	0	0	0	0	0
Grass	97.1	2	0	0	336	8	0	0	0	0	0
Open Soil	85.7	0	0	3	0	18	0	0	0	0	0
Brown Roof	82.6	0	0	0	0	0	19	0	4	0	0
Cement	87.0	0	1	2	0	0	0	20	0	0	0
Play Area	78.3	0	2	2	0	0	0	1	18	0	0
White Roof	87.5	0	1	0	0	0	0	0	0	7	0
Shadow	95.2	0	3	0	0	0	0	0	0	0	60
TOTAL		402	67	23	418	38	20	22	22	11	87
Reliability Accuracy (%)		99.5	89.6	56.5	80.4	47.4	95.0	90.9	81.8	63.6	69.0
OVERALL CLASS PERFORMANCE = 85.7%											
Kappa Statistic (X100) = 79.6%. Kappa Variance = 0.000221											

Table 29

Recreational (2) error matrix for MLC classification results.

Class Name	PA (%)	Grass	Open Soil	Asphalt	Prairie Veg	Shadow	Water	Evergreen Canopy	Deciduous Canopy	White Roof	Brown Roof
Grass	100.0	86	0	0	0	0	0	0	0	0	0
Open Soil	100.0	0	36	0	0	0	0	0	0	0	0
Asphalt	98.7	0	1	74	0	0	0	0	0	0	0
Prairie Veg	89.6	5	0	0	43	0	0	0	0	0	0
Shadow	100.0	0	0	0	0	30	0	0	0	0	0
Water	100.0	0	0	0	0	0	207	0	0	0	0
Evergreen Canopy	88.9	0	0	0	0	0	0	64	8	0	0
Deciduous Canopy	82.1	0	0	0	0	15	0	238	1158	0	0
White Roof	100.0	0	0	0	0	0	0	0	0	14	0
Brown Roof	100.0	0	0	0	0	0	0	0	0	0	6
TOTAL		91	37	74	43	45	207	302	1166	14	6
Reliability Accuracy (%)		94.5	97.3	100.0	100.0	66.7	100.0	21.2	99.3	100.0	100.0
OVERALL CLASS PERFORMANCE = 86.5%											
Kappa Statistic (X100) = 76.0%. Kappa Variance = 0.000184											

Table 30

Recreational (2) error matrix for ECHO classification results.

Class Name	PA (%)	Grass	Open Soil	Asphalt	Prairie Veg	Shadow	Water	Evergreen Canopy	Deciduous Canopy	White Roof	Brown Roof
Grass	100.0	86	0	0	0	0	0	0	0	0	0
Open Soil	100.0	0	36	0	0	0	0	0	0	0	0
Asphalt	98.7	0	1	74	0	0	0	0	0	0	0
Prairie Veg	89.6	5	0	0	43	0	0	0	0	0	0
Shadow	100.0	0	0	0	0	30	0	0	0	0	0
Water	100.0	0	0	0	0	0	207	0	0	0	0
Evergreen Canopy	91.7	0	0	0	0	0	0	66	6	0	0
Deciduous Canopy	83.9	0	0	0	0	15	0	212	1184	0	0
White Roof	100.0	0	0	0	0	0	0	0	0	14	0
Brown Roof	100.0	0	0	0	0	0	0	0	0	0	6
TOTAL		91	37	74	43	45	207	278	1190	14	6
Reliability Accuracy (%)		94.5	97.3	100.0	100.0	66.7	100.0	23.7	99.5	100.0	100.0
OVERALL CLASS PERFORMANCE = 88.0%											
Kappa Statistic (X100) = 78.2%. Kappa Variance = 0.000173											

Table 31

Recreational (2) error matrix for SAM classification results.

Class Name	PA (%)	Grass	Open Soil	Asphalt	Prairie Veg	Shadow	Water	Evergreen Canopy	Deciduous Canopy	White Roof	Brown Roof
Grass	100.0	86	0	0	0	0	0	0	0	0	0
Open Soil	100.0	0	36	0	0	0	0	0	0	0	0
Asphalt	100	0	0	75	0	0	0	0	0	0	0
Prairie Veg	93.8	3	0	0	45	0	0	0	0	0	0
Shadow	100.0	0	0	0	0	30	0	0	0	0	0
Water	100.0	0	0	0	0	0	207	0	0	0	0
Evergreen Canopy	70.8	0	0	0	1	1	0	51	19	0	0
Deciduous Canopy	81.6	29	0	0	238	49	0	63	1684	0	0
White Roof	100.0	0	0	0	0	0	0	0	0	14	0
Brown Roof	100.0	0	0	0	0	0	0	0	0	0	6
TOTAL		118	36	75	284	80	207	114	1703	14	6
Reliability Accuracy (%)		72.9	100.0	100.0	15.8	37.5	100.0	44.7	98.9	100.0	100.0
OVERALL CLASS PERFORMANCE = 84.7%											
Kappa Statistic (X100) = 68.3%. Kappa Variance = 0.000202											

APPENDIX B: MINIMUM NOISE TRANSFORM COVARIANCE MATRIX

The following table (Table 32) shows the covariance matrix from the first 25 of the 248 eigenvector bands generated from MNF analysis. This matrix was selected from study area subset commercial area (1) as an example.

Table 32

A portion of covariance matrix generated from MNF transform of commercial area (1) as an example dataset.

Band	Band 1	Band 2	Band 3	Band 4	Band 5	Band 6	Band 7	Band 8	Band 9	Band 10
1	-0.001797	-0.001599	-0.001879	-0.002544	-0.001945	-0.002054	-0.001166	-0.001024	-0.001273	-0.000468
2	0.001786	0.001286	0.000218	-0.000208	-0.000562	-0.000809	-0.001763	-0.001318	-0.000866	-0.001385
3	0.002033	0.000945	0.000633	0.000434	-0.000109	-0.000968	-0.001162	-0.001427	-0.002103	-0.001487
4	-0.000379	0.000212	-0.000152	0.000406	0.000334	-0.000051	-0.000574	0.000107	0.000146	-0.000327
5	-0.000868	-0.001881	-0.00153	-0.00231	-0.002116	-0.001404	-0.00146	-0.000257	0.000678	0.000337
6	-0.000619	-0.000657	0.001592	0.002623	0.00289	0.003254	0.002285	0.001825	0.001776	0.000039
7	-0.002195	-0.001515	-0.001484	-0.000769	-0.000646	-0.000188	-0.000701	-0.000119	-0.00074	-0.000384
8	-0.000751	-0.00099	0.000008	0.001294	0.000912	0.00115	0.000767	0.000809	0.001084	0.001603
9	-0.003867	-0.002729	-0.003292	-0.002265	-0.002342	-0.001404	-0.001255	0.00051	0.000181	0.000648
10	0.000789	0.000853	0.001334	0.001144	0.000371	0.000574	-0.000106	-0.000639	-0.000109	-0.000758
11	-0.001802	-0.001589	-0.000931	-0.000718	-0.000071	0.000326	-0.000369	0.000496	-0.000489	0.000613
12	-0.000583	-0.000077	0.000553	0.000234	0.000404	0.000408	-0.000259	-0.000258	0.00041	-0.0003
13	0.001858	0.002401	0.00157	0.00124	0.001178	0.000371	0.001217	0.000785	-0.000411	0.000573
14	0.000839	0.000961	-0.000927	-0.001737	-0.001789	-0.001215	-0.000211	0.000214	0.000007	0.000613
15	-0.000749	-0.000727	0.000058	0.000043	0.00054	0.000702	-0.000276	0.000839	0.000088	0.000201
16	0.002885	0.003184	0.000875	-0.00058	-0.000482	-0.000221	-0.00012	-0.001535	-0.000406	-0.00124
17	0.002699	0.00257	0.001815	-0.000336	-0.000314	-0.000194	0.000075	-0.000085	-0.000002	0.000328
18	0.001576	0.001889	0.001792	-0.000525	-0.000967	-0.001654	-0.000692	-0.000898	-0.001008	-0.000934
19	0.009881	0.007067	0.005601	0.002746	0.001302	0.000659	-0.000259	-0.002346	-0.00247	-0.002431
20	-0.001611	-0.001588	-0.002076	-0.002435	-0.001494	-0.002117	0.000317	0.000869	0.001454	0.001387
21	0.006061	0.007576	0.003579	0.003205	0.001392	0.001393	-0.000197	0.000092	-0.001342	-0.001775
22	-0.002541	-0.003521	-0.003165	-0.004773	-0.005563	-0.00443	-0.002302	-0.000455	0.000474	0.000156
23	-0.005375	-0.006223	-0.006251	-0.004145	-0.004728	-0.002417	-0.001317	0.000151	0.000086	0.001716
24	0.00184	0.000647	0.000399	-0.004156	-0.002972	-0.003642	-0.002985	-0.004141	-0.00212	-0.001848
25	-0.005364	-0.004288	-0.004259	-0.001376	-0.001317	0.00222	0.00035	0.000506	0.001375	0.000901

Continued on the next page

Band	Band 11	Band 12	Band 13	Band 14	Band 15	Band 16	Band 17	Band 18	Band 19	Band 20
1	0.000116	-0.000014	0.000115	0.000323	0.000293	0.000611	0.001014	-0.000289	0.000542	0.000545
2	-0.000793	-0.00054	-0.000295	0.000201	0.00024	0.000702	0.000976	0.000719	0.000695	0.000611
3	-0.002013	-0.001075	-0.001027	-0.001019	-0.000826	0.000021	0.00027	-0.000973	0.000777	0.000193
4	-0.000787	-0.000367	-0.000222	0.000567	0.000086	-0.000265	-0.000443	0.000307	-0.000853	-0.000904
5	0.000722	0.001236	0.001108	0.001106	0.001551	0.000866	0.000706	0.001155	0.000267	0.000286
6	-0.000574	-0.000845	-0.000239	-0.00003	0.000096	-0.000389	0.000505	0.00036	0.000922	0.000339
7	-0.00048	-0.000462	-0.00042	-0.000421	-0.000665	-0.000331	-0.000342	-0.001347	0.000402	-0.000158
8	0.00033	0.000776	0.000524	0.000693	0.000492	0.000474	-0.000192	0.000504	-0.000638	0.000237
9	0.00101	0.000357	-0.000548	-0.000139	0.000117	0.000127	-0.000311	-0.001255	-0.001487	-0.001462
10	-0.001241	-0.001648	-0.000599	-0.000981	-0.000688	0.000019	-0.000438	-0.000231	0.001049	0.000055
11	0.000367	-0.000069	-0.000252	-0.000277	-0.000975	-0.000024	-0.000308	-0.002126	-0.000697	0.000002
12	0.000391	-0.000287	0.0001	-0.000166	-0.000597	-0.000307	-0.000646	0.000339	-0.000055	0.000748
13	0.000028	-0.000028	-0.000484	-0.000306	0.000148	0.001126	0.001047	-0.001135	-0.000296	-0.000141
14	0.000663	0.001137	0.000896	0.000702	0.000509	-0.000222	-0.000096	0.000297	-0.0011	-0.000786
15	0.000426	-0.000359	0.000585	0.000693	0.000581	0.000849	0.000977	-0.000789	0.000872	-0.000939
16	-0.000921	-0.000825	-0.000459	-0.000465	-0.000844	-0.000648	0.000888	0.001374	-0.000354	0.000567
17	-0.000479	-0.000364	-0.000329	-0.000892	-0.000801	-0.001436	-0.000515	0.000179	-0.000236	-0.000866
18	-0.002274	-0.001022	-0.000403	0.000283	-0.000273	0.000294	-0.000431	0.001388	0.000549	0.001067
19	-0.003397	-0.00288	-0.000665	-0.001288	-0.002191	-0.001613	0.000337	0.000321	0.00187	0.001939
20	0.00215	0.003005	0.002602	0.000506	0.001928	0.000638	0.000949	0.001353	-0.002235	0.000006
21	-0.001271	-0.000151	-0.000942	-0.001084	-0.000767	-0.000185	0.000626	-0.000065	0.000199	-0.000627
22	0.001384	0.003719	0.002332	0.002428	0.003228	0.002013	0.001209	0.003067	0.001051	0.000792
23	0.00218	0.002685	0.002559	0.002232	0.002916	0.003513	0.002341	0.001571	0.001027	0.001912
24	-0.000169	0.000775	0.001562	0.000605	0.000547	0.000181	0.001412	0.004917	0.003029	0.00219
25	0.002083	-0.000392	-0.000161	0.00043	-0.000012	0.00029	-0.00154	-0.003059	0.001045	0.001464

Continued on the next page

Band	Band 21	Band 22	Band 23	Band 24	Band 25
1	0.00036	-0.000516	-0.000344	0.000004	-0.00103
2	0.001044	0.000868	0.000006	0.000669	0.000611
3	0.001695	0.000199	0.001185	0.001157	0.000598
4	-0.000224	0.000403	0.000203	0.000584	0.000963
5	-0.000335	0.000535	0.000165	0.000184	0.000038
6	0.000881	0.000565	0.001045	0.000245	0.000388
7	0.000511	-0.000291	-0.000141	0.000252	-0.000016
8	-0.000632	0.00025	0.000413	-0.000068	-0.000226
9	-0.001845	-0.001997	-0.003153	-0.001791	-0.002342
10	0.000252	0.000682	0.001079	0.000796	0.001417
11	0.000056	-0.001042	0.00004	0.000664	-0.000293
12	0.000839	-0.000284	0.000104	-0.00013	0.000514
13	0.000741	-0.000909	0.000145	0.000979	-0.000083
14	-0.001086	-0.001156	-0.001349	-0.001621	-0.001634
15	0.000771	0.000275	-0.000243	-0.000244	-0.001278
16	0.000943	0.001106	0.000478	0.000418	0.001322
17	-0.000543	0.000355	-0.000226	0.000451	0.000551
18	0.001049	0.001917	0.001489	0.001931	0.002531
19	0.002405	0.002479	0.004109	0.00231	0.001901
20	-0.002372	-0.000326	-0.002818	-0.001353	-0.001211
21	0.000345	-0.000821	-0.001642	-0.000416	-0.000932
22	0.000491	0.000698	0.000947	0.000965	0.00137
23	0.001361	0.001814	0.001925	0.001735	0.001769
24	0.002599	0.004087	0.004698	0.002586	0.002932
25	0.001527	0.00042	0.000828	0.001907	-0.000064

APPENDIX C: MINIMUM NOISE TRANSFORM EIGENVALUES

Eigenvector loadings are for 248 bands, with eigenvector band consisting of a MNF band digital number that is multiplied by an eigenvector loading. The sum of each one of the 248 individual bands results in the final eigenvector values. The highest value has the most variance or information, and is the most important band. The band containing the next most variance is the second most important band, and so on. The eigenvector associated with the largest eigenvalue has the same direction as the first principal component, and the eigenvector associated with the second largest eigenvalue determines the direction of the second principal component.

The table in this appendix shows the eigenvalues of the top 25 bands that have most variance. Each column represents a study area.

Table 33

Eigenvalues for the first 25 bands in each study area.

	Eigenvalues					
Band	Commercial (1)	Commercial (2)	Residential (1)	Residential (2)	Recreation (1)	Recreation (2)
1	27.95115	43.93014	16.7136	51.53808	27.10446	105.7139
2	15.99375	26.25997	12.22388	20.88525	15.58878	45.37423
3	14.41654	17.28657	10.04768	13.87338	14.15177	24.15439
4	13.84108	12.39557	8.708817	12.10634	10.85209	18.3776
5	10.43413	11.03386	6.593699	11.23188	9.995477	15.71481
6	8.833206	9.09674	5.932341	9.378101	8.388093	10.51723
7	6.438119	6.836935	5.15567	7.860804	7.622527	9.031202
8	6.085381	6.608133	4.431514	7.213422	6.252172	8.309512
9	5.745343	6.07634	4.007607	6.434815	5.784421	7.6706
10	5.039288	5.876482	3.846846	5.989498	5.533586	7.05955
11	4.671094	5.660641	3.402437	5.639558	5.016357	6.119651
12	4.477443	5.135531	3.162879	5.221786	4.702112	5.791444
13	4.022547	4.685622	3.078211	4.80538	4.408929	5.217487
14	3.831801	4.606922	2.891924	4.258289	4.109159	4.478615
15	3.58317	4.435442	2.828739	4.134301	3.749538	3.775705
16	3.297357	4.093186	2.718439	3.81429	3.429909	3.372467
17	3.111881	3.969339	2.657234	3.568297	3.263923	3.247348
18	3.00554	3.486478	2.462425	3.298751	3.086746	3.045834
19	2.81108	3.273533	2.405207	3.113874	2.919661	2.928023
20	2.683256	3.145601	2.301127	2.88693	2.779034	2.777711
21	2.614775	2.998698	2.2308	2.822761	2.594128	2.628495
22	2.445394	2.942664	2.113077	2.564783	2.444241	2.460323
23	2.362281	2.746178	2.063796	2.452416	2.350597	2.338045
24	2.207309	2.641241	1.960164	2.350468	2.105755	2.199324
25	1.988631	2.459091	1.878336	2.293767	2.063944	2.041441